THE UNIVERSITY OF CALGARY

OTA DESIGN
AND
BIQUAD FILTER IMPLEMENTATION

by

Jeffrey L. LaFrenz

A THESIS
SUBMITTED TO THE FACULTY OF GRADUATE STUDIES
IN PARTIAL FULFILLMENT OF THE REQUIREMENTS FOR THE
DEGREE OF
MASTER OF SCIENCE

DEPARTMENT OF
ELECTRICAL ENGINEERING

CALGARY, ALBERTA
March, 1988

ISBN 0-315-42500-8

THE UNIVERSITY OF CALGARY
FACULTY OF GRADUATE STUDIES

The undersigned certify that they have read, and recommend to the Faculty of Graduate Studies for acceptance, a thesis entitled, "OTA Design and Biquad Filter Implementation" submitted by Jeffrey L. LaFrenz in partial fulfillment of the requirements for the degree of Master of Science.

Supervisor, Dr. J. W. Haslett
(Electrical Engineering)

Dr. L. E. Turner
(Electrical Engineering)

B. Nowrouzian
Dr. B. Nowrouzian
(Electrical Engineering)

Dr. G. M. Birtwistle
(Computer Science)

Date March 30, 1988

ABSTRACT

This thesis describes the design, fabrication and characterization of seven types of bipolar Operational Transconductance Amplifier (OTA) structures for the purpose of implementing a biquad filter topology. The resulting biquad filter is an extremely flexible circuit, allowing for nine different filter outputs (three lowpass, three bandpass, a highpass and two notch responses) and for easy adjustment of filter performance parameters. However, it has a relatively simple structure, requiring few components for its implementation.

The primary consideration in the design of these OTA structures is that they fit into the cell structure of the semi-custom substrates available from Linear Technology Incorporated (LTI). For this reason, the designs are limited to those which can be implemented using single or dual cells. A biquad filter structure is then implemented from the OTA's designed to fit such a restriction.

The standard design tools do not satisfactorily predict the output responses of the above filter configurations. To overcome this, a scheme is derived which enables an easy design of these filters and a simple means of predicting their responses.

Initially, all the seven OTA's are characterized to enable a better understanding of their performance. From the OTA characteristics, lumped models for the filter structures are developed and applied to obtaining design equations and predictive

algorithms. The design process is automated through the use of specialized programs developed for the purpose.

The design process is shown to be quite effective, and the filter responses are shown to be in excellent agreement with those predicted by the algorithms.

ACKNOWLEDGEMENTS

The author wishes to express his appreciation for the guidance and tolerance of Dr. J. W. Haslett throughout his research.

Also appreciated is Linear Technology Incorporated, for the free use of their fabrication facilities in the implementation of the Operational Transconductance Amplifiers. In addition NSERC is appreciated for providing the funding.

For assistance in the design and implementation of circuits used in the research, the author would like to thank Art, Brij and Warren.

For the care and understanding of the author's parents and sister during the difficult times, thanks is not enough.

To the author's friends and fellow graduate students, thank you, and best of luck in your future endevours.

And finally to Brydon, whose friendship and warped sense of humor kept the author going when the path seemed darkest. We strive mightily, but eat and drink as friends.

To those who understood

and those who are willing to understand.

TABLE OF CONTENTS

Chapter 6

LIST OF TABLES

LIST OF FIGURES

LIST OF SYMBOLS

C_1	biquad filter capacitor 1
C_2	biquad filter capacitor 2
C_{cm}^{+}	OTA non-inverting input common mode capacitance
C_{cm}^{-}	OTA inverting input common mode capacitance
C_d	OTA differential input capacitance
C_{IN}	OTA input capacitance
C_o	OTA output capacitance
$D(s)$	denominator polynomial
$D_{IM}(\omega)$	Ideal Magnitude Denominator Polynomial
$D_M(\omega)$	Lumped Model Magnitude Denominator Polynomial
f	frequency (Hz)
f_n	natural or center frequency (Hz)
g_m	OTA transconductance gain
i_b	small signal transistor base current
i_{OUT}	OTA output current
I_{BIAS}	OTA bias current
I_C	DC transistor collector current
I_E	DC transistor emitter current
k	Boltzmann constant
$N(s)$	numerator polynomial
q	electron charge
Q	quality factor
$r_{bb'}$	parasitic base resistance
$r_{b'e}$	intrinsic common emitter input resistance
r_d	transistor dynamic resistance
r_o	transistor output resistance
R_{cm}^{+}	OTA non-inverting input common mode resistance
R_{cm}^{-}	OTA inverting input common mode resistance
R_d	OTA differential input resistance
R_E	emitter resistor
R_{IN}	OTA input resistance
R_L	load resistor
R_o	OTA output resistance

R_{OFF}	offset resistance
T	temperature in Kelvin
v_d	differential input voltage
v_{IN}	input voltage
v_{OUT}	output voltage
V_{CC}	positive supply voltage
V_{EE}	negative supply voltage
$V_{IN}(s)$	frequency domain input voltage
$V_{OUT}(s)$	frequency domain output voltage
β	common-emitter current gain
ε_1	lumped model error term 1
ε_2	lumped model error term 2
ε_3	lumped model error term 3
ε_4	lumped model error term 4
ω	radian frequency (rad/s)
ω_n	natural or center frequency (rad/s)

OTA SYMBOLS

2T	2 Transistor Mirror OTA
3T1	Wilson Mirror OTA
3T2	3 Transistor Mirror OTA
DP1	Wilson Mirror OTA with Darlington Pair Input Stage
DP2	3 Transistor Mirror OTA with Darlington Pair Input Stage
M1	Modified Wilson Mirror OTA
M2	Modified 3 Transistor Mirror OTA

FILTER SYMBOLS

BP1a	Bandpass Ia filter
BP1b	Bandpass Ib filter
BP2	Bandpass II filter
HP	Highpass filter
LP1a	Lowpass Ia filter
LP1b	Lowpass Ib filter
LP2	Lowpass II filter
Na	Notch a filter
Nb	Notch b filter

CHAPTER 1

INTRODUCTION TO OTA FILTER DESIGN

Linear Technology Incorporated (LTI), a Canadian company, requires flexible, active device circuits for inclusion in their semi-custom bipolar product line. These circuits are required to use a small chip area so as to fit into LTI's cell layout and, if possible, into a single cell. The circuits are not required to have a large dynamic range. Minimal size is of the most importance. From such circuits, filter structures are to be developed, which are also to be included as part of their product line.

The active device chosen for implementation here is the *Operational Transconductance Amplifier* (OTA). There are several types of amplifier circuits (i.e. voltage, current, transconductance, transresistance), but the majority of the existing filter designs utilize the operational amplifier (op-amp) as the primary active device. Many practical filter design methods are based on this approach.

It has become apparent, however, that op-amp based filters have several major limitations. It is often not practical to use these filters at high frequencies due to the limited bandwidth of most op-amps. The full integration of such filters is more difficult than that of structures using OTA's. This is mainly due to the fact that an op-amp takes up much more silicon area than an OTA.

As the process of filter design can be extremely time consuming and tedious, it is desirable to have a filter circuit which is easy to implement, while not placing limitations on the designer in the choice of filter parameters.

An analog circuit is presented here which enables the designer to change the filter performance parameters, and in fact the filter type, in a simple manner. This filter belongs to a family of circuits known as biquad filters, and uses as its basic building block the OTA. Existing op-amp base biquad filter structures do not allow the same design flexibility and simplicitiy [1], offered by OTA based biquad filters. Op-amp based biquads are much more difficult to tune, require more components, and do not exhibit the range of filter types available with OTA based biquad filters [2].

It is only very recently that the potential of OTA based filters has been realized. As Geiger et al.[3] point out

> "these structures offer improvements in design simplicity and programmability when compared to op-amp based structures as well as reduced component count."

They go on to illustrate this statement through the design of many OTA based filters, most of which are exceedingly simple in concept, while maintaining a large degree of flexibility.

The standard filter parameters of the majority of these filters are directly proportional to the transconductance gain, g_m, of the OTA. As g_m is proportional to an external bias current, control of filter parameters can easily be accomplished. In fact, several researchers have recently proposed tunable filters based upon this principle [4]-[5].

Due to the recent popularity of OTA based filters, a plethora of proposals for filter designs can be considered. However, when the choice is restricted to those cases which provide the maximum flexibility and minimum complexity, the number becomes limited. Of these, the design which appears to be the best is that of the biquad filter [2].

Unfortunately, as very little study has been conducted on these filters until just recently, the existing design equations are mainly based on the ideal model of the OTA. It will be shown later that this model gives rise to results which are often quite different from the actual performance. Design tools such as HSPICE [6], which are supposed to take into account known non-idealities, also fall short of predicting the actual performance (due to the process variations not being fully accounted for).

A need exists then for some method whereby the filter performance can be predicted accurately. It would also be beneficial if a design methodology could be developed to make the process of filter design easier and more accurate, not requiring extensive tuning. This will be shown to be possible through the use of lumped OTA models.

A lumped model is developed to take into account the non-idealities which plague the majority of designs. Stray capacitances and resistances are lumped together at the inputs and outputs, and the corresponding design equations are thereby derived.

Fabrication of the filter designs was provided by Linear Technology Incorporated. LTI expected the OTA's designed, and the filters incorporating them to be integrated using their semi-custom bipolar process [7], and to be included as part of their product line. LTI's process is based upon cell design, where a cell is a block containing several transistors and resistors in a fixed layout. They have several different substrates which vary in the number of cells contained, and the number of external components available. However, the internal structure of the cells in all the different substrates remains the same. For this reason, the designs presented here will be oriented towards placement in the cell structure and will not use external components, since they vary from substrate to substrate.

Chapter 2 describes the steps required to design and implement OTA's in LTI's semi-custom bipolar process. Chapter 3 illustrates the steps required to characterize the OTA's, and the lumped model obtained from this characterization. The actual implementation of biquad filters using the OTA's, and the determination of a practical design technique for the filters is covered in Chapter 4. The results obtained from measuring the biquad filters implemented is shown in Chapter 5, as is a comparison with the lumped model predictions. Conclusions and suggestions for future work are presented in Chapter 6.

CHAPTER 2

OPERATIONAL TRANSCONDUCTANCE AMPLIFIER DESIGN

2.1 Operational Transconductance Amplifiers

An OTA is basically a differential voltage input, single ended current output device with a variable gain (Figure 2.1). The output current of the OTA is proportional to the differential input voltage, with the proportionality factor being the OTA transconductance gain, g_m. However, unlike operational amplifiers, the gain itself is variable, and is set through the use of an external bias current. This variable gain property is what makes the OTA so useful in filter design.

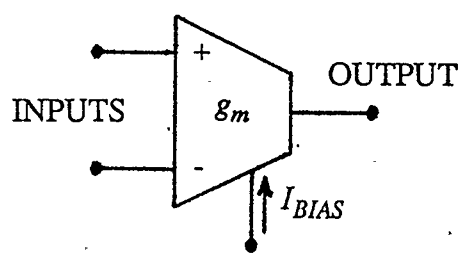

Figure 2.1 The OTA Symbol

The basic structure of an OTA is shown in Figure 2.2. It consists of a differential pair, whose operating current is supplied through a current mirror from the external bias source, and a series of current mirrors (two PNP mirrors and one NPN mirror) to carry the current signal to the output.

When the voltages applied to the differential pair are the same, the current mirrors on the output stage have cancelling currents, and thus there is no excess current to flow through the output. If the differential inputs are not at the same voltage, an imbalance occurs in the two output current mirrors. This imbalance causes the current supplied from the top mirror to be either greater or lesser than the current required by the bottom mirror. Such a difference in currents will be balanced by sourcing or sinking current from the output. This is the basic principle of an OTA.

2.2 Current Mirror Considerations

A current mirror is a circuit which in effect duplicates a current, producing a second current of the same orientation and, ideally, the same magnitude as the original current. The current transfer ratio is defined as the ratio of the output current to the input current, and it is desired that this ratio be as close to unity as possible. There are a variety of circuits which approximate this. Some of the more common configurations are shown in Figure 2.3.

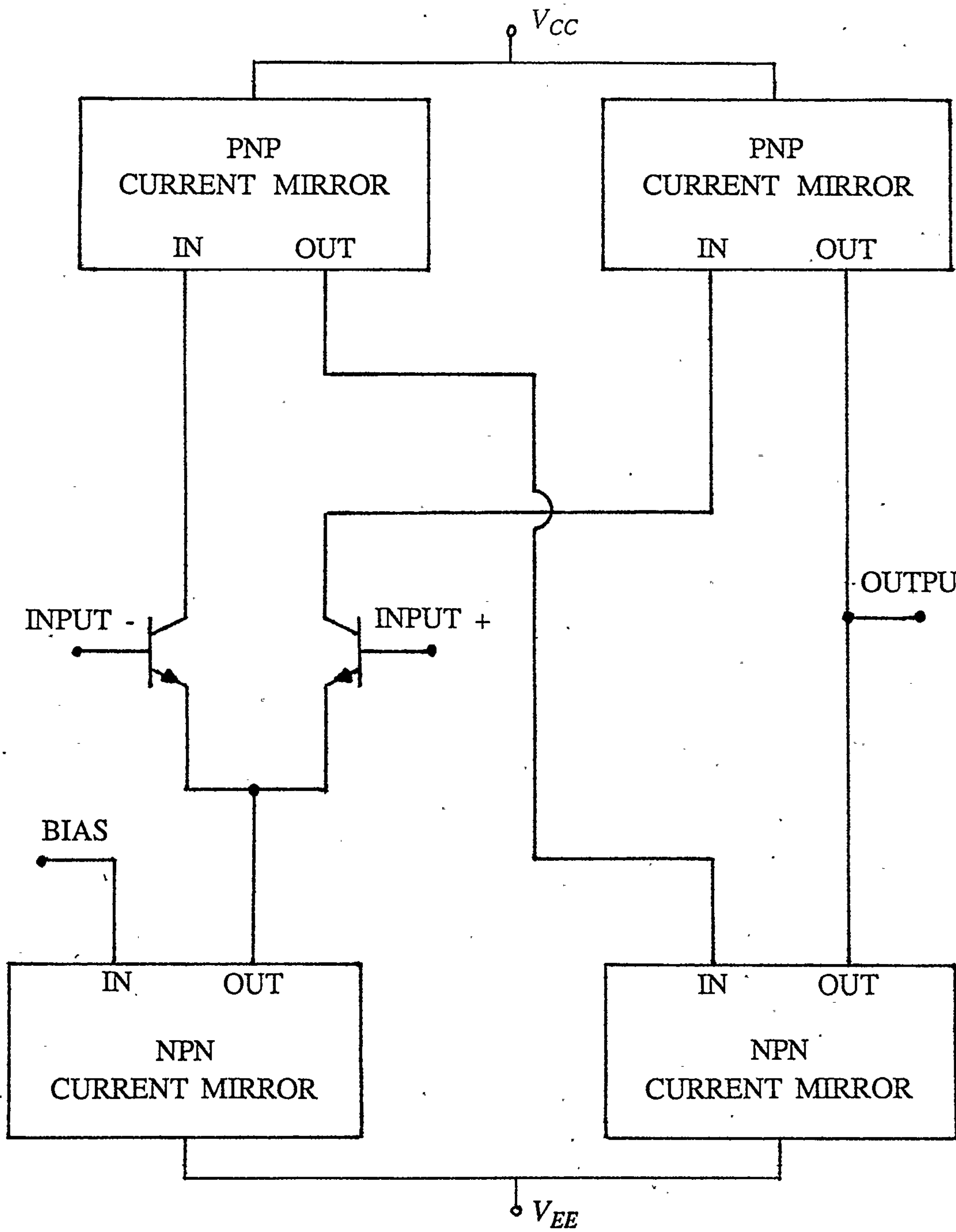

Figure 2.2 OTA Block Diagram

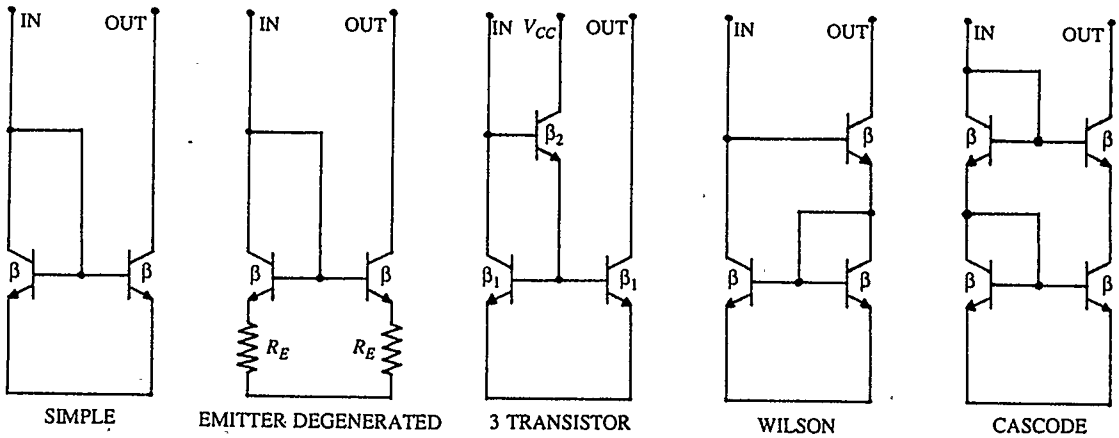

Figure 2.3 Current Mirror Configurations

The best OTA performance is achieved from current mirrors which exhibit the most accurate current transfer ratio and a high output resistance. Values for these parameters can be derived from consideration of the small signal transistor model shown in Figure 2.4, where β is the common emitter current gain, $r_{bb'}$ is a small resistor, r_o is quite a large resistor and the resistance $r_{b'e}$ is defined as follows:

$$r_{b'e} = (\beta + 1)r_d \tag{2.1}$$

where

$$r_d = \frac{nkT}{qI_E}. \tag{2.2}$$

In the above equation k is the Boltzmann constant, T is the temperature in degrees Kelvin, q is the charge of an electron, I_E is the dc current flowing through the emitter and n is a generation-recombination factor which is usually in the range of 1 to 2.

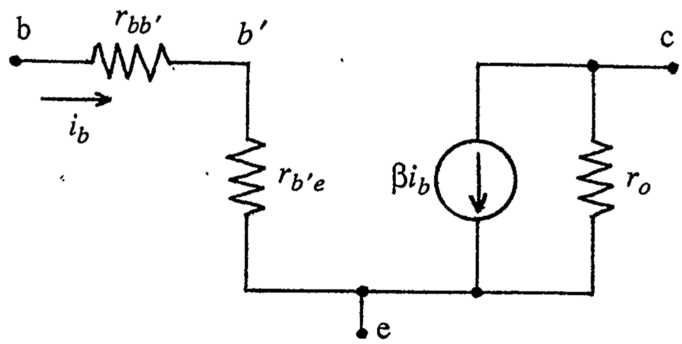

Figure 2.4 Small Signal Transistor Model - Common Emitter Configuration

The current transfer ratio for each of the current mirrors in Figure 2.3 can then be defined using the transistor model shown in Figure 2.4. The calculations are performed assuming that all transistors have matching β's, with the exception of the 3 transistor mirror where $\beta_2 < \beta_1$ due to bias mismatch. Typical β mismatch on transistors is much less than 10% for the technology used [7]. The nominal value of the transfer ratio is much more important for choosing a mirror than the small variations due to β mismatch.

In general, PNP transistors have much lower β's than NPN transistors. This can be seen in Figure 2.5. This is due to the lateral geometry commonly used in the integration of PNP transistors. For this reason, the current transfer ratio becomes more important when dealing with PNP mirrors. In addition, as an ideal current source has infinite small signal resistance, it is important to have as high a resistance as possible on the output of mirror circuits. The current transfer ratio, and the corresponding output resistance for each of the current mirrors shown in Figure 2.3 are tabulated in Table 2.1.

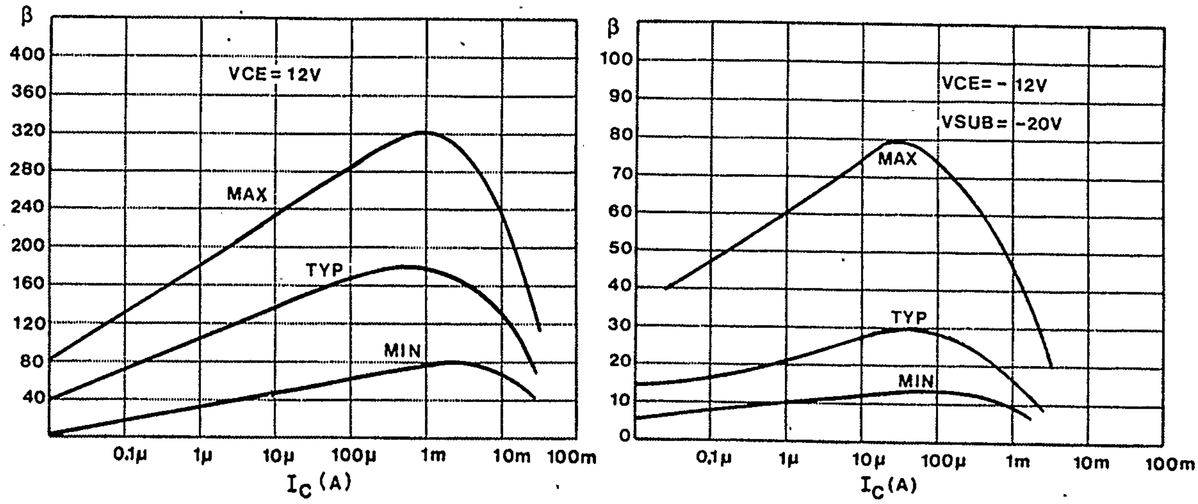

(a) NPN

(b) PNP
(with both collectors connected together)

Figure 2.5 DC Current Gain vs. Collector Current for LTI Transistors
By Permission of LTI.

From the performance viewpoint the Wilson mirror configuration has the best current transfer ratio, while maintaining a reasonably high output resistance. However, due to the limited amount of silicon area available for integration, the size becomes an important factor too, and may dictate the use of a different mirror structure. This will be considered in the next section.

2.3 Implementation of a Current Mirror

As the relative performance capabilities of the current mirrors has been determined, it now becomes important to consider the technology and layout into which they are to be integrated. For the purpose of this thesis the OTA's were developed in connection with LTI's [7] technology. LTI uses a semi-custom bipolar process, therefore the transistors and other integrable components are predefined and fixed in position. The design task consists of determining the

Mirror	Current Transfer Ratio	Output Resistance, Current Source Drive
2 Transistor	$\frac{\beta}{\beta+2}$	r_o
Emitter Degenerated	$\frac{\beta}{\beta+2}$	$\approx\frac{\beta}{2}r_o,\ r_b<R_E<r_o, \beta>>1$ $r_b\ = r_{bb'}+r_{b'e}$
3 Transistor	$\frac{\beta_1(\beta_2+1)}{\beta_1\beta_2+\beta_1+2}$	r_o
Wilson	$\frac{\beta(\beta+2)}{\beta^2+2\beta+2}$	$\approx\frac{\beta}{2}r_o,\ \beta>>1$
Cascode	$\frac{\beta^2}{\beta^2+4\beta+2}$	$\approx\beta r_o$

Table 2.1 Current Mirror Characteristics

optimal means of connecting the various components using metal traces. As each of the various substrates available from LTI use cells as the common layout element, designs will be based upon placement into such a layout.

Each cell (see Figure 2.6) consists of six NPN transistors and two split collector PNP transistors. As the basic design of an OTA requires two PNP current mirrors and two NPN current mirrors (see Figure 2.2), execpt for the most simple current mirrors, the design will require the use of more than one cell for a

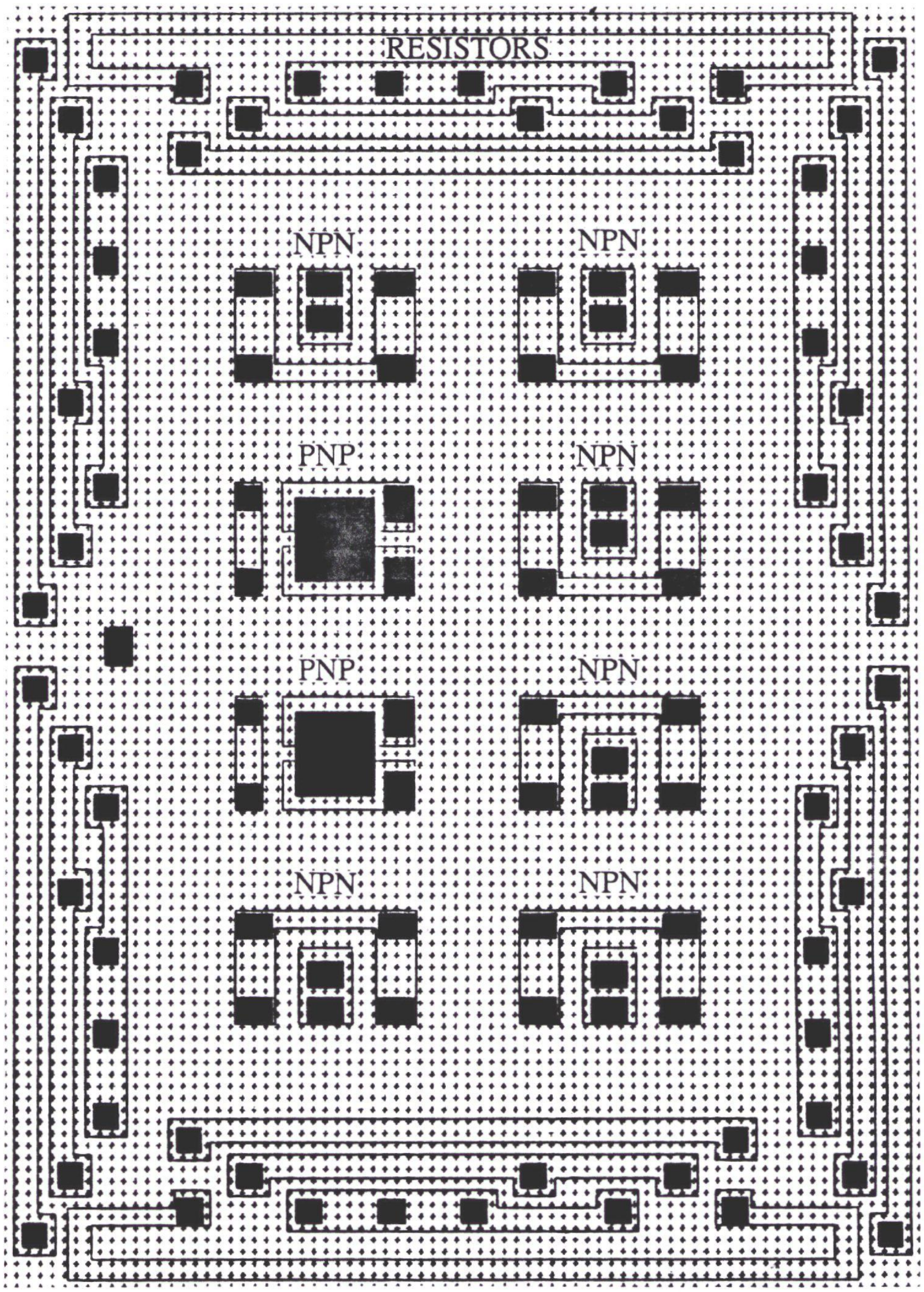

Figure 2.6 LTI Cell Layout

complete OTA. However, as the simpler mirror structures have worse performances, a trade off exists between maximum performance and minimum size.

As there are more NPN transistors in each cell than PNP transistors, the size constraint pertains more to the PNP mirrors than to the NPN mirrors. In addition, as was earlier indicated, the β of the PNP transistors is significantly smaller than the β of the NPN transistors. This means that performance limitations of the mirrors will be more readily apparent when dealing with the PNP transistors. For these reasons the following discussion of current mirror implementation will be limited to that of the PNP mirrors.

To minimize the size, the simple two transistor current mirror can be implemented using a single split collector PNP transistor (Figure 2.7). The disadvantage of this configuration is that it cannot be emitter degenerated (i.e. the emitters are connected directly to the supply rail and cannot be separated and

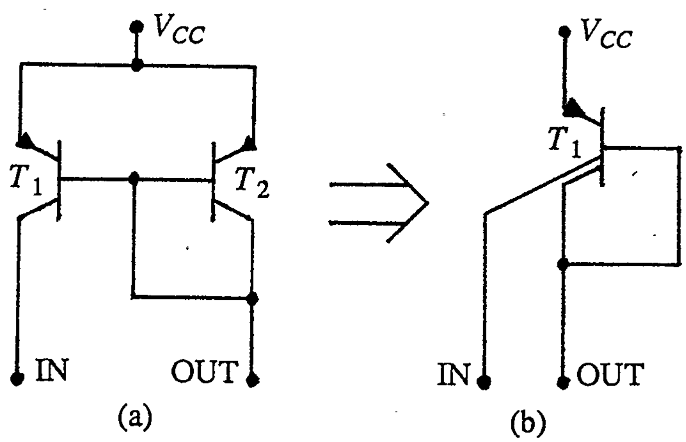

Figure 2.7 Split Collector Implementation of a 2 Transistor Current Mirror

individually reconnected through resistors, as there is actually only one emitter) to provide a better output resistance (see Table 2.1). However, an implementation with emitter degenerated current mirrors could be accomplished if double the number of PNP transistors were available. The problem with such an arrangement is that it requires two cells for a complete OTA implementation. In this case a current mirror such as the Wilson mirror, which gives the same output resistance and a much better current transfer ratio, is preferable.

The Wilson mirror can be easily implemented using two split collector transistors, as shown in Figure 2.8. The split collector implementation will have the same current transfer ratio as the original Wilson current mirror providing the β's of all the transistors are the same. Unfortunately transistors T_3 and T_4 in Figure 2.8(b) will carry only half of the bias currents of transistors T_1 and T_2, so this is not strictly the case, but the small change in β that this represents will not have a noticeable effect on the transfer ratio.

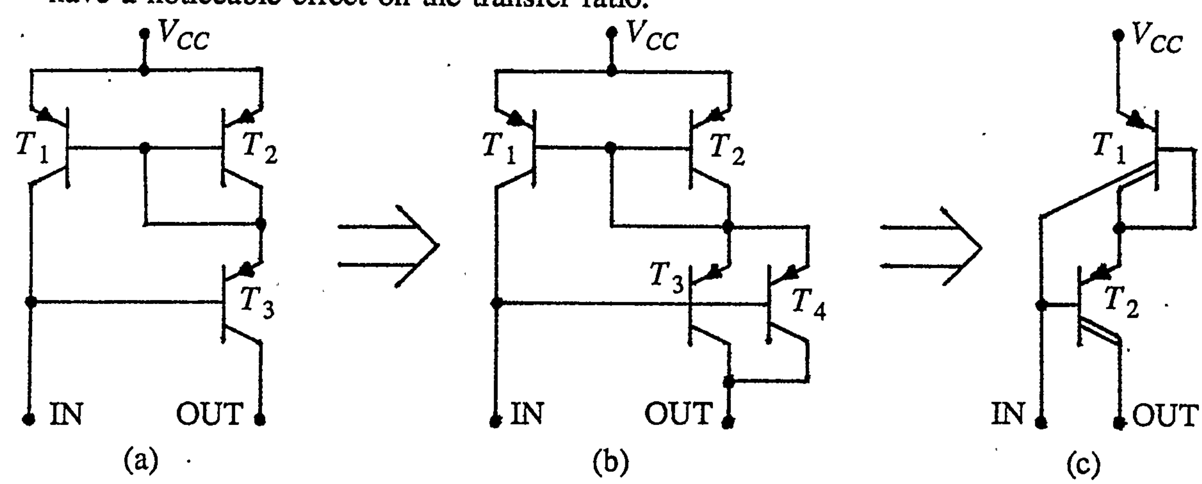

Figure 2.8 Split Collector Implementation of a Wilson Current Mirror

2.4 Lumped Model OTA

In the ideal case, the small signal model of an OTA is that shown in Figure 2.9. However, due to the process limitations this ideal model is never achieved in practice. Instead, non-idealities produce stray capacitances and resistances, which can greatly affect the performance of any circuit containing the OTA.

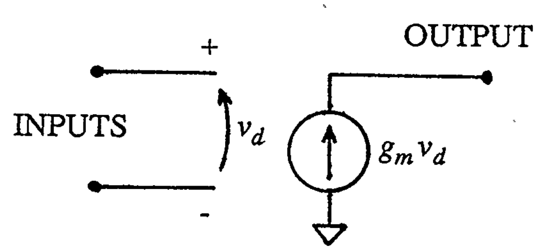

Figure 2.9 OTA Small Signal Model (Ideal)

To alleviate these problems somewhat, the ideal OTA model is replaced with a lumped model (Figure 2.10) in which the stray impedances are replaced with lumped equivalents at the circuit inputs and outputs. Such a model can then be used to determine the performance of the circuits utilizing these OTA's.

2.5 OTA Implementation

The simplest possible configuration for an OTA is that utilizing only 2 transistor mirrors and the basic differential pair (Figure 2.11(a)). This circuit requires six NPN transistors and two split collector PNP transistors, and can thus be implemented entirely in a single cell (Figure 2.11(b)).

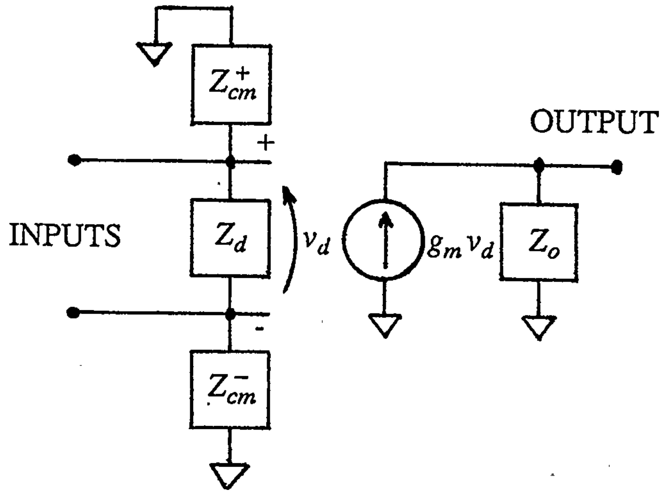

Figure 2.10 OTA Small Signal Model (Lumped)

In much the same manner, an OTA using the Wilson mirror can be designed as shown in Figure 2.12. However, this design will require two cells (Figure 2.12(b)), and if the size constraint is important the improvement in performance may not justify the doubling of the required silicon area.

It should be noted that the NPN mirror on the bias input is not as critical to the performance as that on the output, so this mirror is kept unchanged through all the designs considered. The bias input mirror mainly sets the operating point of the OTA and has little to do with the performance at that point.

For comparison, an OTA using simple 3 transistor mirrors was also designed, and is shown in Figure 2.13. While the mirrors in this configuration have the advantage over those of the 2 transistor mirror OTA in having a somewhat better current transfer characteristic, the output resistance of the mirrors is no better. In fact, the mirrors in the Wilson mirror configuration, which take up the same area,

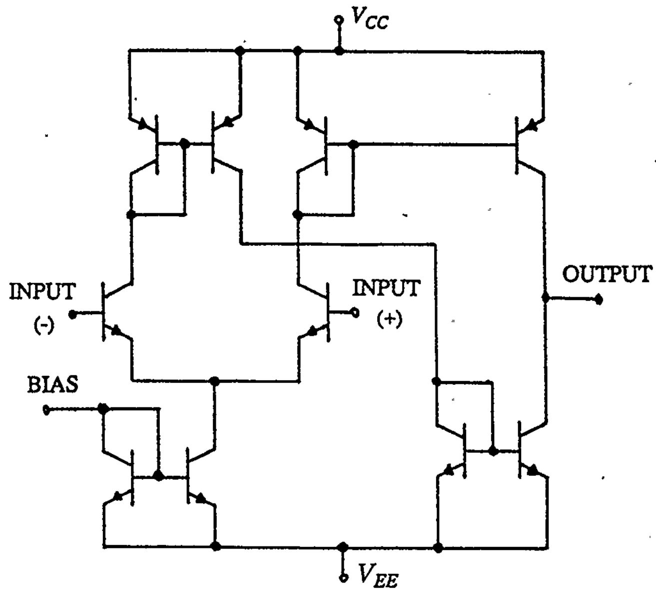

(a)

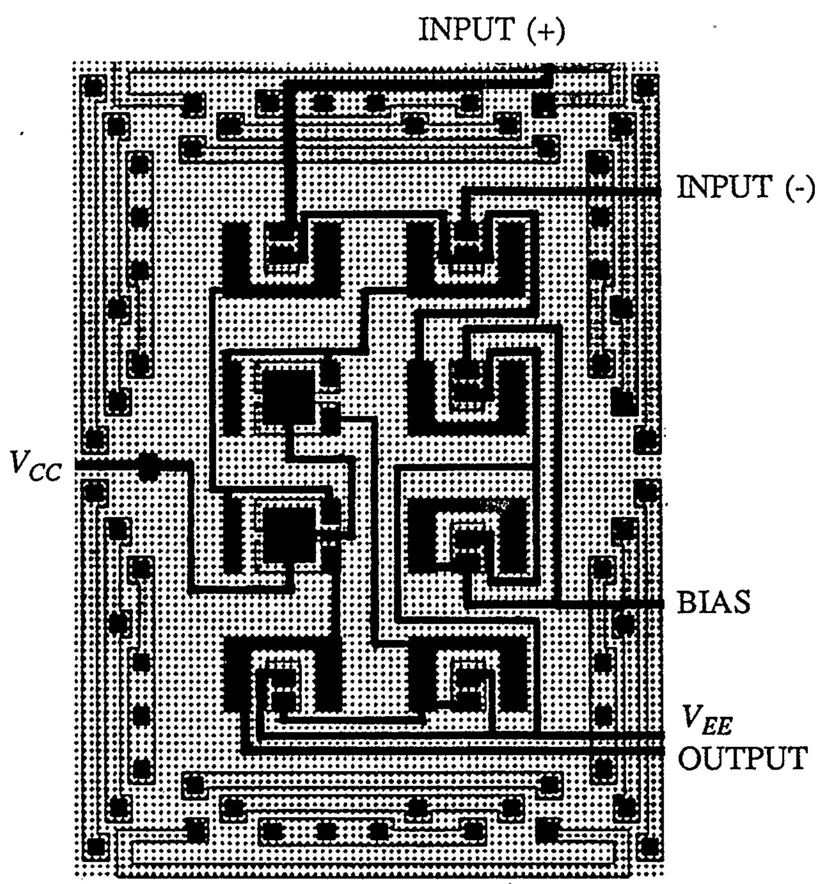

(b)

Figure 2.11 2 Transistor Mirror OTA Design and Implementation

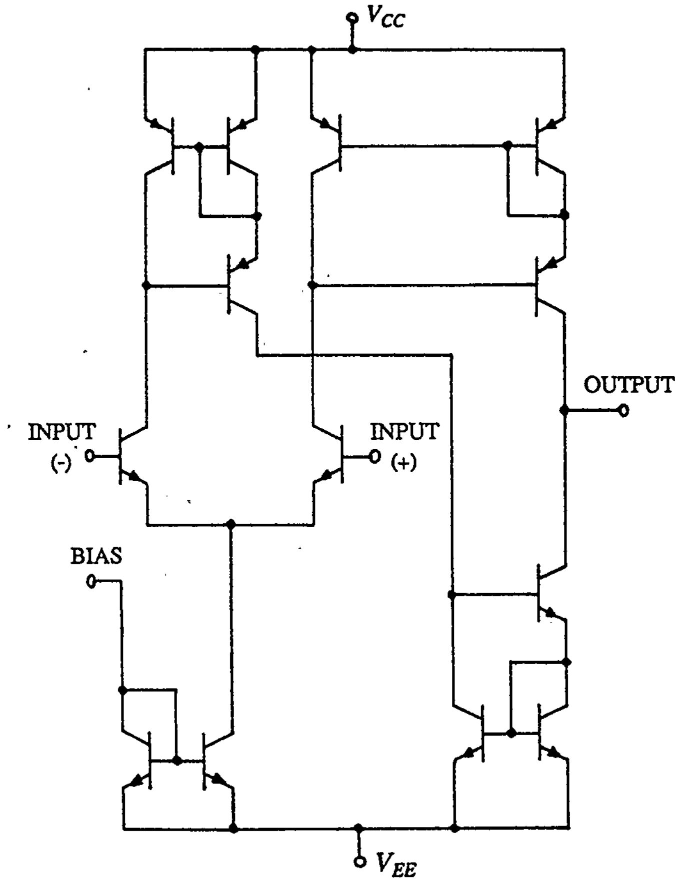

(a)

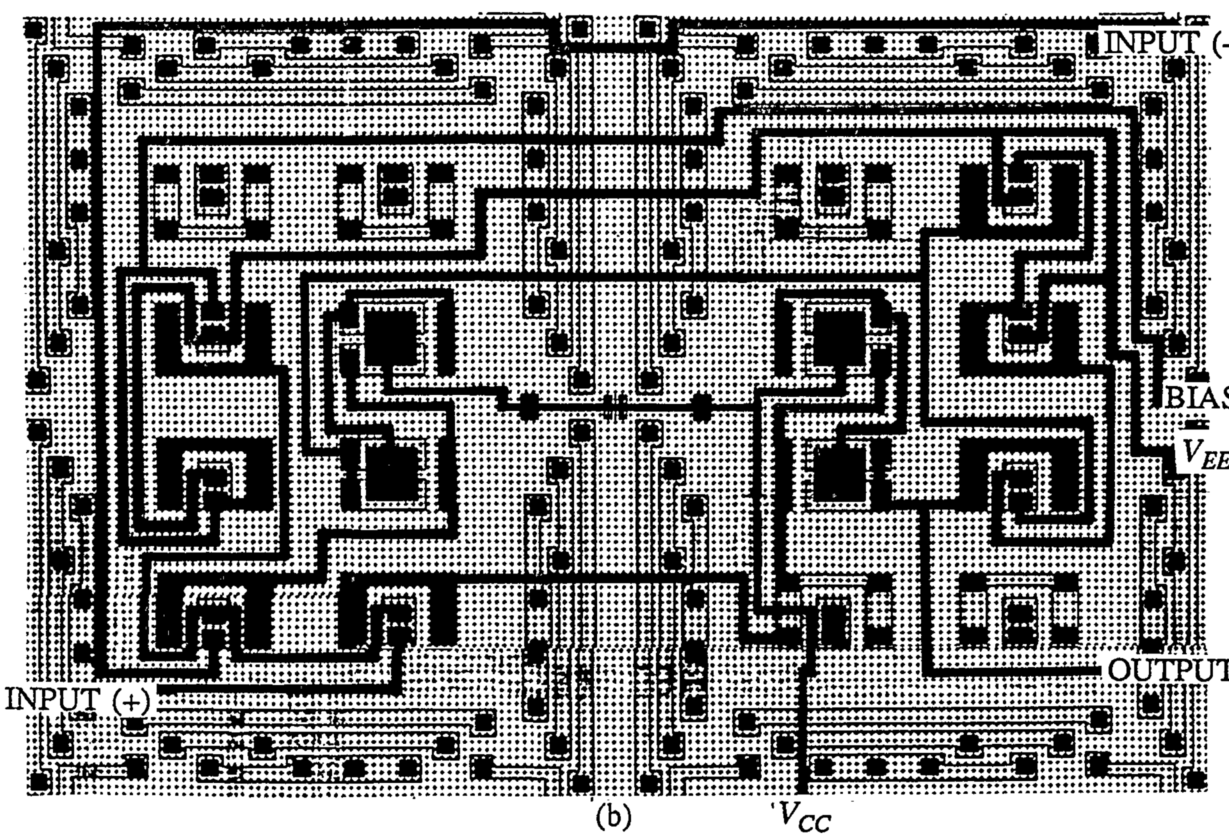

(b)

Figure 2.12 Wilson Mirror OTA Design and Implementation

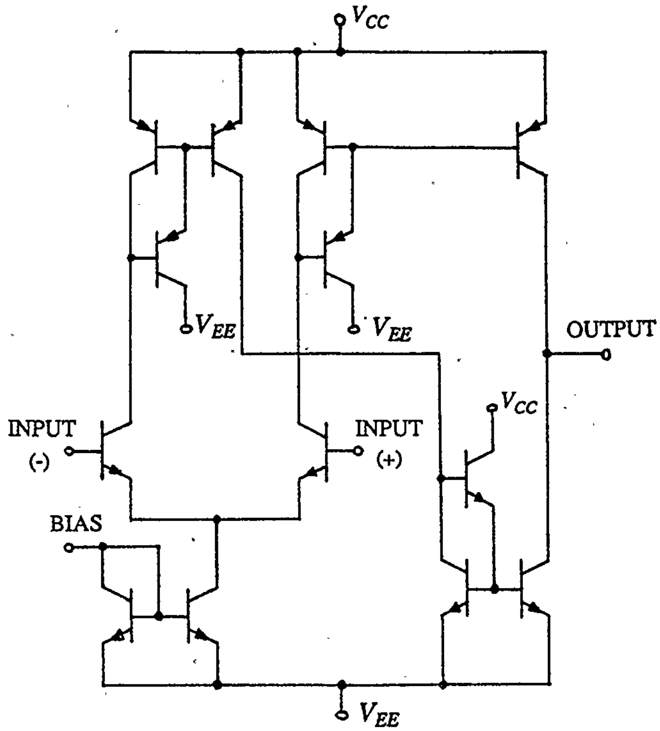

(a)

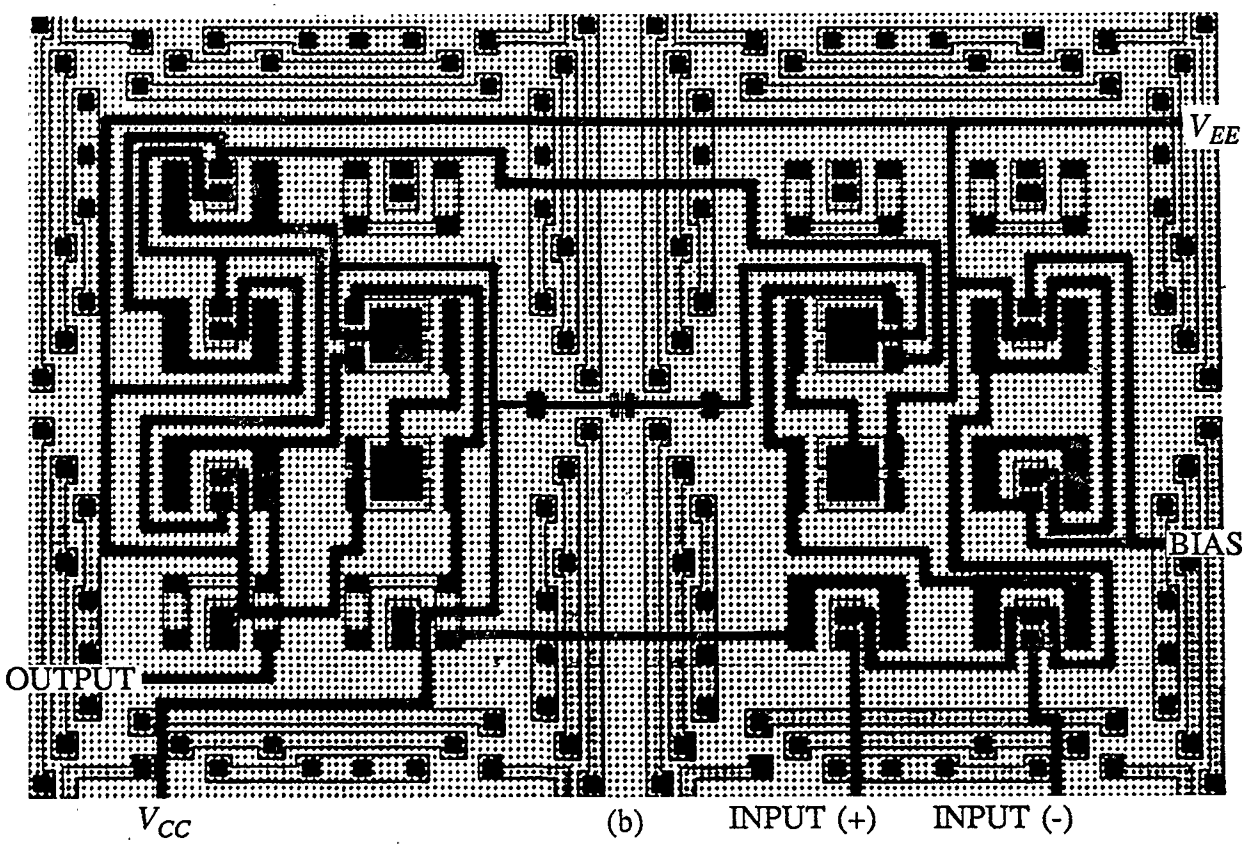

(b)

Figure 2.13 3 Transistor Mirror OTA Design and Implementation have a much better output resistance and a somewhat better transfer ratio as well.

As there are many cases in which a single cell design would be preferable a modified configuration of the OTA was proposed (Figure 2.14). This configuration has the same nominal g_m as the normal Wilson mirror OTA while only requiring a single cell. The output resistance of such a configuration will be somewhat less than that of the Wilson mirror OTA, but will be better than that of the simple 2 transistor configuration. Again, for comparison, a similar circuit using the simple 3 transistor mirrors was designed (Figure 2.15).

Since the normal Wilson configuration does not use all the transistors in both of the cells it occupies, an OTA with a differential pair having better input characteristics, that of the Darlington pair, was also designed (See Figure 2.16). Such a differential pair will have much higher input resistance, but, as will be seen (Chapter 3), produces an overall g_m approximately half that of the normal Wilson configuration. Finally, to act as a comparison, a 3 transistor mirror equivalent was included (Figure 2.17).

It should be noted that throughout this thesis the figures will refer to the Wilson mirror OTA as 3T1, the 3 transistor mirror OTA as 3T2, the 2 transistor mirror OTA as 2T, the modified Wilson mirror OTA as M1, the modified 3 transistor mirror OTA as M2, the Darlington pair Wilson mirror OTA as DP1 and the Darlington pair 3 transistor mirror OTA as DP2. This is done for convenience, as the long form is somewhat unwieldy. These abbreviations are also included in the list of symbols for reference.

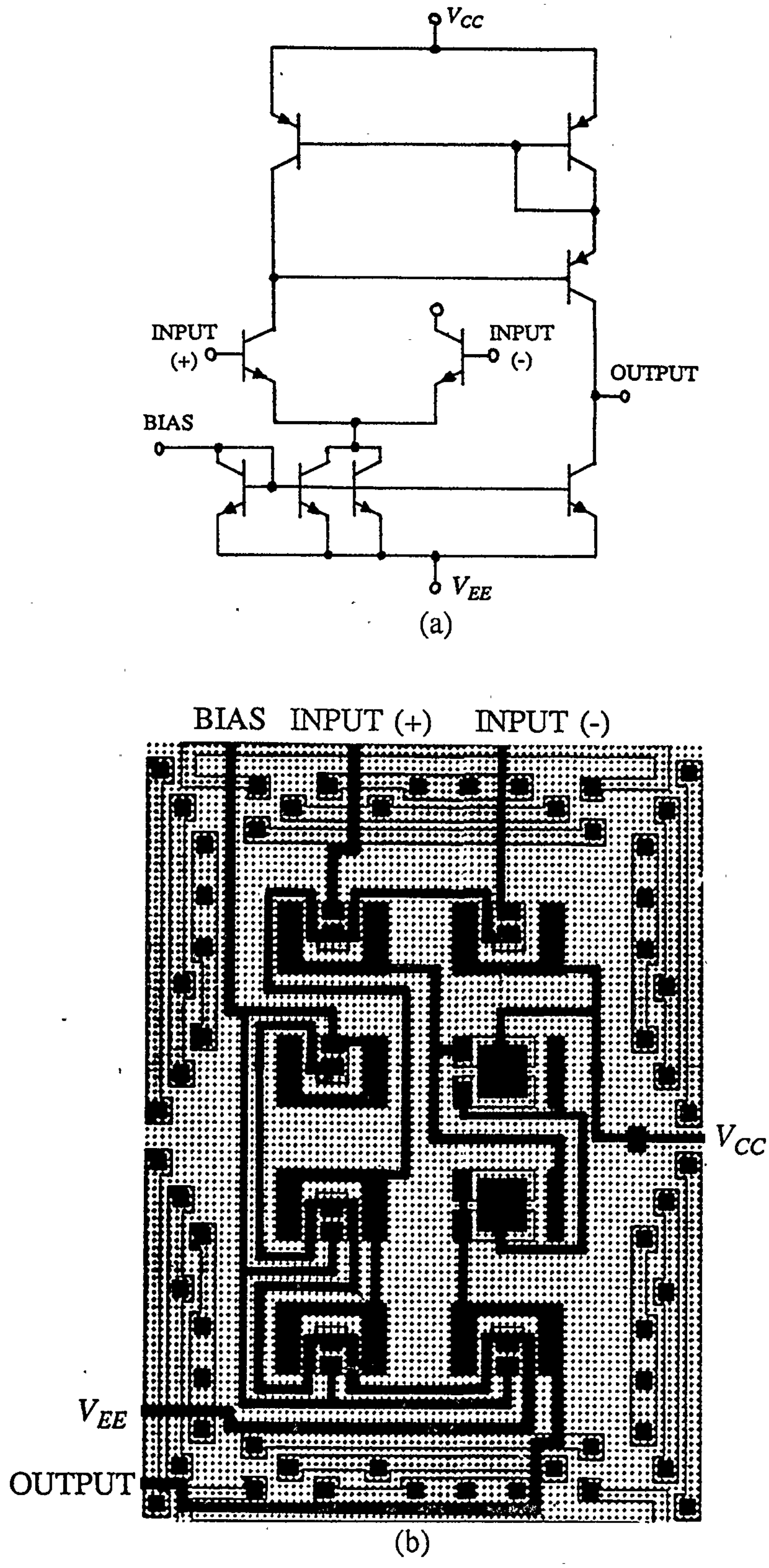

Figure 2.14 Modified Wilson Mirror OTA Design and Implementation

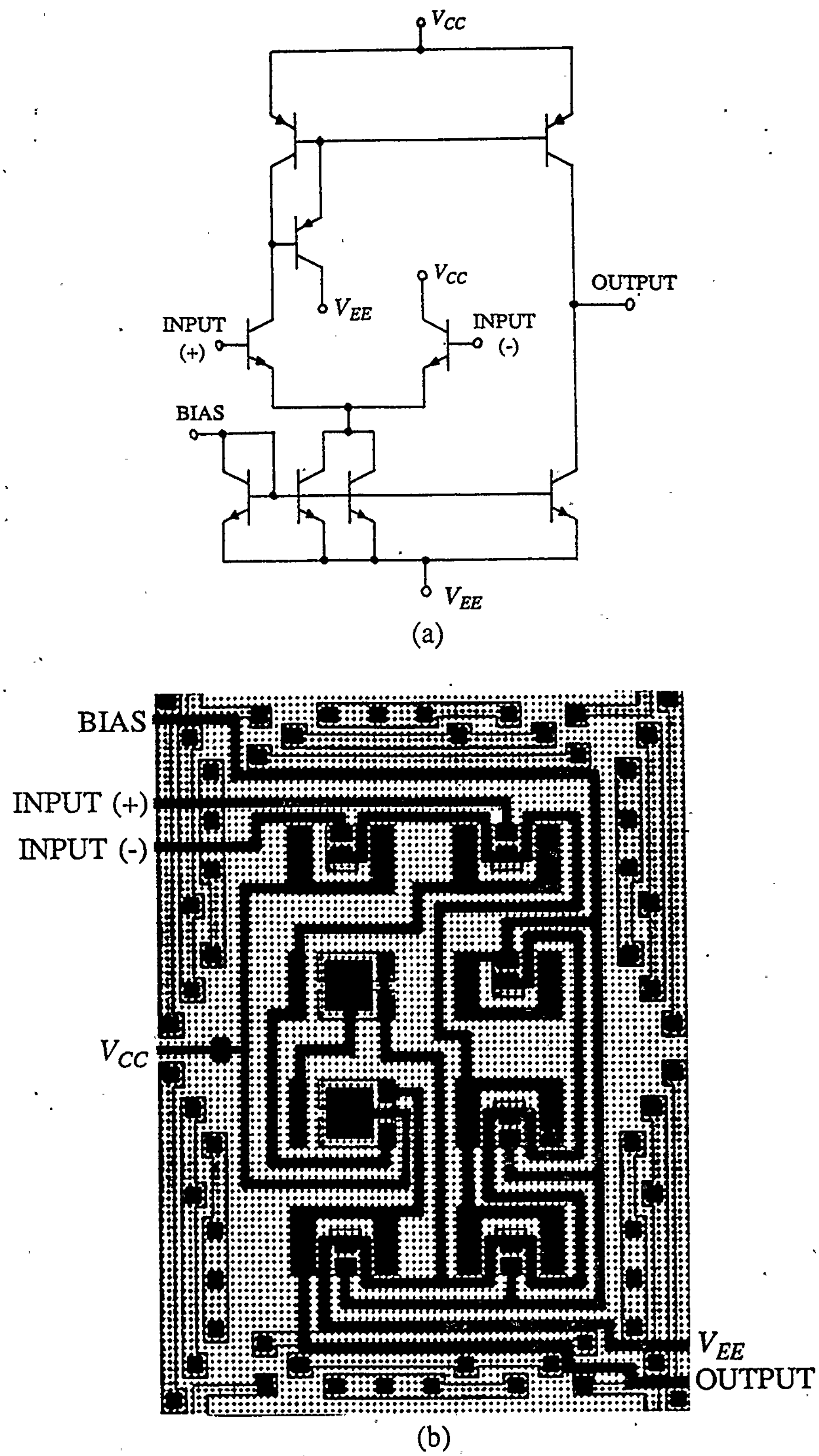

Figure 2.15 Modified 3 Transistor Mirror OTA Design and Implementation

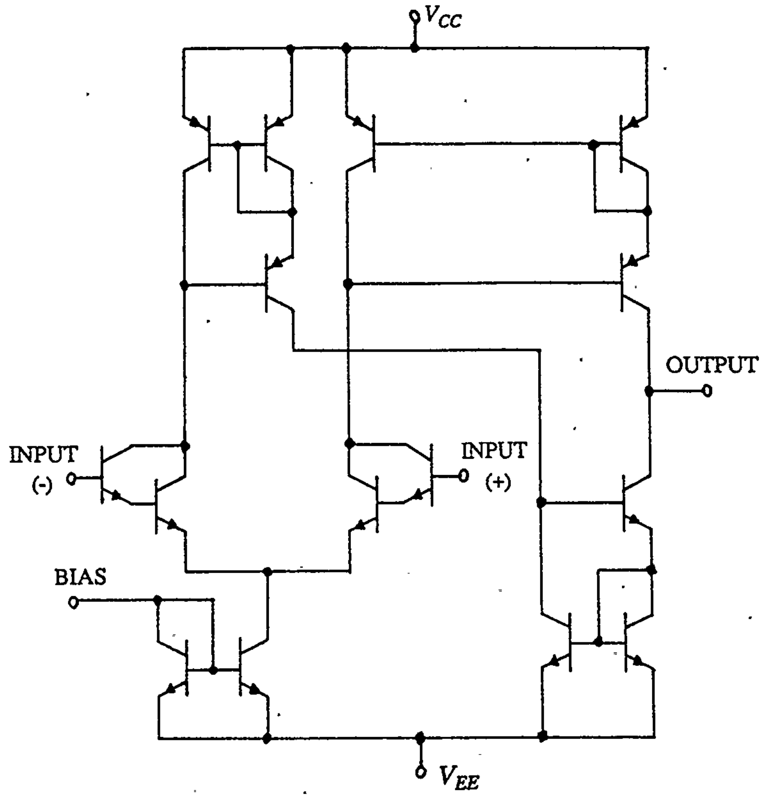

(a)

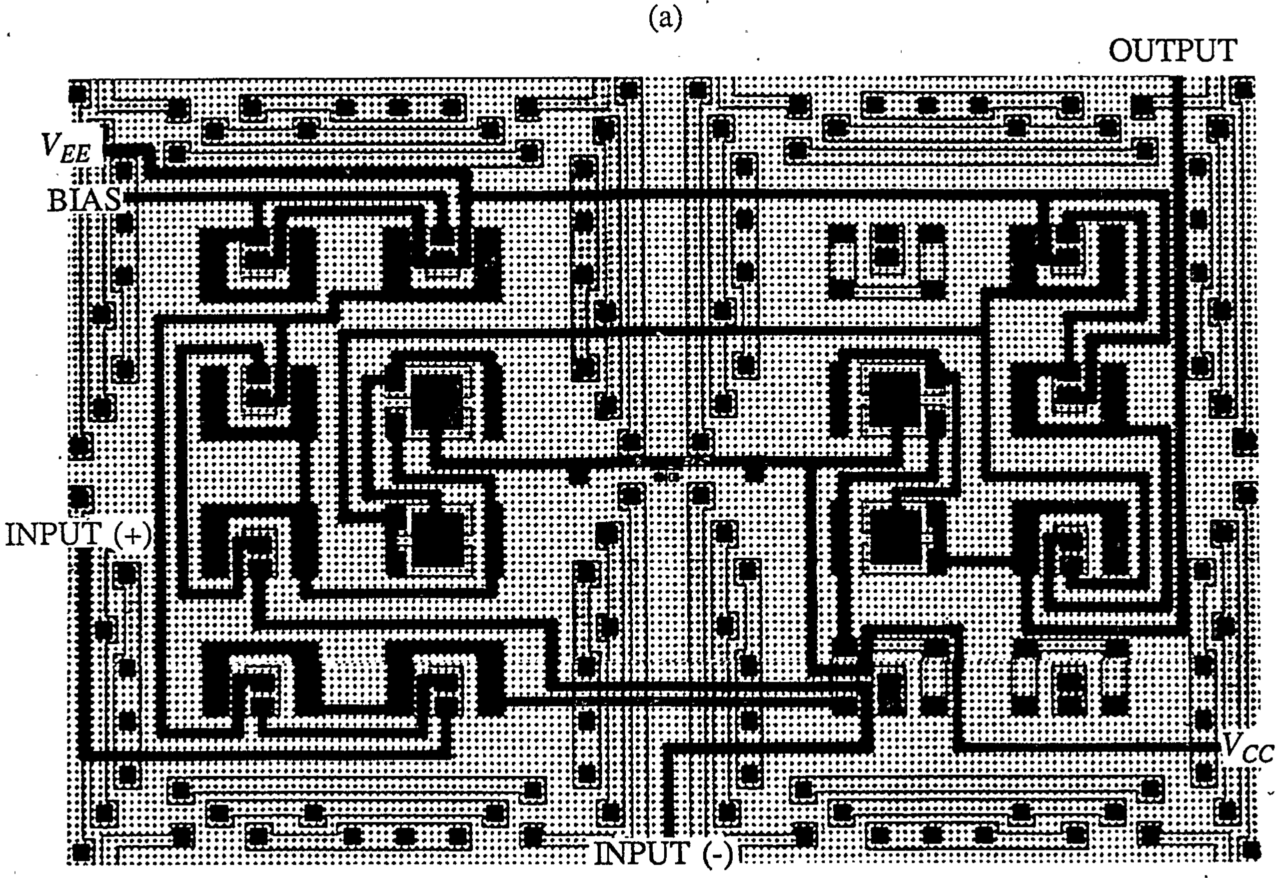

(b)

Figure 2.16 Darlington Pair Wilson Mirror OTA Design and Implementation

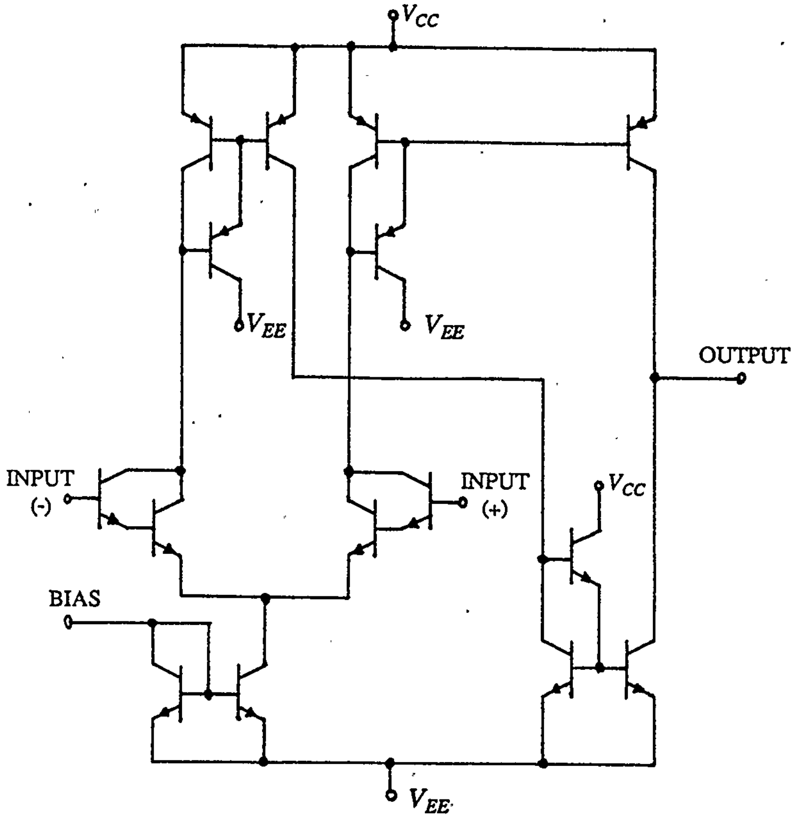

(a)

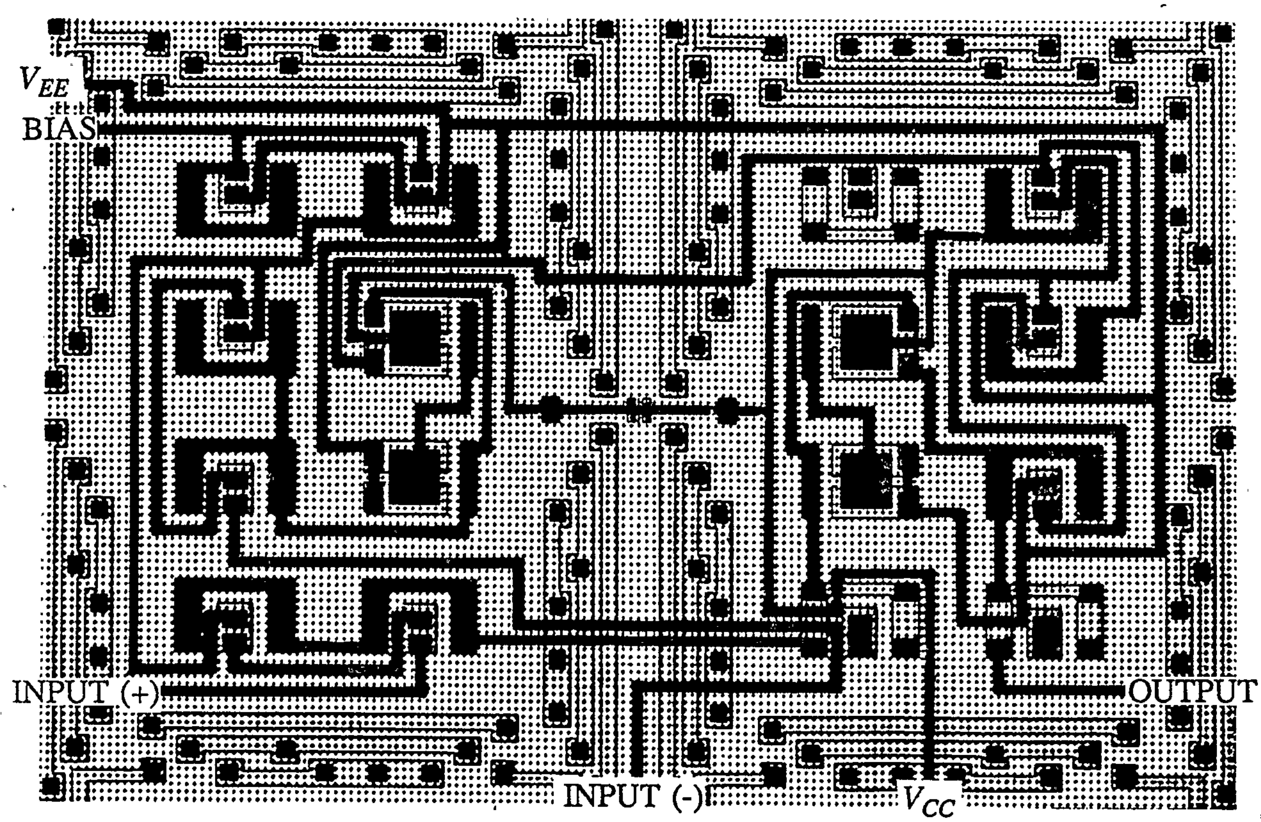

(b)

Figure 2.17 Darlington Pair 3 Transistor Mirror OTA Design and Implementation

In order to confirm the feasibility of the designs chosen, all were first implemented using the kit parts provided by LTI for prototyping. Kit parts are chips with a selection of components from the actual technology used, such as transistors, resistors, etc., brought out to external pins. This enables the designer to test whether the design chosen is practicable prior to the expense of actual chip manufacture. Through basic tests all the designs were determined to be functional, and it was decided to go ahead with their integration.

The complete implementation of all the above OTA's used a single LA 251 substrate from LTI [7]. This semi-custom substrate contains twelve cells, 40 bonding pads for signal connection to external pins, and a few extra components external to the cells. The external components were not considered in the design as each of the semi-custom chip substrates available from LTI has a different external component layout, while maintaining the same internal cell layout [7]. Using components external to the cells nullifies the benefits of modular cell design.

The completed design of the seven different OTA structures is shown in Figure 2.18. This chip was integrated courtesy of LTI. Due to the expense involved in producing 40 pin packages, which would be required if all OTA types were brought out at the same time, a different method was employed. The final product from LTI was returned in two different package types, one with four of the OTA's brought out to the pins and the other with the remaining three OTA's (Figure 2.19). The internal chip remains the same for both package types, but different OTA's were connected to the external pins.

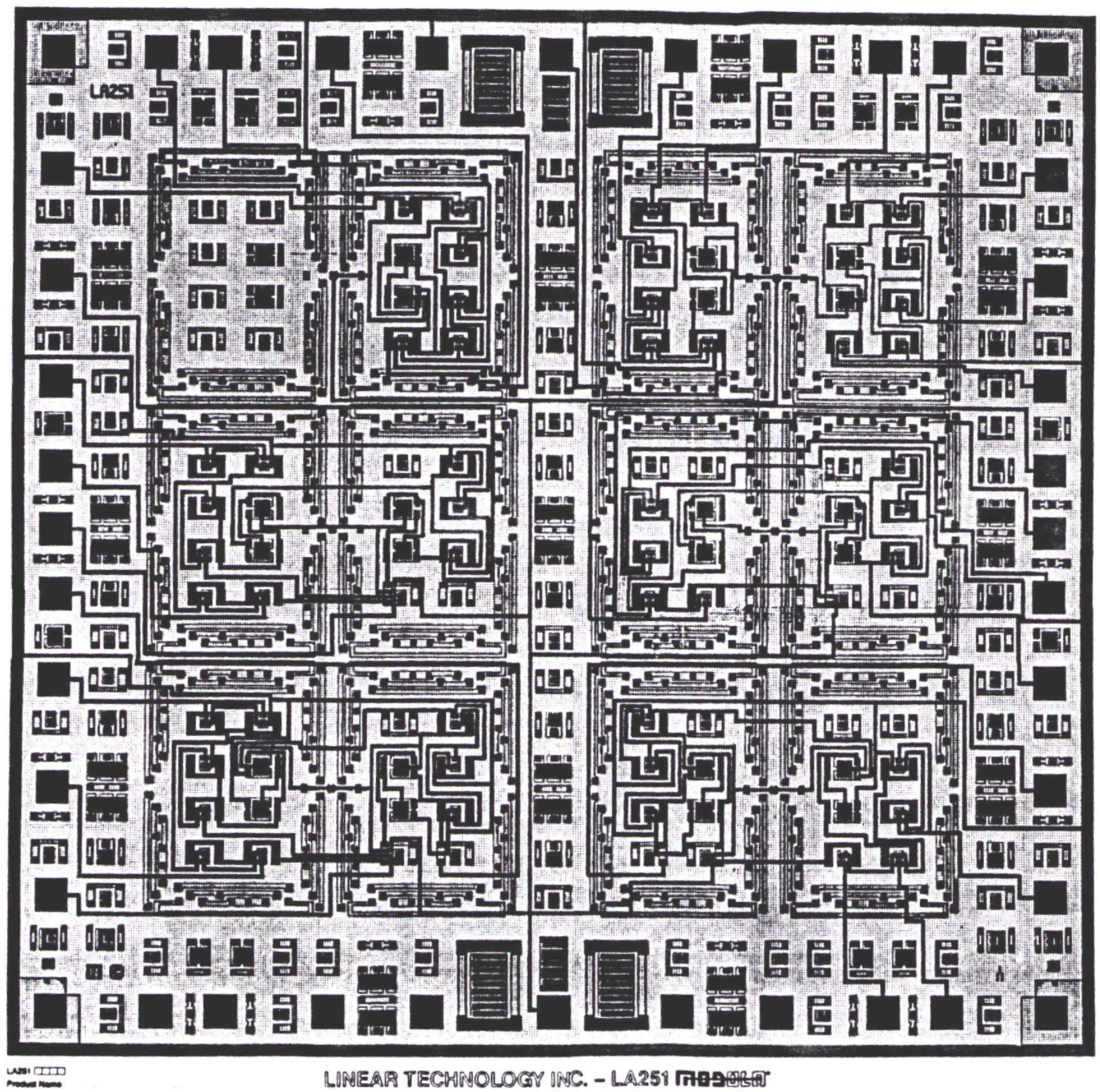

Figure 2.18 LA 251 Implementation of OTA Designs

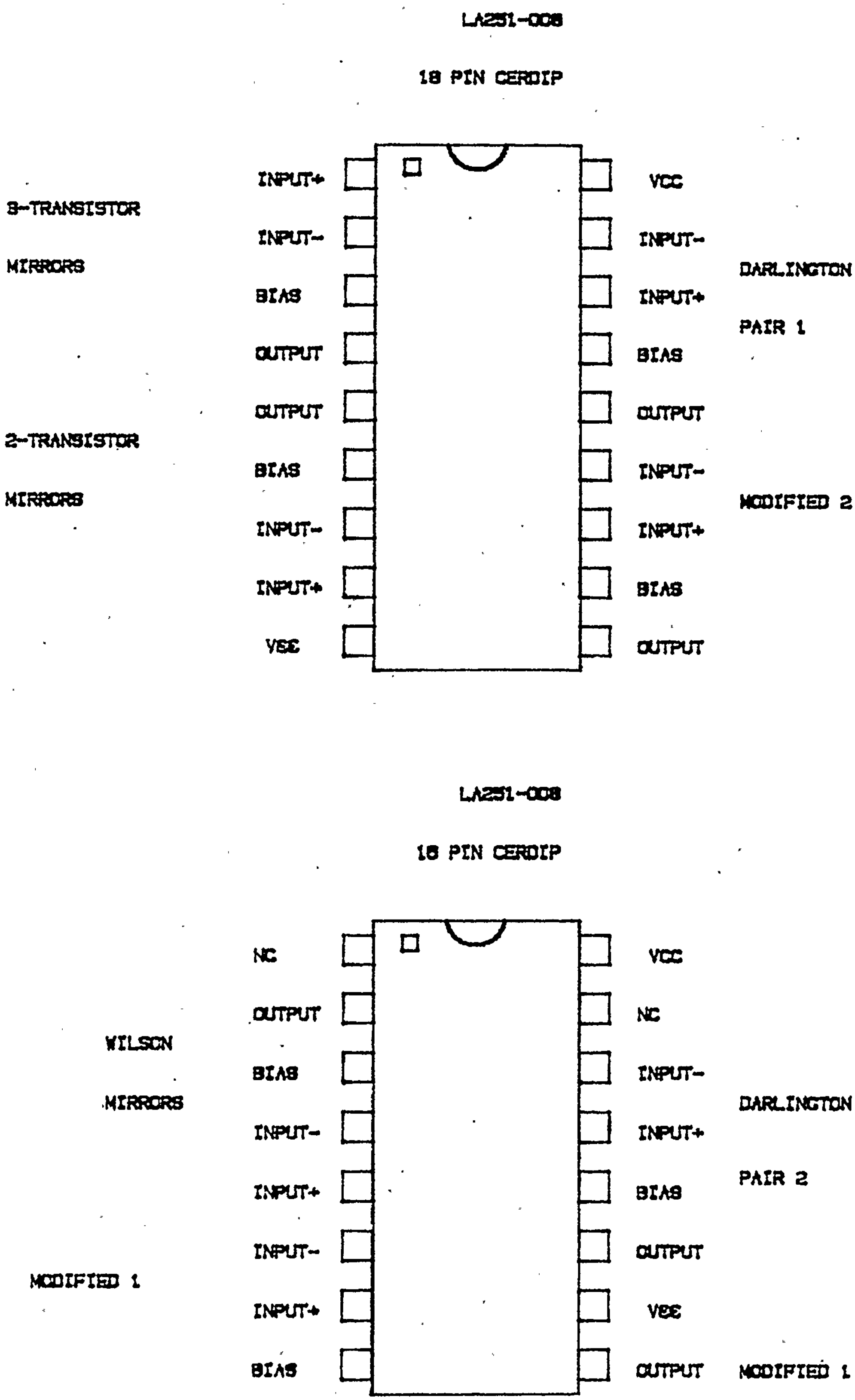

Figure 2.19 OTA Pin Diagrams

CHAPTER 3

OPERATIONAL TRANSCONDUCTANCE AMPLIFIER CHARACTERIZATION

In order to develop the lumped model of the OTA discussed in Chapter 2, it is first necessary to measure the relevant resistances and capacitances, as well as the transconductance gain. As the bias current determines the operating point of the OTA, it is appropriate to measure all of the relevant characteristics relative to this current. For this reason, all the measurement schemes discussed in this chapter vary the bias current to obtain the range of parameter measurements.

3.1 Measurement of Transconductance Gain

Due to the nature of the OTA, it is necessary to measure a small signal current. The output resistance of the OTA, and the very low signal levels it operates at, make the measurement of such a current very difficult. Thus, it is necessary to have a measurement circuit which can eliminate the effects of the output resistance while converting the output current into a form which can be more easily measured. Such a circuit is that shown in Figure 3.1.

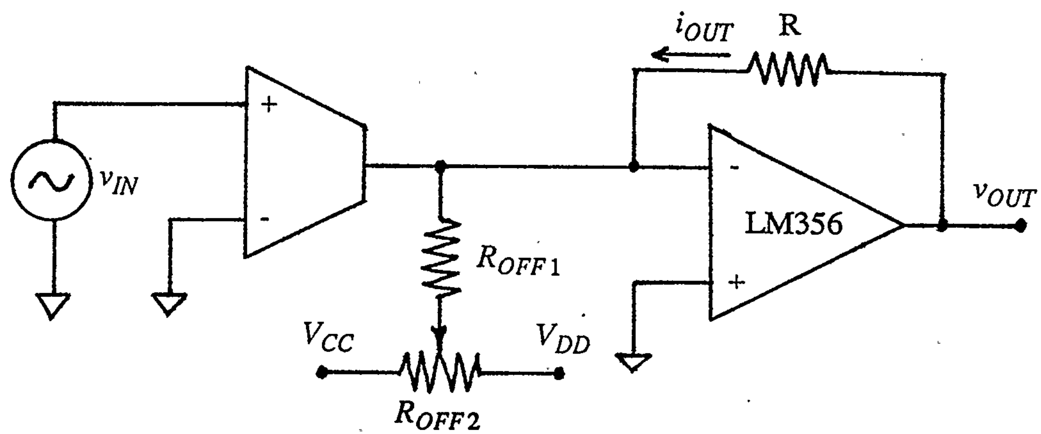

Figure 3.1 OTA Transconductance Gain Measuring Circuit

The OTA input signal, v_{IN}, is kept at approximately 6 mV_{pp} so as to stay well within the limited dynamic range of the OTA (≈ 20 mV_{pp}. With the other input is grounded, v_{IN} becomes the differential voltage. The frequency of the signal is kept low (≈ 50 Hz) so that the parasitic capacitances do not affect the measurements.

The output of the OTA is fed into the input of the inverting op-amp configuration. The OTA output is held at DC ground by the op-amp, so that the output resistance will not affect the magnitude of the small signal output. Any DC offset which may appear at the output of the OTA, whether due to the OTA or the op-amp, is zeroed out through the use of the two resistors labeled R_{OFF1} and R_{OFF2}. The small signal output current of the OTA is converted into the small signal output voltage, v_{OUT}, by passage through the resistor R.

The small signal output current of the OTA will vary by around three decades over the range of bias currents used. For this reason the resistor R must be reduced as the output current is increased in order to maintain a reasonable voltage at the circuit output. The results of a measurement run using a Wilson mirror OTA is shown in Table 3.1. The value of g_m is determined from the equation

$$g_m = \frac{v_{OUT}}{v_{IN}} \frac{1}{R} \tag{3.1}$$

for each value of bias current.

To act as a comparison, theoretical values for g_m can also be generated. If the input transistors of Figure 2.2 are replaced with the small signal model of

I_{BIAS} (μA)	R ($k\Omega$)	v_{OUT} / v_{IN} (dB)	g_m (μmho)
6.5	100	-17.8	128
10	80	-16.0	196
20	40	-15.9	397
40	20	-15.8	803
80	10	-15.7	1627
100	10	-13.7	2048
200	8	-9.4	4199
400	4	-8.8	9000
800	2	-7.7	20429
1000	2	-5.4	26623
2000	1	-5.6	52033

Table 3.1 Gain Measurement Example Using Wilson Mirror OTA

Figure 2.4, the equivalent small signal model of the OTA is formed (Figure 3.2). The resistance r_o is ignored since all collectors feed low impedance points in the circuit. It is also assumed that the input transistors are matched. A_{p1} and A_{p2} are the current transfer ratios of the PNP mirrors, and A_{n1} is the current transfer ratio of the NPN mirror.

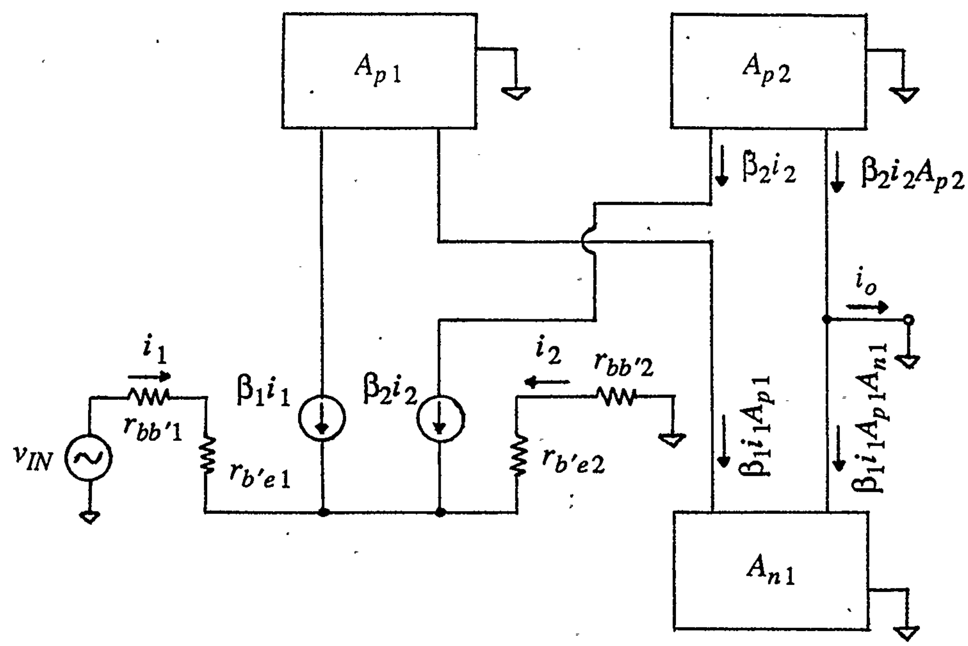

Figure 3.2 Simplified Small Signal OTA Model

It is easy to show that $i_2 = -i_1$, so

$$i_o = -\beta_n i_1 (A_{p2} + A_{p1} A_{n1}) \tag{3.2}$$

where β_n is the common emitter gain of the NPN transistors. It is also easy to show that

$$i_1 = \frac{v_{IN}}{2(r_{bb'} + r_{b'e})} \tag{3.3}$$

and therefore

$$g_m = \frac{i_o}{v_{IN}} = \frac{-\beta_n}{2(r_{bb'} + r_{b'e})}(A_{p2} + A_{p1}A_{n1}). \tag{3.4}$$

If the current transfer ratios of the mirrors are assumed to be close to unity and β_n is large, then equations 2.1 and 2.2 allow the simplification of equation 3.4 to

$$g_m \approx \frac{qI_E}{nkT} = \frac{1}{r_d}. \tag{3.5}$$

For OTA's with a normal configuration (Figures 2.11 - 2.13) I_E is effectively half the bias current. For OTA's with the modified configuration (Figures 2.14 - 2.15) the effective I_E is actually equal to the bias current. However, the output mirrors of the modified OTA's effectively halve the output current, resulting in an actual output current of the same nominal value as that of the normal configuration.

Equation 3.5 will be quite accurate for the Wilson mirror and modified Wilson mirror OTA's. The 2 transistor, 3 transistor and modified 3 transistor OTA's will not be quite as well represented by equation 3.5, because the transfer ratios of the mirrors used in these OTA's are not as good as the transfer ratio of the Wilson mirror. Equations for g_m could also be generated for those OTA's using other than Wilson mirrors, but it is a much more difficult task. As the Wilson mirror is the best mirror ideally, it is expected that OTA's using it will be the primary ones chosen for filter implementation; thus the basic equations were considered sufficient.

For the Darlington pair OTA's, the generation of the theoretical value for g_m is somewhat different. Figure 3.3 shows the small signal equivalent of a

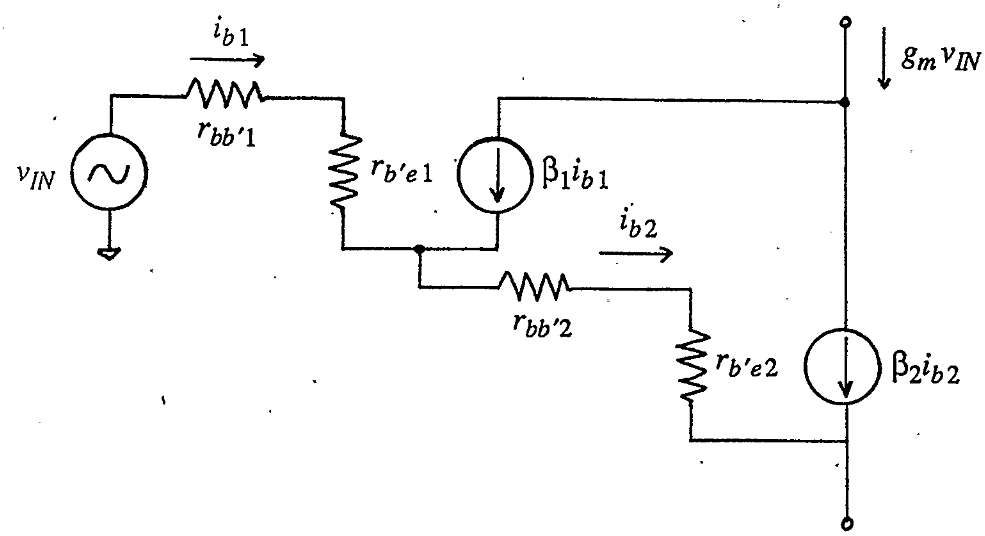

Figure 3.3 Simplified Small Signal Darlington Pair Model

Darlington pair. Again, r_o is ignored. If the transfer ratios of the mirrors are assumed to be unity again, it is easy to show that

$$g_m = \frac{[\beta_1 + \beta_2(\beta_1 + 1)]}{r_1 + (\beta_1 + 1)r_2} \tag{3.6}$$

where r is just $(r_{bb'} + r_{b'e})$, and

$$I_{E1} = \frac{I_{E2}}{\beta_2 + 1}. \tag{3.7}$$

If $r_{bb'}$ is ignored, then the substition of equations 2.1 and 2.2 into 3.6 result in

$$g_m = \frac{[\beta_1 + \beta_2(\beta_1 + 1)]}{(\beta_1 + 1)(\beta_2 + 1)} \frac{qI_{E2}}{2nkT}. \tag{3.8}$$

If $\beta_2 >> 1$ (note that $\beta_1 >> 1$ is not required), then

$$g_m \approx \frac{qI_{E2}}{2nkT} = \frac{1}{2r_d}. \tag{3.9}$$

As for the normal configuration, I_{E2} is half the bias current. It is interesting that the final g_m is half that of the normal configuration, a result which will be verified by the transconductance measurements.

In order to get a more accurate value for the measured g_m, the transconductance for six different OTA's of the same type were found at each bias current. These six values were averaged together to give the value of g_m used for that OTA at each bias current. Figure 3.4 shows the average g_m for all the seven OTA's, with error bars at each measurement point showing the maximum and minimum values, and the expected theoretical values. As was indicated, the g_m's for the Darlington pair configurations are approximately half of those for the equivalent configurations with a normal differential pair. Also, the theory for g_m is much closer for the OTA's using Wilson mirrors than for the other OTA's, as was expected. The OTA's do not operate well for bias currents over about 1 mA. As all of the filters designed later in this thesis use bias currents under 400 μA, this does not cause a problem.

In an attempt to determine the bandwidth of the OTA circuits, the frequency of the input to the circuit of Figure 3.1 was swept from 0Hz up to over 1MHz before distortion was noted. However, this does not perhaps truly indicate the bandwidth of the OTA. Attempts to determine whether it was the OTA or the op-amp which limited the range were not conclusive. It is sufficient, though, to say that the OTA will operate through at least the effective range found.

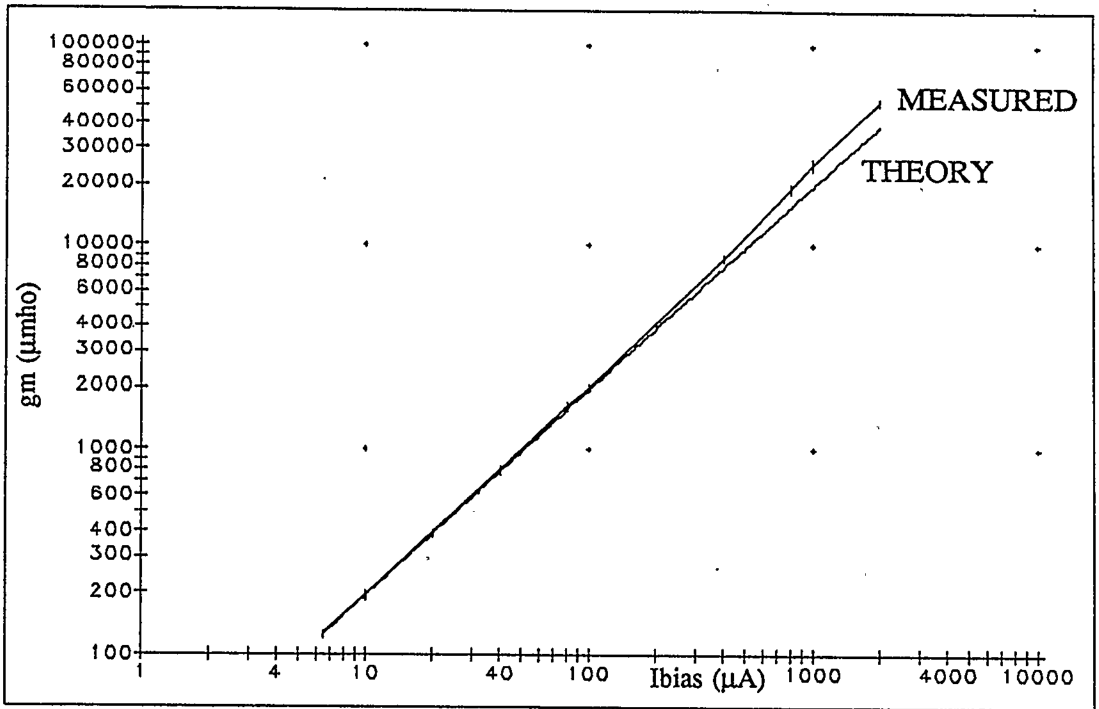

(a) 3T1

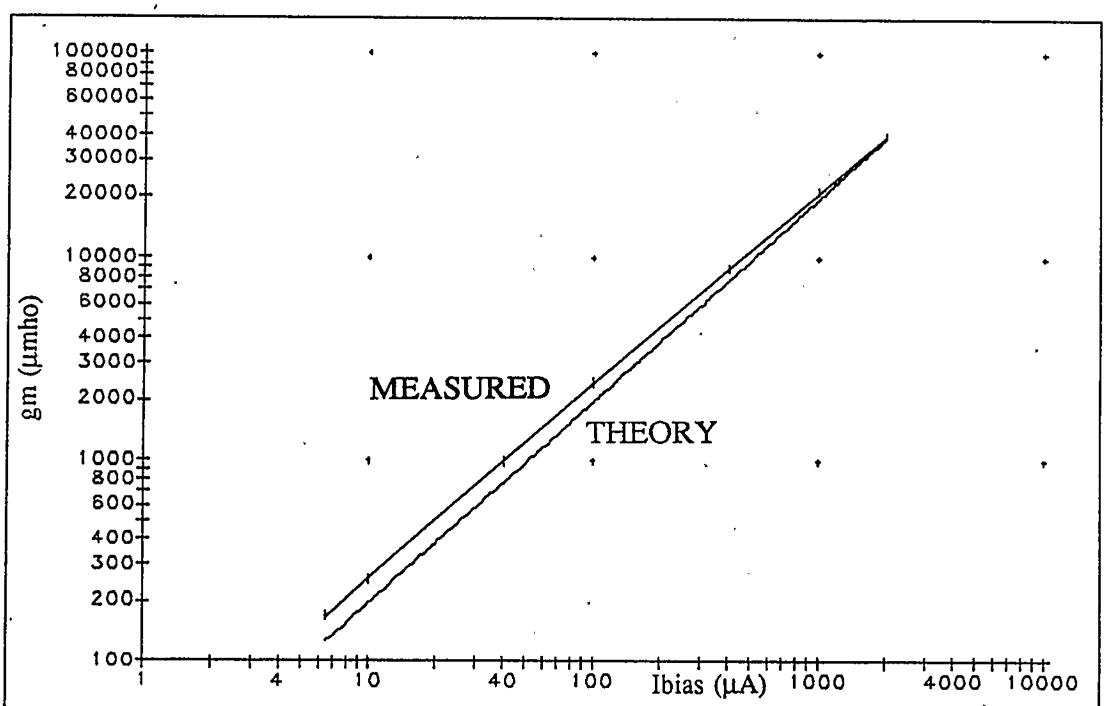

(b) 3T2

Figure 3.4 Average Transconductance vs Bias Current for All OTA Types

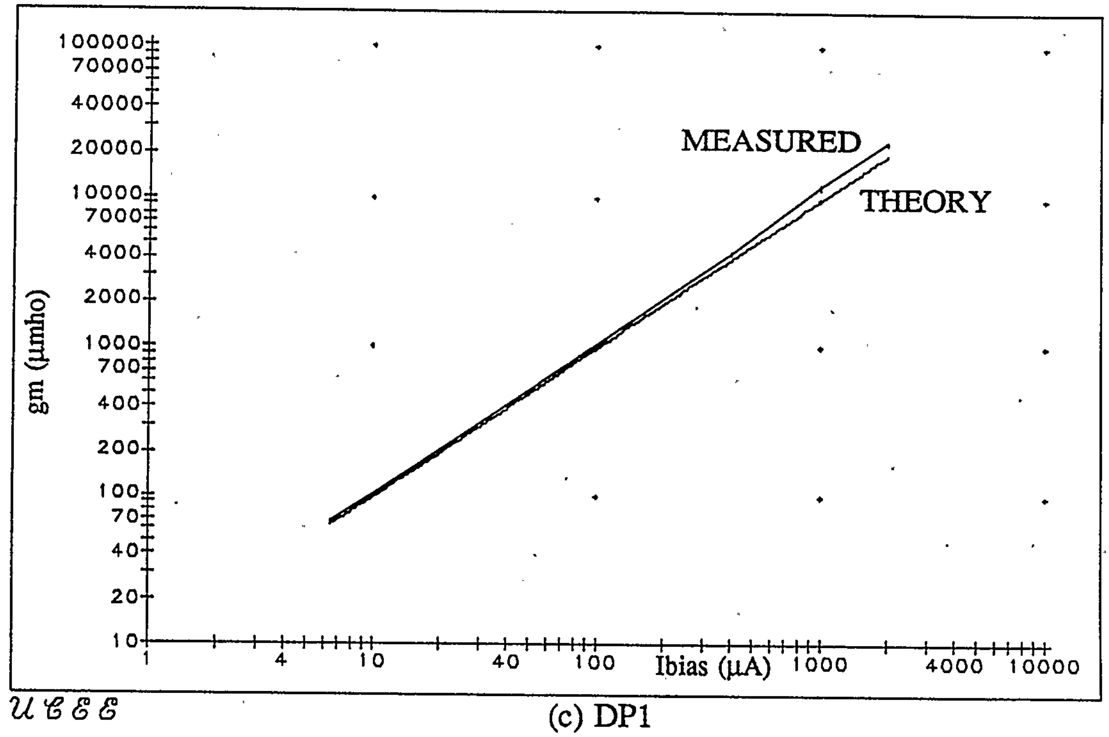

(c) DP1

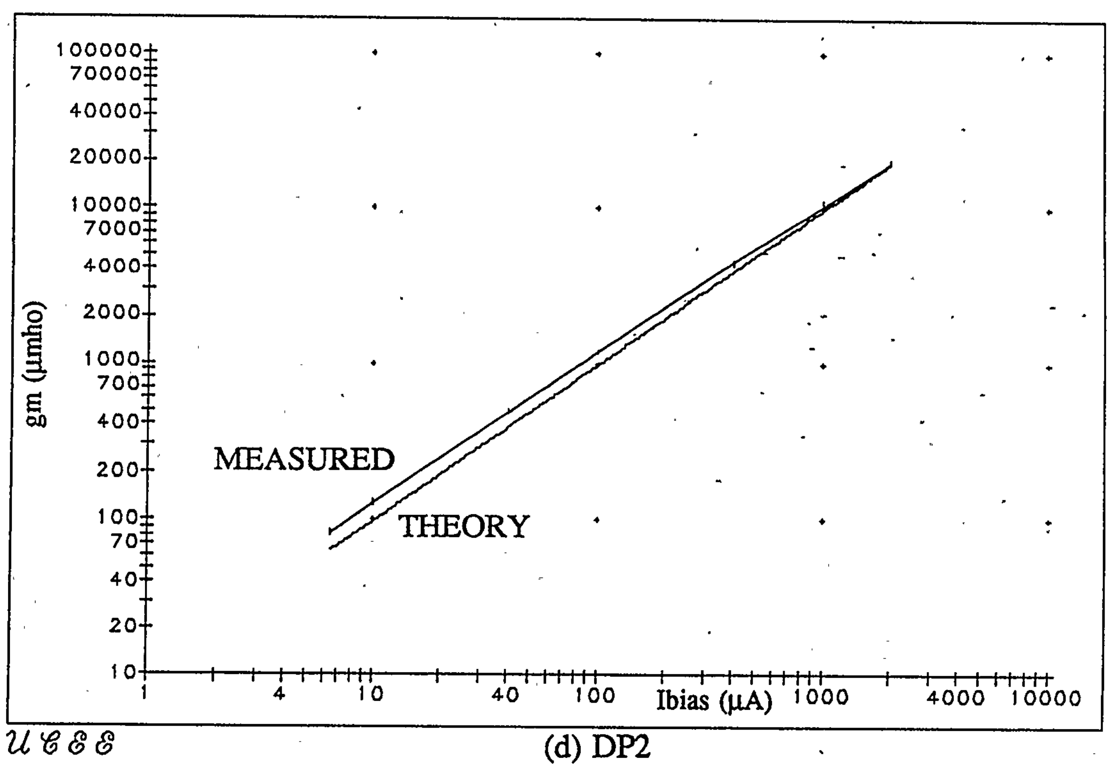

(d) DP2

Figure 3.4 Continued

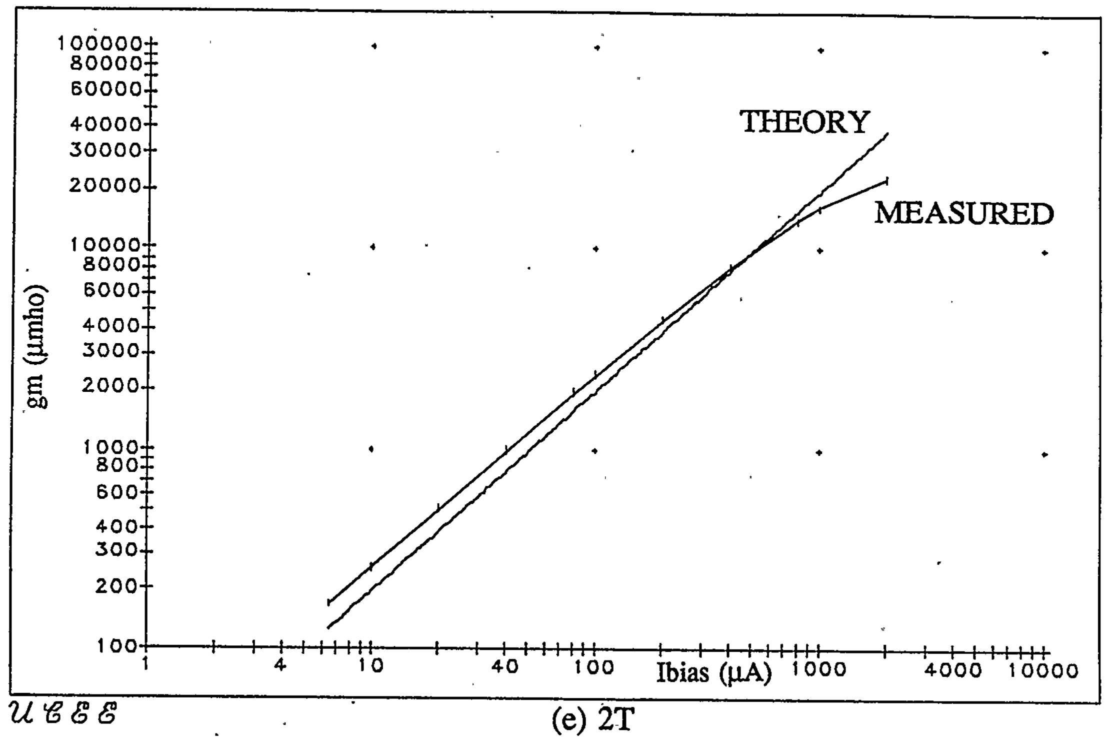

(e) 2T

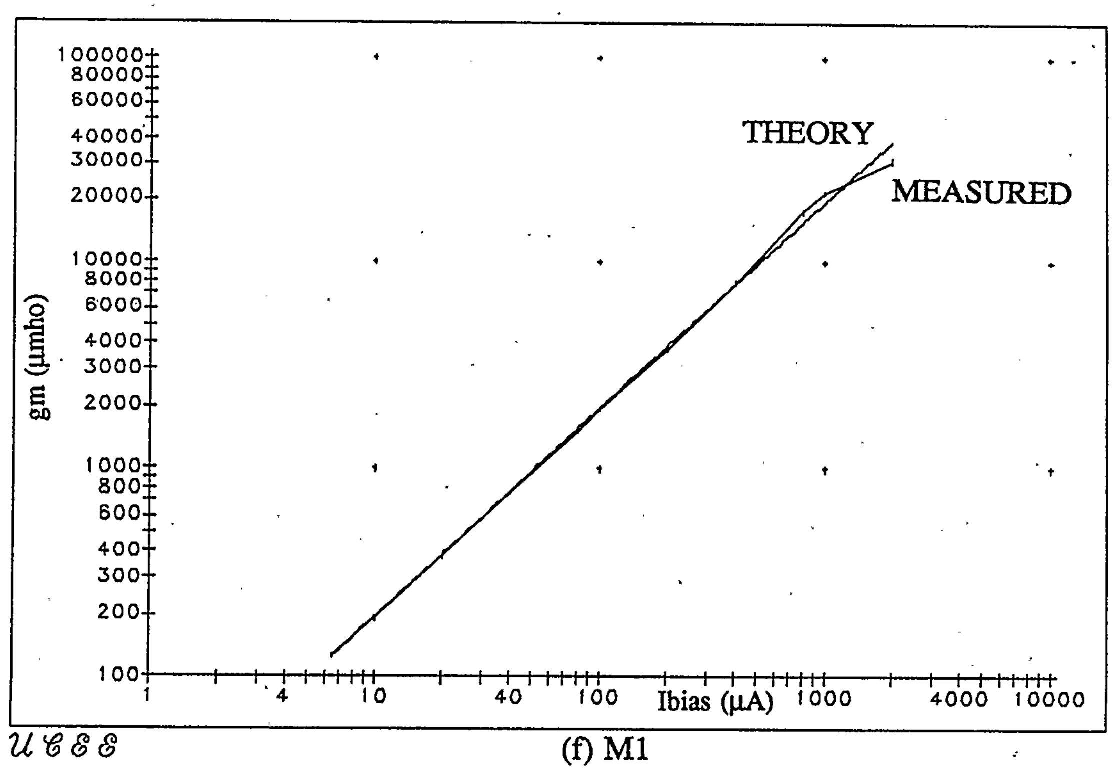

(f) M1

Figure 3.4 Continued

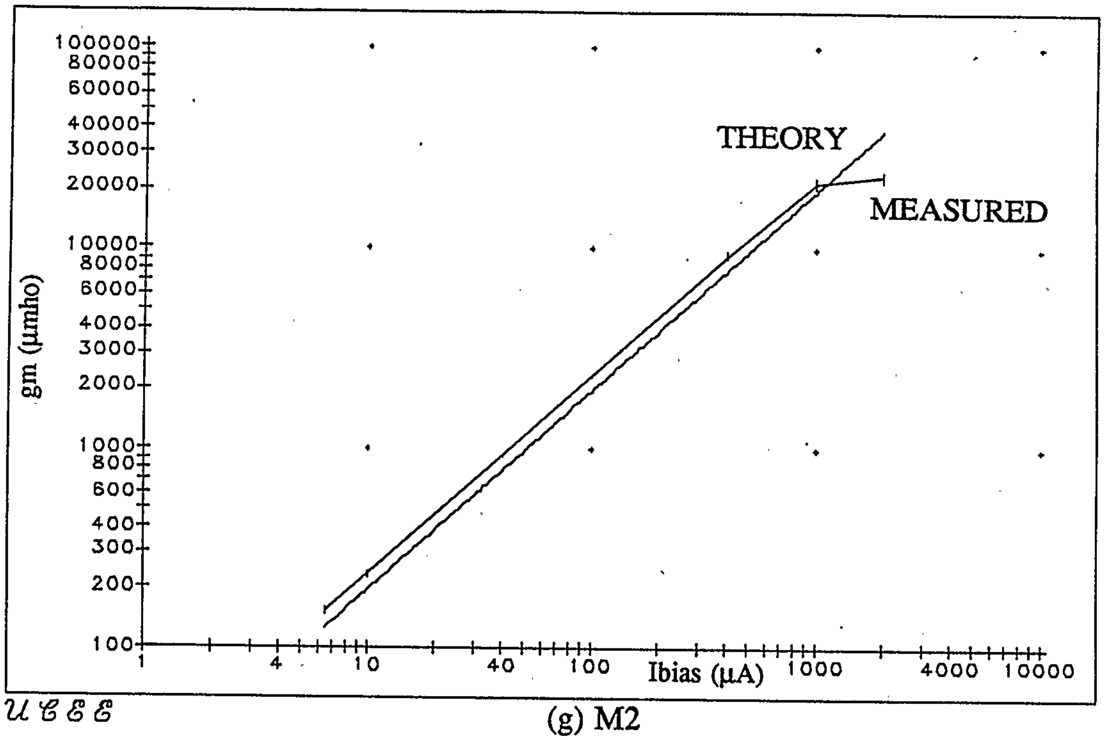

(g) M2

Figure 3.4 Continued

3.2 Measurement of Output Impedances

The measurement of output resistance must also be done at low frequency so that stray capacitances do not affect the measurements. A knowledge of the g_m at each bias current allows the determination of the output current at each point, since the output current is simply the differential input voltage multiplied by the transconductance gain.

It is a simple matter then to place a known resistance on the output of the OTA and measure the voltage drop across it. Unfortunately the output voltage cannot be simply probed as would be desired, because the measurement probe itself has a finite resistance. To overcome this problem an op-amp follower circuit is added to the output of the circuit to get the final configuration shown in Figure 3.5. The effective resistance of the op-amp used (LM 356) to ground is so large that it can be neglected.

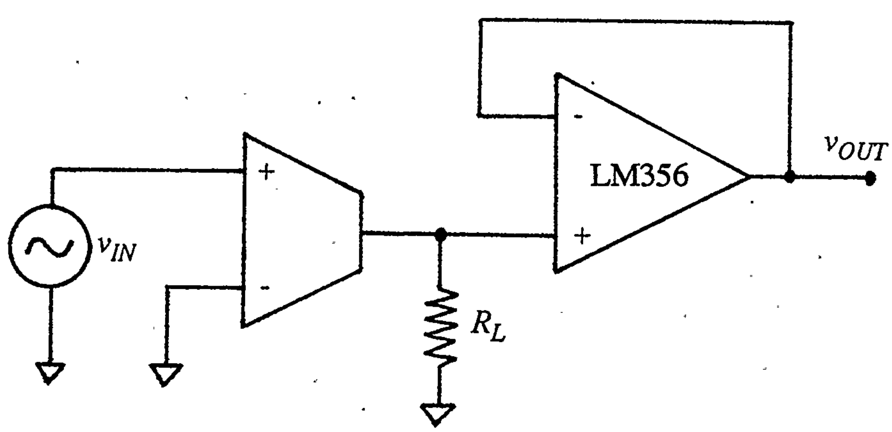

Figure 3.5 OTA Output Resistance Measuring Circuit

Using the same Wilson mirror OTA as for the transconductance gain measurement example, a measurement run is performed for the output resistance. The results are shown in Table 3.2. The output resistance can be calculated from the equation

$$R_o = \frac{1}{\frac{v_{IN}}{v_{OUT}} g_m - \frac{1}{R_L}}. \tag{3.10}$$

As with the g_m measurement, six different OTA results were averaged together to give the resistance value used. Figure 3.6 shows the average values for all of the OTA types with error bars representing the maximum and minimum values. As was expected, the OTA's using Wilson mirrors had the highest output

I_{BIAS} (μA)	R_L ($k\Omega$)	v_{OUT} / v_{IN} (dB)	R_o ($k\Omega$)
6.5	116930	41.7	506950
10	116930	44.7	350006
20	116930	48.8	170588
40	77880	50.2	83509
80	38240	50.1	40468
100	38240	50.95	31345
200	19390	50.6	13822
400	5910	47.85	5119
800	1996	44.7	1453
1000	996	42.1	920
2000	196	34.15	196

Table 3.2 Output Resistance Measurement Example Using Wilson Mirror OTA

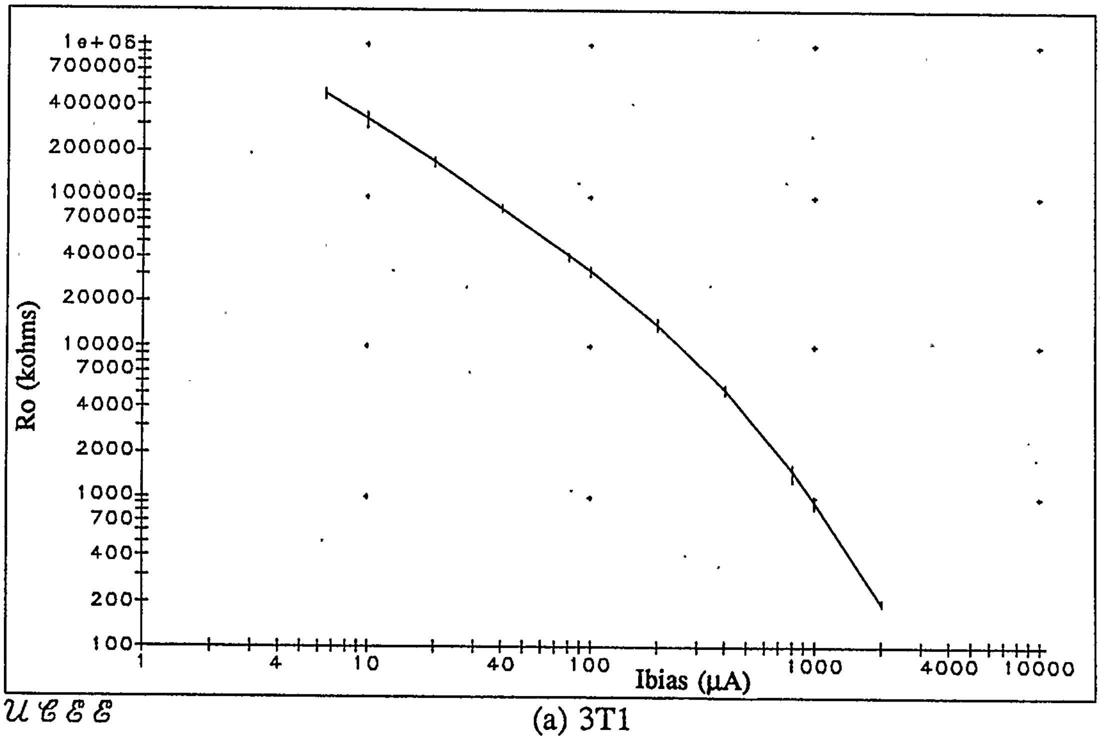

(a) 3T1

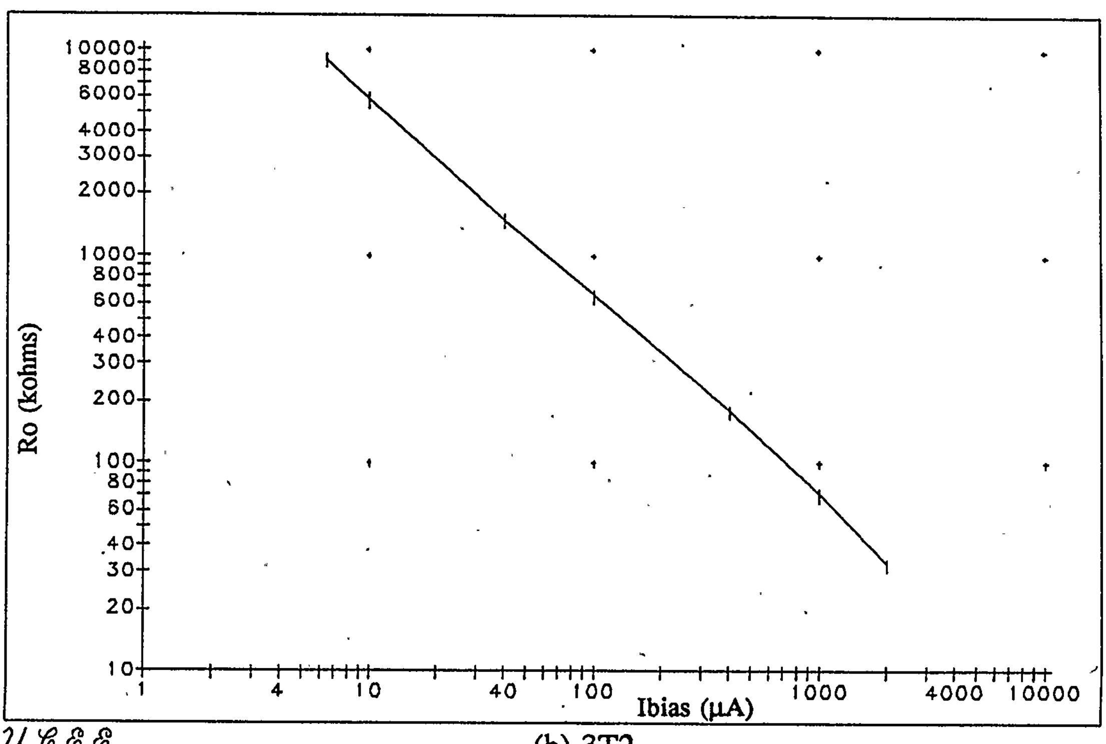

(b) 3T2

Figure 3.6 Average Output Resistance vs Bias Current for All OTA Types

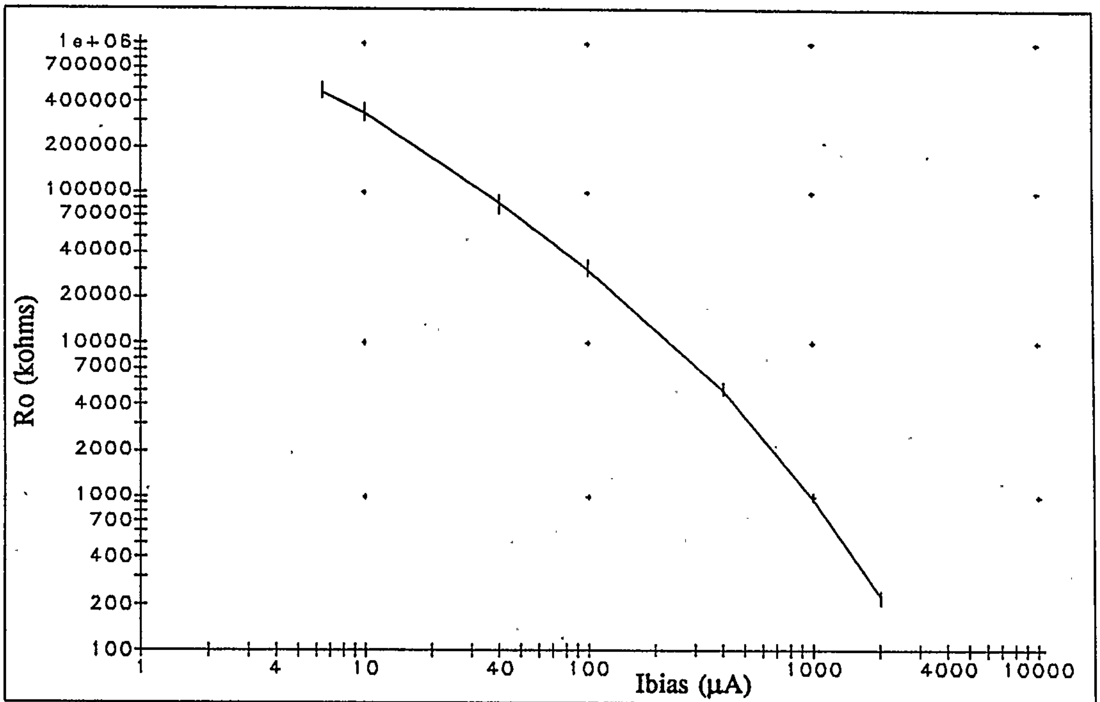

UCEE

(c) DP1

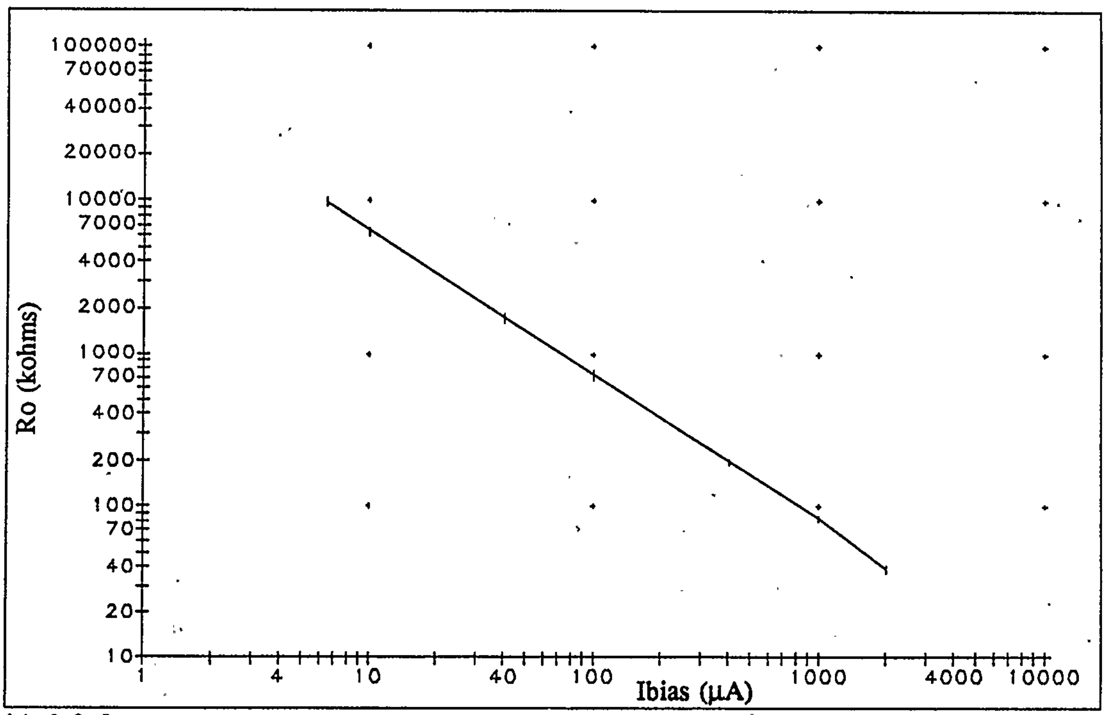

UCEE

(d) DP2

Figure 3.6 Continued

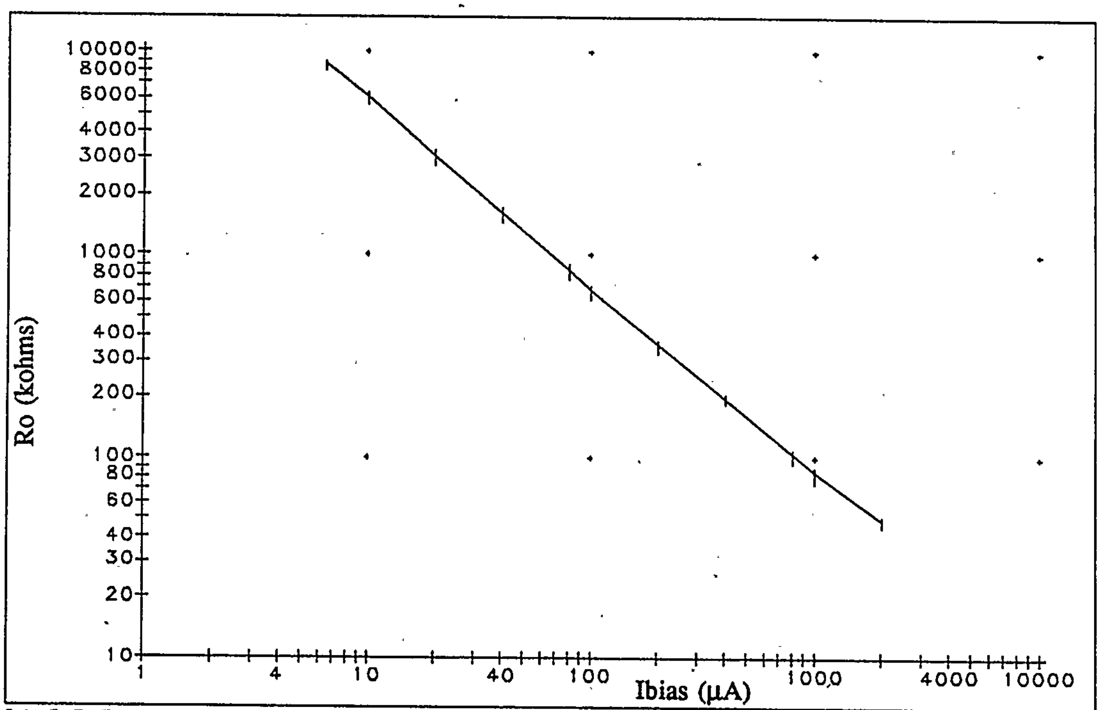

UCEE

(e) 2T

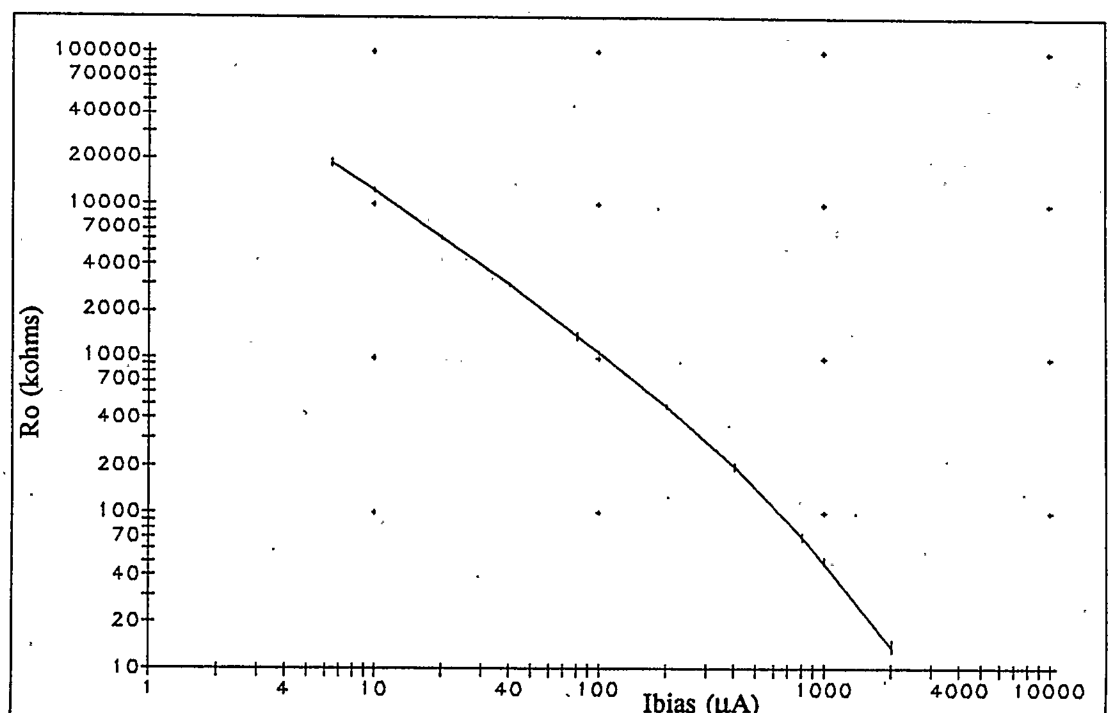

UCEE

(f) M1

Figure 3.6 Continued

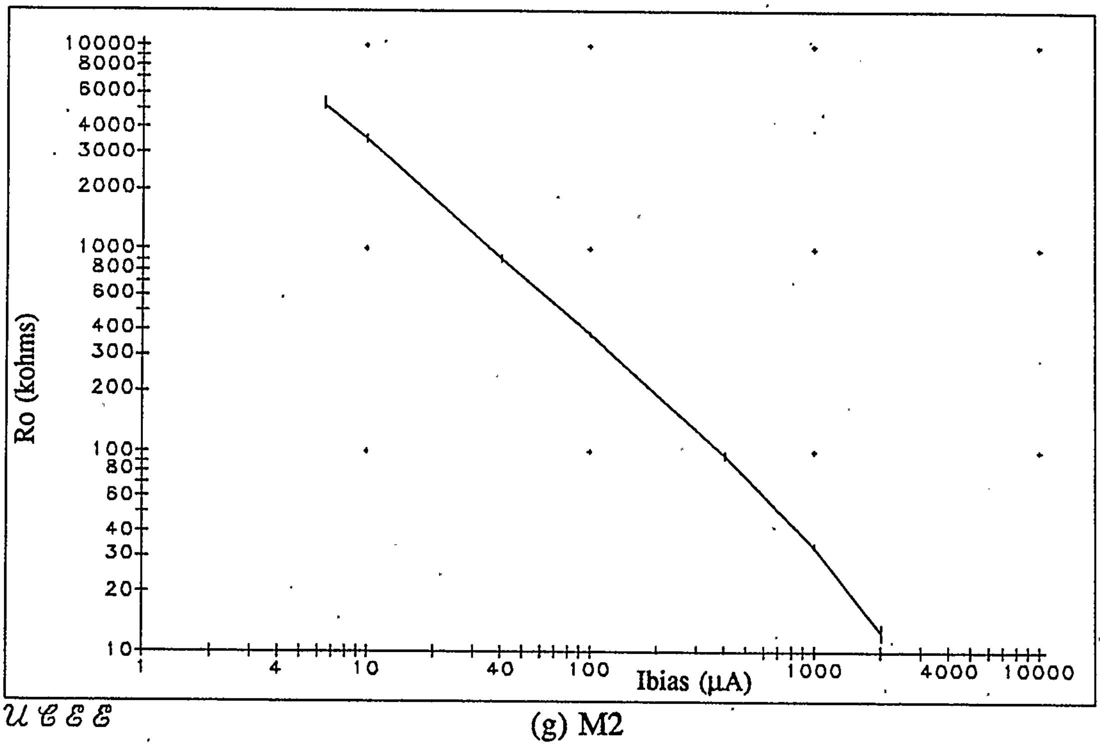

(g) M2

Figure 3.6 Continued

resistance. The theory of output resistance is very difficult to develop, so was not included here.

Measurement of the output capacitance was completed using the same circuit as that used to measure the output resistance. The frequency of the input signal was increased until the output signal dropped by 3 dB. At that point the output capacitance can be found from the equation

$$C_o = \frac{1}{2\pi f R} \tag{3.11}$$

from which the capacitance of the op-amp must be subtracted, and where

$$R = \frac{R_o R_L}{R_o + R_L}. \tag{3.12}$$

From experimental measurements it was found that the output capacitance was essentially independent of the bias current.

As there is some small fixed capacitance associated with the op-amp itself, a value for it was determined and subtracted from the above equation for C_o to determine its actual value. The value of op-amp capacitance was determined by paralleling more op-amps with the one already in place and measuring the increase in the output capacitance associated with each additional op-amp. The results obtained from these measurements and calculations are shown in Table 3.3.

OTA	2T	3T1	3T2	M1	M2	DP1	DP2
C_o (pF)	7.6	9.1	9.5	9.4	9.2	9.1	8.5

Table 3.3 OTA Output Capacitances

3.3 Measurement of Input Resistances

There are three resistances associated with the inputs to the OTA, common mode resistances from the inputs to ground (R_{cm}^{+} and R_{cm}^{-}), and the differential resistance (R_d). To determine these resistances the circuit of Figure 3.7 was implemented.

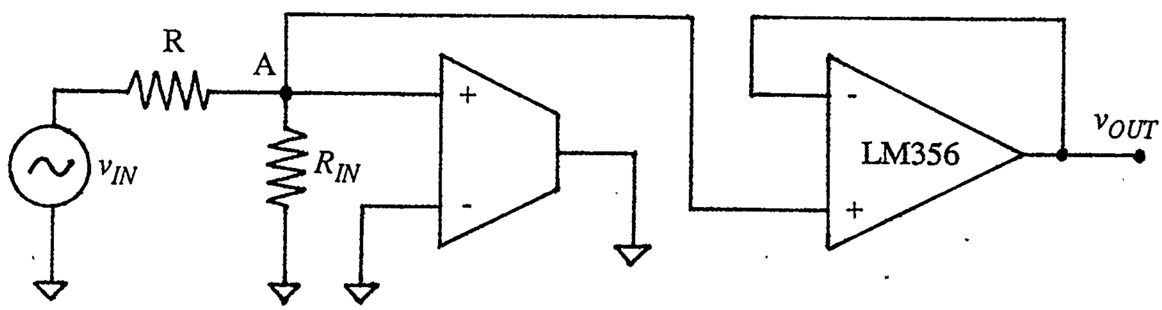

Figure 3.7 OTA Input Resistance Measuring Circuit

Initially, point A is connected to the positive OTA input with the negative input grounded as shown. This allows the measurement of the parallel combination of R_{cm}^{+} and R_d. Connection of point A to the negative terminal with the positive terminal grounded gives the parallel combination of R_{cm}^- and R_d. Connection of point A to both terminals gives the parallel combination of R_{cm}^+ and R_{cm}^-.

The resistance R essentially forms a voltage divider with the input resistance of the OTA. The op-amp follower circuit is again required for the measurement due to probe resistance. The input resistance is then determined from the equation

$$R_{IN} = R\frac{\dfrac{v_{OUT}}{v_{IN}}}{1-\dfrac{v_{OUT}}{v_{IN}}}. \tag{3.13}$$

The common mode resistances are expected to be large, and through experimental work it was determined that they are so large as to be unmeasureable, at all levels of bias current.

Based upon this observation, the only significant input resistance becomes that of R_d. It was further determined that the values of R_d could be broken down into three main categories, by the configuration of the OTA to which they belong. The R_d for both OTA's with a Darlington pair input stage were considered as one category. Those OTA's having the modified configuration also had matching input resistance. The final category then, was the OTA's with a normal configuration.

This result can also be determined theoretically. For both the normal differential pair OTA's and those with the modified configuration, the input stage can be replaced by that shown in Figure 3.8. This equivalent circuit is derived by replacing the bias current mirror with a small signal open circuit. This is reasonable as the bias current mirror is effectively a DC current source, which has

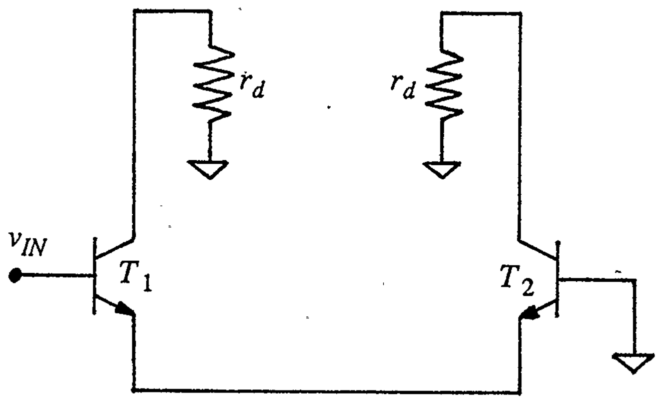

Figure 3.8 Circuit Equivalent of Normal Input Stage

a large output resistance compared to the resistance looking into the emitter of T_2. The signal carrying mirrors were replaced with a resistance to small signal ground (these resistances have no effect on the value of R_d). The resistance from the input to ground of such a configuration is actually the parallel combination of R_d and R_{cm}^+. However, as the common mode resistance is extremely large, the resistance will be effectively R_d.

If the transistors are replaced by the small signal model of the transistor described in Chapter 2 (Figure 2.4), then ordinary circuit analysis allows the derivation of the following equation:

$$R_d = 2(r_{bb'} + r_{b'e}) \tag{3.14}$$

$$\approx 2(\beta + 1)\frac{nkT}{qI_E} \tag{3.15}$$

if $r_{b'e}$ is assumed to be much larger than $r_{bb'}$. For OTA's with a normal configuration I_E is effectively half the bias current. For OTA's with a modified configuration the effective I_E is actually equal to the bias current.

For the Darlington pair configuration the calculations become somewhat more complex. The equivalent circuit for a Darlington pair input stage is shown in Figure 3.9. This circuit is derived using the same assumptions as those used for the normal input stage. The difference in the calculations is due to the fact that the I_E of transistors T_1 and T_4 is actually the I_B of transistors T_2 and T_3, respectively. Standard circuit equations for transistors can be used through ordinary circuit analysis to yield the following equation:

$$R_d = r_{b1} + r_{b2}(\beta' + 1) + r_{b3}(\beta' + 1) + r_{b4} \tag{3.16}$$

where

$$r_b = r_{bb'} + r_{b'e}. \tag{3.17}$$

Using equations 2.1 and 2.2 and assuming $r_{b'e} >> r_{bb'}$ results in the equation

$$R_d \approx 4(\beta' + 1)(\beta + 1)\frac{nkT}{qI_E}. \tag{3.18}$$

β' is the common emitter gain of transistors T_1 and T_4, β is the common emitter gain of transistors T_2 and T_3 and I_E is half the bias current. The values of β can

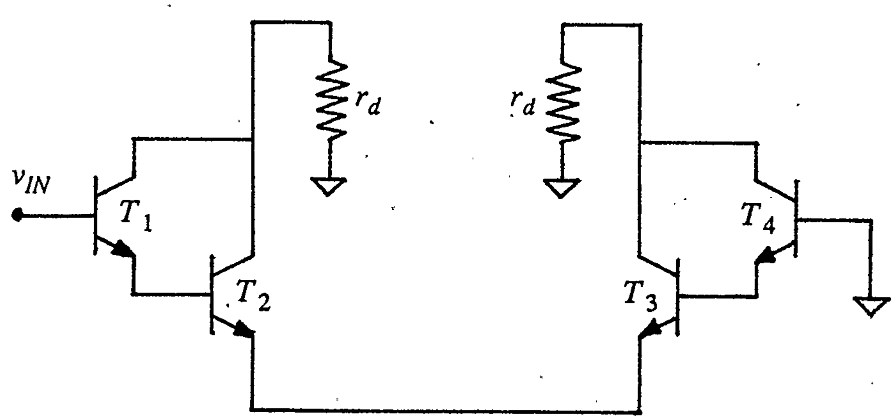

Figure 3.9 Circuit Equivalent of Darlington Pair Input Stage

be found from the graph of Figure 2.6(a) since

$$I_C = \frac{\beta}{\beta + 1} I_E. \tag{3.19}$$

Plots of the theoretical R_d for the maximum, minimum and typical values of β are compared to the measured value of R_d in Figures 3.10 - 3.12 for the three different configurations. As can be seen, the measured values fall well within the theoretical range.

3.4 Measurement of Input Capacitances

The measurement circuit for input capacitances (Figure 3.13) is similar to that used for input resistances. Resistors R_1 and R_2 form a voltage divider at the input to the OTA. R_2 is much less than the input resistance of the OTA, so R_{IN} can be neglected. From consideration of the circuit it can easily be shown that the output will drop by 3dB at the frequency

$$f = \frac{1}{2\pi C_{IN} R_2} \tag{3.20}$$

from which C_{IN} can be defined as

$$C_{IN} = \frac{1}{2\pi f R_2}. \tag{3.21}$$

As with the output capacitance measurements the capacitance of the op-amp must be subtracted from equation 3.18 to give the actual value of C_{IN}. With the circuit as shown, C_{IN} will be the parallel combination of C_{cm}^{+} and C_d. With point A connected to the negative terminal of the OTA and the positive terminal grounded, C_{IN} will be C_{cm}^{-} in parallel with C_d. With both terminals connected to

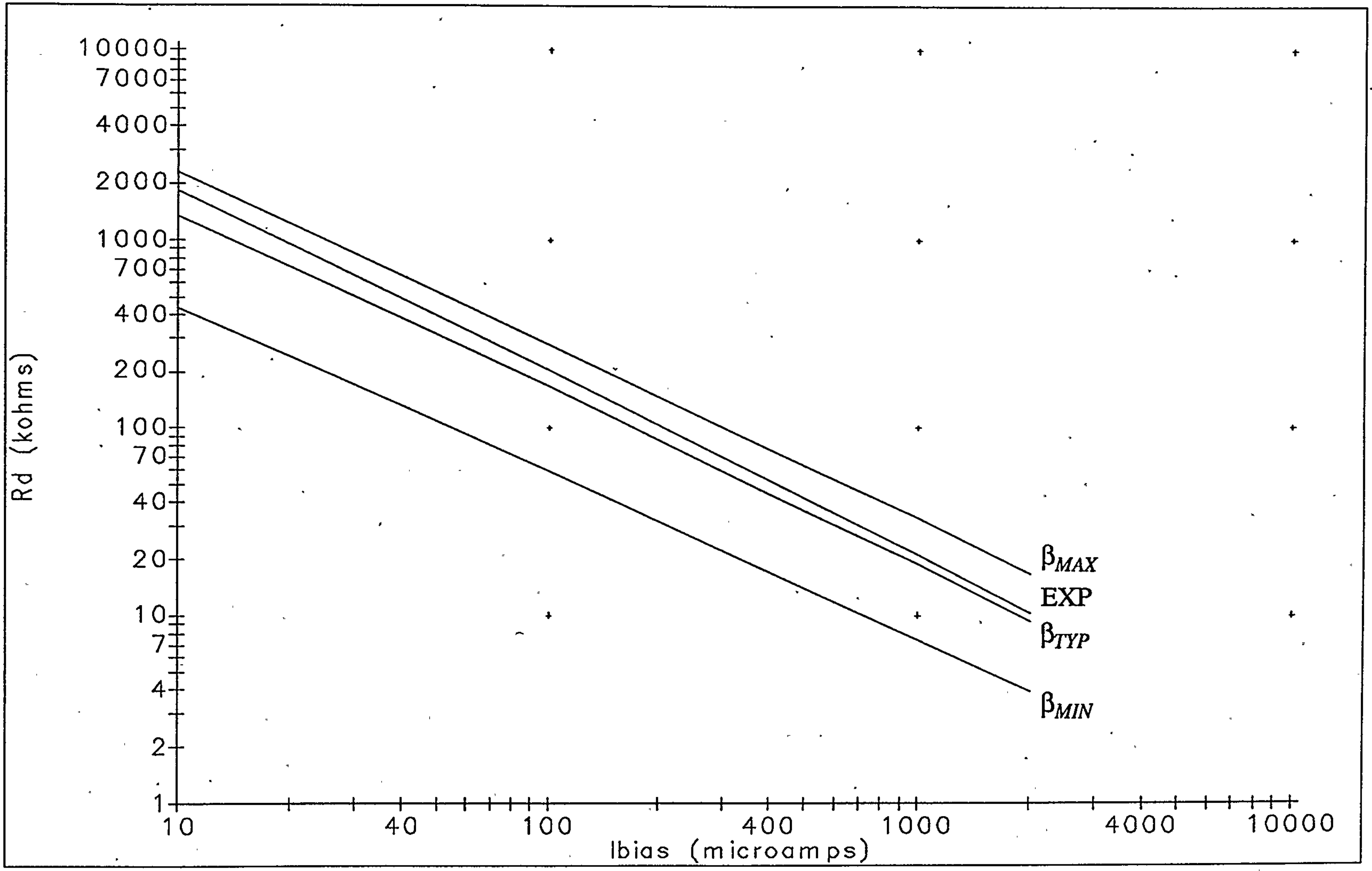

UCEE Rd of Normal Input Stage (Theory vs. Experiment)

Figure 3.10 Differential Resistance vs Bias Current for Normal Configuration

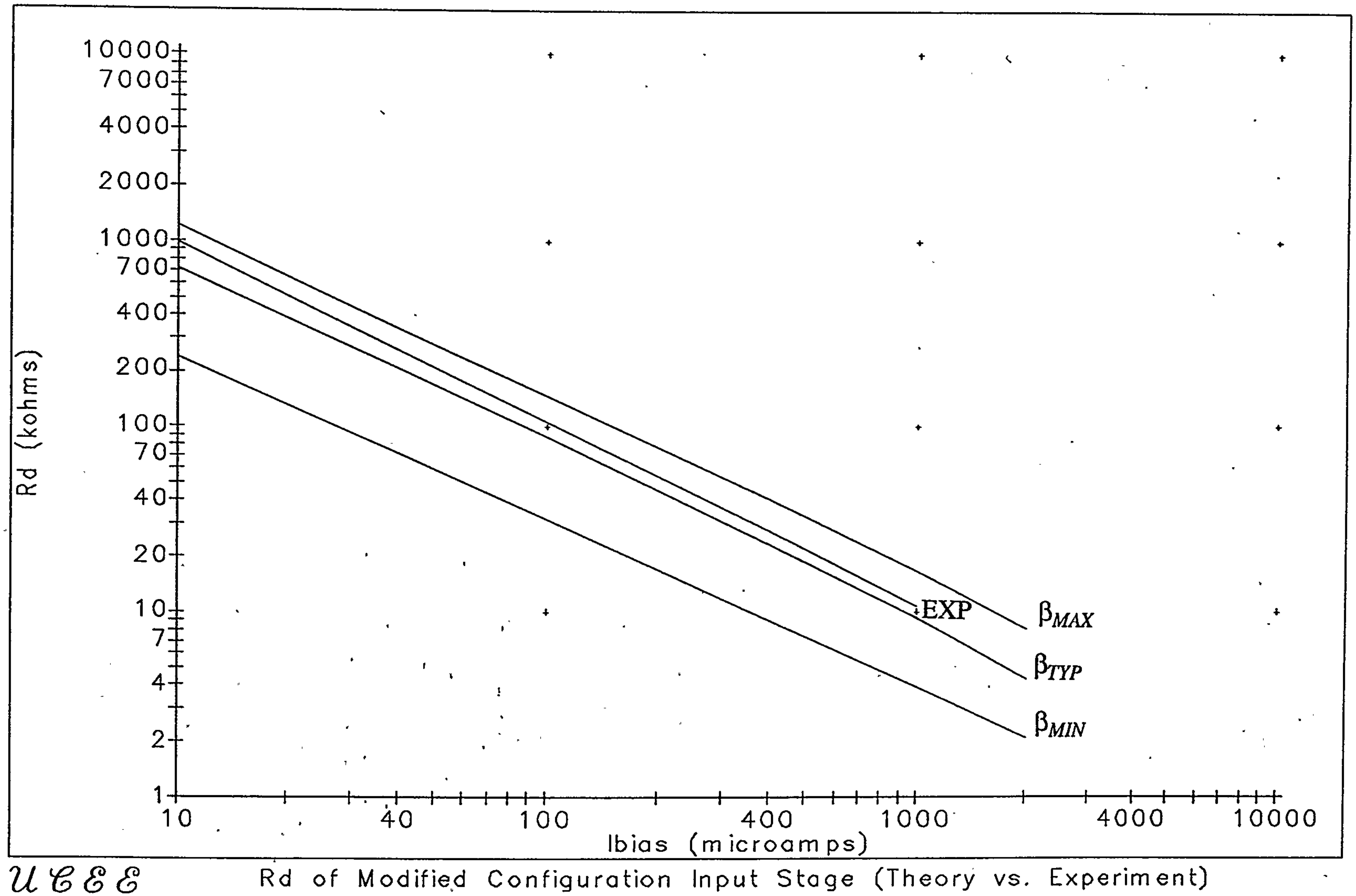

Figure 3.11 Differential Resistance vs Bias Current for Modified Configuration

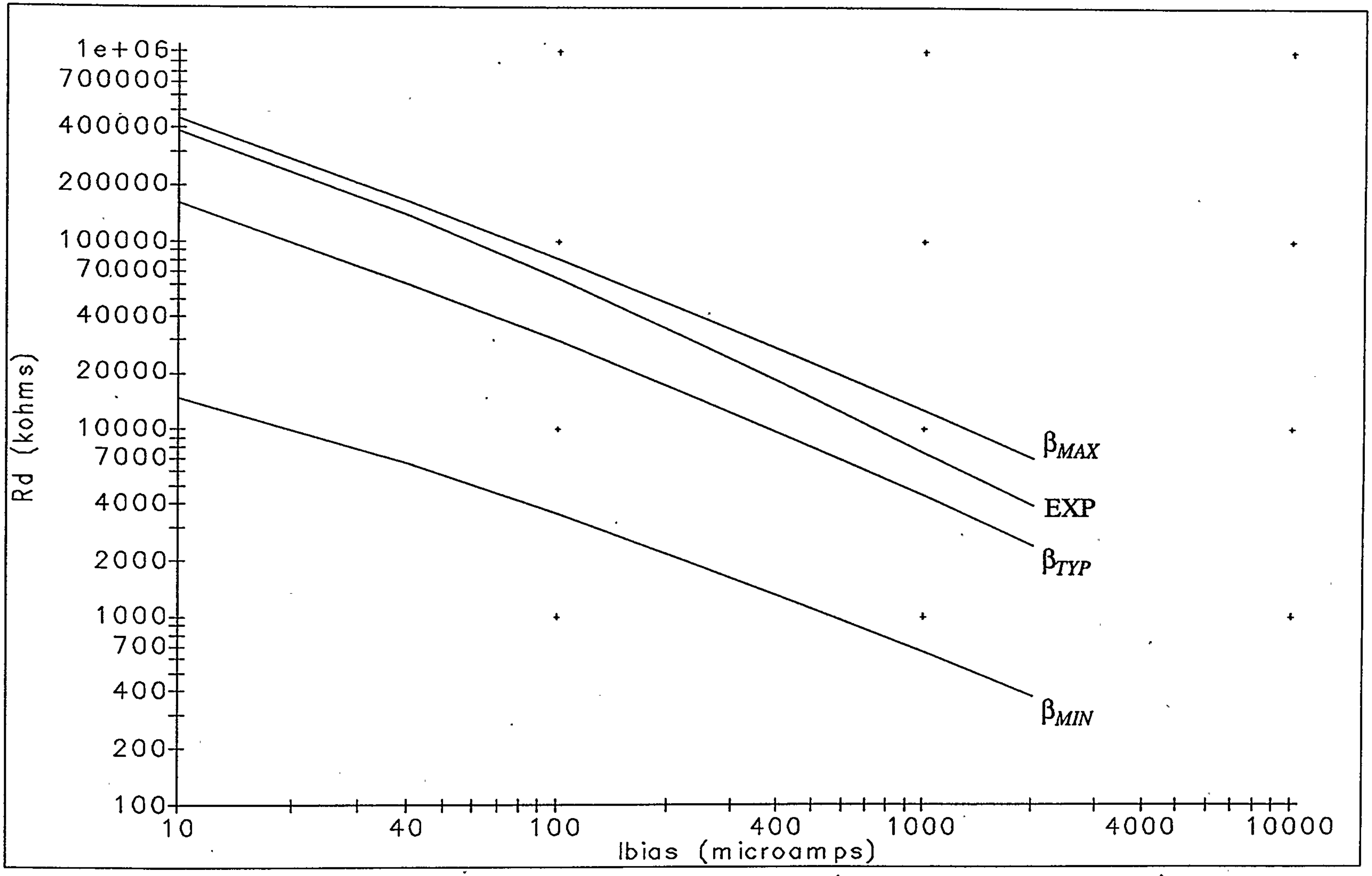

𝒰𝒞ℰℰ Rd of Darlington Pair Input Stage (Theory vs. Experiment)

Figure 3.12 Differential Resistance vs Bias Current for Darlington Pair Configuration

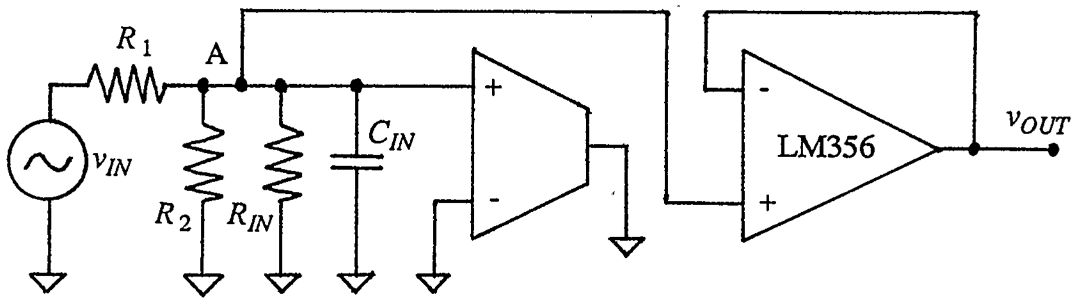

Figure 3.13 OTA Input Capacitance Measuring Circuit

point A the parallel combination of C_{cm}^{+} and C_{cm}^{-} will be measured. It was determined that the common mode input capacitances, C_{cm}^{+} and C_{cm}^{-}, are independent of the bias current (Table 3.4), while C_d is a linearly increasing function of it (Figure 3.14).

Complete records of all the measurements made are available in a report sent to LTI [8]. These are not included within the thesis due to their large quantity.

OTA	C_{cm}^{+} (pF)	C_{cm}^{-} (pF)
2T	5.7	5.7
3T1	6.7	6.7
3T2	6.8	6.8
M1	5.8	4.5
M2	8.8	6.0
DP1	7.5	7.5
DP2	6.7	6.7

Table 3.4 OTA Common Mode Input Capacitances

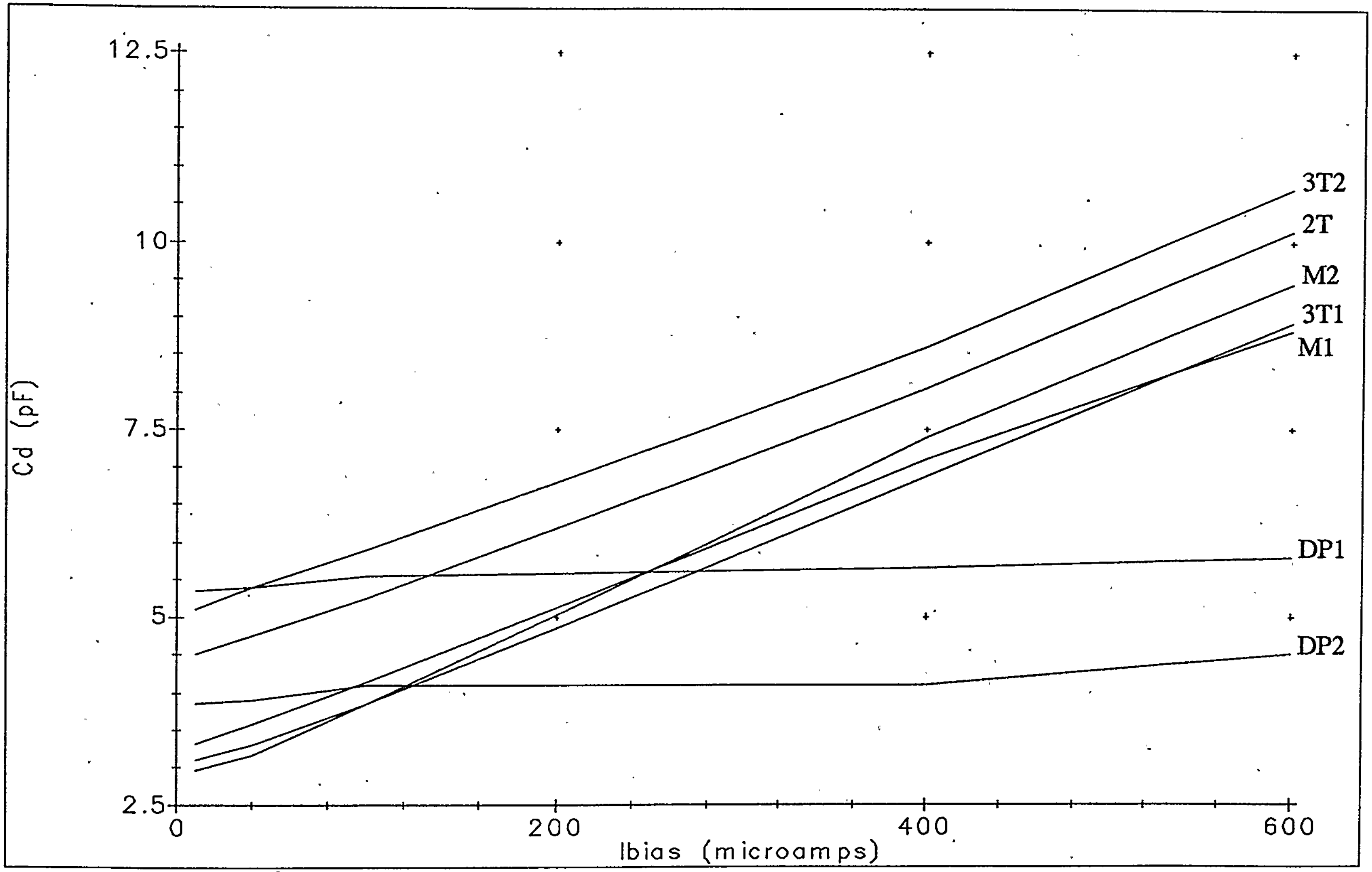

UCEE Cd vs Bias Current for all OTA configurations

Figure 3.14 Differential Capacitance vs Bias Current for all OTA Types

3.5 Modelling of OTA Characteristics

As will be seen in Chapter 4, the filter design equations require specific knowledge of all the OTA parameters. As was shown previously, most of the OTA parameters vary with the applied bias current. In general it is unlikely that the operating points chosen will be at the measuring points used. This leaves the designer with the inconvenience of determining the parameters from their respective graphs.

As graphical determination is not really acceptable, due to the large number of parameters whose value must be found, it was decided to model each of the parameters through standard quadratic curve fitting algorithms using the least squares method. A program was written to analyze each plot and output the equation of a curve which best fit it. An example of such a fit is shown in Figure 3.15 where the solid line is the measured response, and the dotted line is the curve fit output. This has the added convenience of allowing for the possibility of fully automating the design process once the parameter equations have been determined. This is in fact done in Chapter 4.

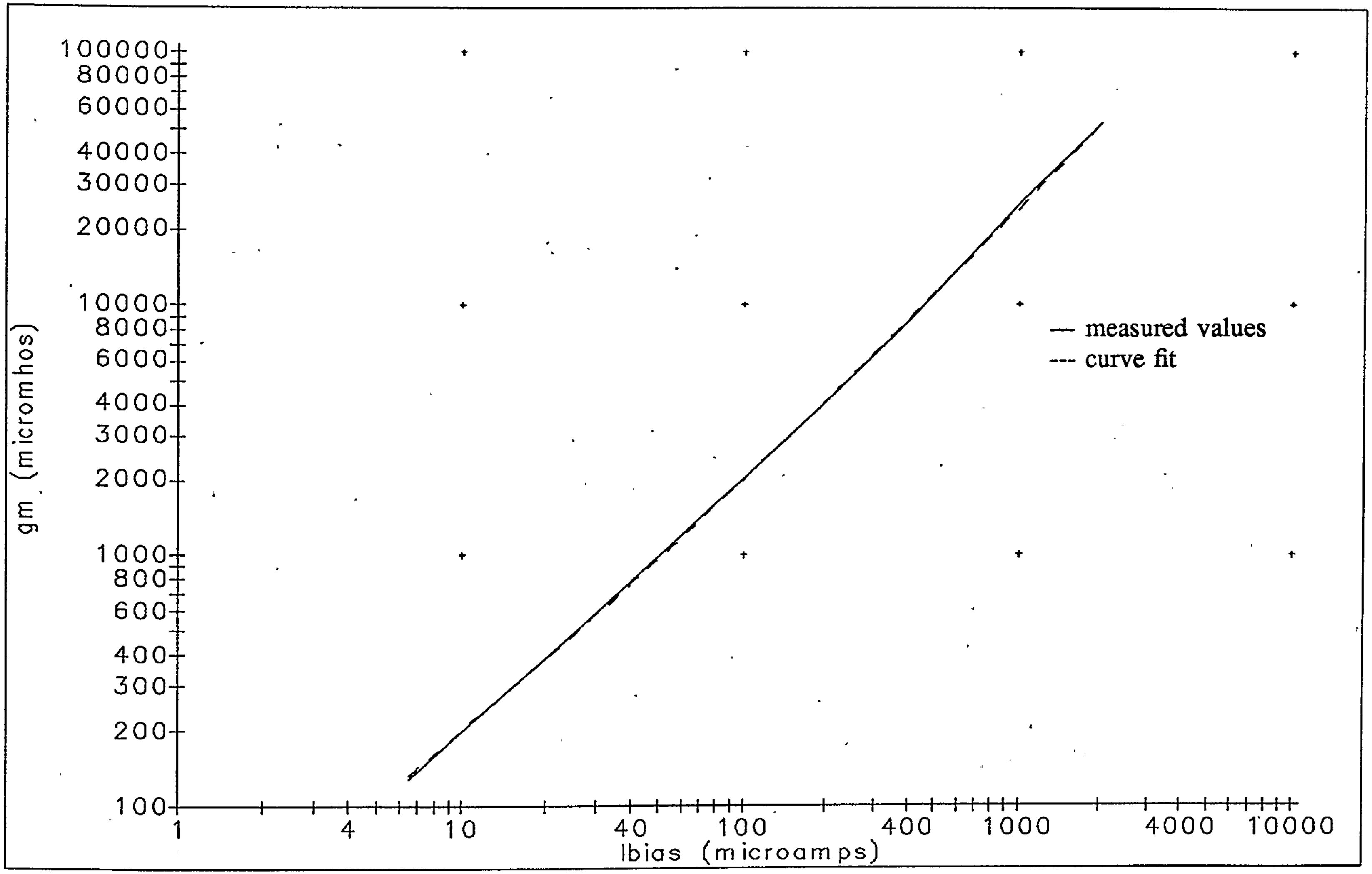

UCEE Fit of average gm vs Ibias for LTI OTA 3T1

Figure 3.15 Example of Curve Fit to Data Values

CHAPTER 4

BIQUAD FILTER DESIGN AND IMPLEMENTATION

4.1 The OTA Based Biquad Filter

Of the filter designs for OTA's in recent literature, the one which gives the best tradeoff between maximum flexibility and minimum complexity is the biquad filter. The biquad filter is capable of producing many different filter responses and, due to the variable gain nature of the OTA, the operating parameters may be easily manipulated. However, it is a fairly simple circuit. The OTA based biquad filter requires only three OTA's and two capacitors (Figure 4.1). The various inputs

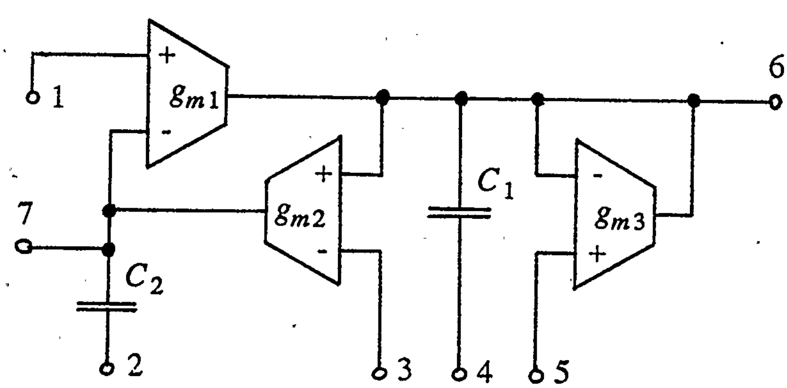

Figure 4.1 Biquad Filter Circuit

(labeled 1-5) are connected either to the input signal or ground, and the filter response is derived from one of the two outputs (6 and 7).

Malvar [2] has determined the combinations of inputs and outputs which produce useful filter responses. If the OTA's in Figure 4.1 are replaced by their ideal small signal model (Figure 2.9), the ideal transfer functions for the available filter types may be easily determined through standard circuit analysis.

The frequency domain transfer function of a filter response may be represented as

$$\frac{V_{OUT}(s)}{V_{IN}(s)} = \frac{N(s)}{D(s)}. \tag{4.1}$$

It was found that the denominator polynomial is the same for all possible filter types and is given by the equation

$$D(s) = s^2 + s\frac{g_{m3}}{C_1} + \frac{g_{m1}g_{m2}}{C_1C_2}. \tag{4.2}$$

The numerator polynomials for the useful filter responses and the appropriate combinations of inputs and outputs which produce these filter responses are tabulated in Table 4.1.

From the denominator polynomial (Eq. 4.2), the natural frequency, ω_n, and quality factor, Q, can be determined.

FILTER TYPE	NUMERATOR POLYNOMIAL	INPUT NODES	OUTPUT NODE	GROUNDED NODES
LOWPASS I	$\frac{g_{m1}g_{m2}}{C_1C_2}$	3 or 1	6 7	1,2,4,5 2,3,4,5
LOWPASS II	$\frac{g_{m2}g_{m3}}{C_1C_2}$	5	7	1,2,3,4
BANDPASS Ia	$s\,\frac{g_{m1}}{C_1}$	1	6	2,3,4,5
BANDPASS Ib	$s\,\frac{g_{m2}}{C_2}$	4	7	1,2,3,5
BANDPASS II	$s\,\frac{g_{m3}}{C_1}$	5	6	1,2,3,4
HIGHPASS	s^2	4	6	1,2,3,5
NOTCH	$s^2+\frac{g_{m1}g_{m2}}{C_1C_2}$	3,4 or 1,2,3,4	6 6	1,2,5 5

Table 4.1 Biquad Filter Configurations and Ideal Numerator Polynomials

$$\omega_n = \sqrt{\frac{g_{m1}g_{m2}}{C_1C_2}} \tag{4.3}$$

$$Q = \sqrt{\frac{C_1}{C_2}}\sqrt{\frac{g_{m1}g_{m2}}{g_{m3}^2}}. \tag{4.4}$$

As the transconductances (g_{m1}, g_{m2} and g_{m3}) are directly controlled by the appropriate bias currents, ω_n and Q can easily be set to the values desired.

4.2 Lumped Model Biquad Filter Analysis

Biquad filter analysis using the ideal OTA model, while providing a guideline for filter design, does not adequately predict the actual performance of these circuits. It is for this reason that the lumped model of the OTA is to be used. When the OTA's of the biquad filter in the lowpass II configuration are replaced by the lumped model of Figure 2.10, the equivalent circuit of Figure 4.2 is obtained.

From Figure 4.2, a standard circuit analysis gives the transfer function as

$$\frac{V_{OUT}}{V_{IN}} = \frac{g_{m2}(g_{m3} + sC_{d3} + \frac{1}{R_{d3}})}{g_{m1}g_{m2} + (sC_A + \frac{1}{R_A})(g_{m3} + sC_B + \frac{1}{R_B})} \tag{4.5}$$

where

$$C_A = C_2 + C_{cm1}^- + C_{d1} + C_{o2} \tag{4.6}$$

$$C_B = C_1 + C_{o1} + C_{cm2}^+ + C_{d2} + C_{cm3}^- + C_{d3} + C_{o3} \tag{4.7}$$

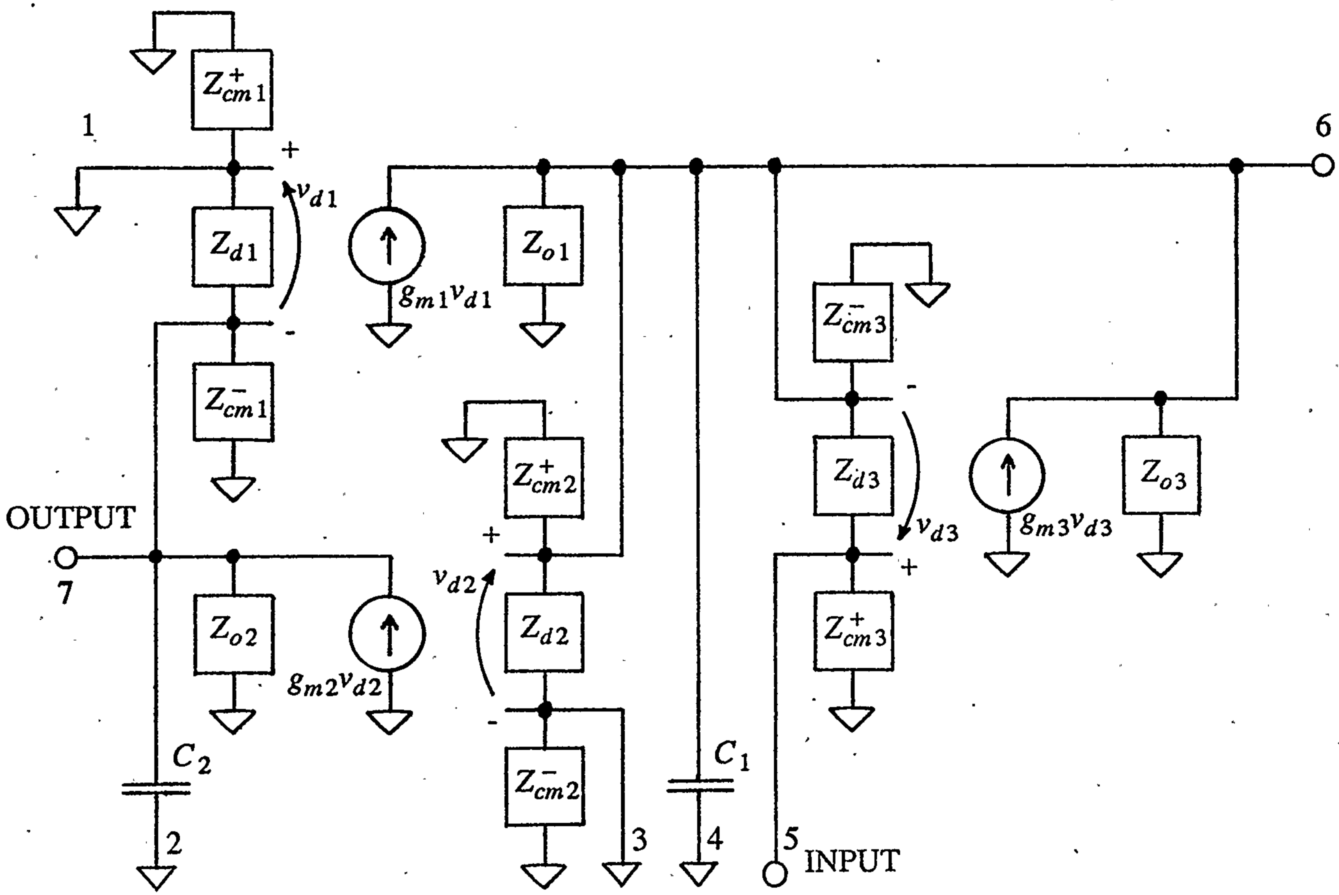

Figure 4.2 Lumped Model Equivalent of Lowpass II Configuration

$$\frac{1}{R_A} = \frac{1}{R_{d1}} + \frac{1}{R_{o2}} \tag{4.8}$$

$$\frac{1}{R_B} = \frac{1}{R_{o1}} + \frac{1}{R_{d2}} + \frac{1}{R_{d3}} + \frac{1}{R_{o3}}. \tag{4.9}$$

Equation 4.5 can be manipulated to form the equation

$$\frac{V_{OUT}}{V_{IN}} = \frac{s\frac{g_{m3}C_{d3}}{C_A C_B} + \frac{g_{m2}(1+g_{m3}R_{d3})}{C_A C_B R_{d3}}}{s^2 + s\left[\frac{1+g_{m3}R_B}{C_B R_B} + \frac{C_A}{C_B R_A}\right] + \frac{1}{C_A C_B}\left[g_{m1}g_{m2} + \frac{1+g_{m3}R_B}{R_A R_B}\right]} \tag{4.10}$$

whose denominator is of the form

$$D(s) = s^2 + s\frac{\omega_n}{Q} + \omega_n{}^2. \tag{4.11}$$

From 4.10 and 4.11, the equations for ω_n and Q can be obtained as

$$\omega_n = \sqrt{\frac{g_{m1}g_{m2}}{C_1 C_2}}\sqrt{\frac{(1+\varepsilon_1)(1+\varepsilon_2)}{(1+\varepsilon_3)}} \tag{4.12}$$

and

$$Q = \sqrt{\frac{C_1}{C_2}}\sqrt{\frac{g_{m1}g_{m2}}{g_{m3}^2}}\sqrt{\frac{(1+\varepsilon_1)(1+\varepsilon_3)}{(1+\varepsilon_2)(1+\varepsilon_4)^2}} \tag{4.13}$$

where

$$\varepsilon_1 = \frac{1 + g_{m3}R_B}{g_{m1}g_{m2}R_A R_B} \tag{4.14}$$

$$\varepsilon_2 = \frac{C_A'}{C_2} \tag{4.15}$$

$$\varepsilon_3 = \frac{C_B'}{C_1} \tag{4.16}$$

$$\varepsilon_4 = \frac{C_A R_A + C_B R_B}{g_{m3} C_A R_A R_B} \tag{4.17}$$

and

$$C_A' = C_A - C_2 \tag{4.18}$$

$$C_B' = C_B - C_1. \tag{4.19}$$

In much a similar manner, the transfer functions for all nine of the available filter types can be derived. As with the ideal case, the denominator polynomial is common to all filter types and is given by the equation

$$D(s) = s^2 + s\left[\frac{1+g_{m3}R_B}{C_B R_B} + \frac{C_A}{C_B R_A}\right] + \frac{1}{C_A C_B}\left[g_{m1}g_{m2} + \frac{1+g_{m3}R_B}{R_A R_B}\right]. \tag{4.20}$$

The numerator polynomials for all nine filter types are shown in Table 4.2.

4.3 Filter Performance Prediction

To examine the sinusoidal response of the filters developed, s is replaced by jω in the transfer functions. From the equations thus derived the magnitude of the filter responses with respect to frequency may be obtained. Phase response calculations were also done, as were phase measurements. The agreement between the calculations and measurements was found to be very good. The large volume of data involved in showing this data precluded their inclusion here. The programs presented in section 4.5 also include the phase calculations, so those who desire more information on the phase responses are refered to [9].

FILTER TYPE	NUMERATOR POLYNOMIAL
LOWPASS Ia	$s^2 \frac{C_{d2}}{C_B} + s\ [\frac{1}{C_B R_{d2}} + \frac{C_{d2}}{C_A C_B R_A}] + \frac{1}{C_A C_B}\ [g_{m1} g_{m2} + \frac{1}{R_A R_{d2}}]$
LOWPASS Ib	$s^2 \frac{C_{d1}}{C_A} + s\ [\frac{1}{C_A R_{d1}} + \frac{C_{d1}(1+g_{gm} R_B)}{C_A C_B R_A}] + \frac{1}{C_A C_B}\ [g_{m1} g_{m2} + \frac{1+g_{m3} R_B}{R_B R_{d1}}]$
LOWPASS II	$s\ \frac{g_{m3} C_{d3}}{C_A C_B} + \frac{g_{m2}(1+g_{m3} R_{d3})}{C_A C_B R_{d3}}$
BANDPASS Ia	$\frac{g_{m1}}{C_A C_B}\ [s\ (C_2 + C_{\bar{c}m1} + C_{o2}) + \frac{1}{R_{o2}}]$
BANDPASS Ib	$s\ \frac{g_{m2} C_1}{C_A C_B}$
BANDPASS II	$s^2 \frac{C_{d3}}{C_B} + s\ [\frac{1+g_{m3} R_{d3}}{C_B R_{d3}} + \frac{C_{d3}}{C_A C_B R_A}] + \frac{1}{C_A C_B}\ [\frac{1+g_{m3} R_{d3}}{R_A R_{d3}}]$
HIGHPASS	$s^2 \frac{C_1}{C_B} + s\ \frac{C_1}{C_A C_B R_A}$
NOTCH a	$s^2 \frac{C_1 + C_{d2}}{C_B} + s\ [\frac{1}{C_B R_{d2}} + \frac{C_1 + C_{d2}}{C_A C_B R_A}] + \frac{1}{C_A C_B}\ [g_{m1} g_{m2} + \frac{1}{R_A R_{d2}}]$
NOTCH b	$s^2 \frac{C_1 + C_{d2}}{C_B} + s\ [\frac{1}{C_B R_{d2}} + \frac{C_1 + C_{d2}}{C_A C_B R_A} + \frac{(C_{\bar{c}m1} + C_{o2}) g_{m1}}{C_A C_B}] + \frac{1}{C_A C_B}\ [g_{m1} g_{m2} + \frac{1}{R_A R_{d2}} + \frac{g_{m1}}{R_{o2}}]$

Table 4.2 Lumped Model Numerator Polynomials

For the ideal case the denominator of the magnitude equations can be written as

$$D_{IM}(\omega) = \sqrt{[g_{m1}g_{m2} - \omega^2 C_1 C_2]^2 + [\omega g_{m3} C_2]^2}. \tag{4.21}$$

For the lumped model prediction the denominator is

$$D_M(\omega) = \sqrt{a^2 + b^2} \tag{4.22}$$

where

$$a = \left[g_{m1}g_{m2} + \frac{1}{R_A}(g_{m3} + \frac{1}{R_B}) - \omega^2 C_A C_B \right] \tag{4.23}$$

and

$$b = \omega \left[\frac{C_B}{R_A} + C_A (g_{m3} + \frac{1}{R_B}) \right]. \tag{4.24}$$

The ideal magnitude response numerator polynomials are shown in Table 4.3. Those for the lumped model analysis are shown in Table 4.4. The lumped model equations are much more complex than those of the ideal model.

4.4 Design of Biquad Filters

For most purposes the easiest method of designing a biquad filter circuit is to first choose the desired ω_n and Q, and then calculate the component values necessary to achieve them. Consideration of the ideal design equations (4.3 and 4.4) shows that there are five unknowns (C_1, C_2, g_{m1}, g_{m2} and g_{m3}) with only two equations. This is a highly under-determined system, so some other assumptions must be made. For almost all practical purposes g_{m1} can be made equal to g_{m2} with no loss of design flexibility. It then becomes necessary to choose practical

FILTER TYPE	MAGNITUDE NUMERATOR POLYNOMIAL
LOWPASS Ia	$g_{m1}g_{m2}$
LOWPASS Ib	$g_{m1}g_{m2}$
LOWPASS II	$g_{m2}g_{m3}$
BANDPASS Ia	$\omega g_{m1}C_2$
BANDPASS Ib	$\omega g_{m2}C_1$
BANDPASS II	$\omega g_{m3}C_2$
HIGHPASS	$\omega^2 C_1 C_2$
NOTCH a	$\sqrt{[g_{m1}g_{m2} - \omega^2 C_1 C_2]^2}$
NOTCH b	$\sqrt{[g_{m1}g_{m2} - \omega^2 C_1 C_2]^2}$

Table 4.3 Ideal Magnitude Response Numerator Polynomials

FILTER TYPE	MAGNITUDE NUMERATOR POLYNOMIAL
LP Ia	$\sqrt{[g_{m1}g_{m2} + \frac{1}{R_A R_{d2}} - \omega^2 C_A C_{d2}]^2 + \omega^2[\frac{C_{d2}}{R_A} + \frac{C_A}{R_{d2}}]^2}$
LP Ib	$\sqrt{[g_{m1}g_{m2} + \frac{1}{R_{d1}}(g_{m3}+\frac{1}{R_B}) - \omega^2 C_B C_{d1}]^2 + \omega^2[\frac{C_B}{R_{d1}} + C_{d1}(g_{m3}+\frac{1}{R_B})]^2}$
LP II	$\sqrt{[g_{m2}(g_{m3}+\frac{1}{R_B})]^2 + \omega^2[g_{m2}C_{d3}]^2}$
BP Ia	$\sqrt{[\frac{g_{m1}}{R_{o2}}]^2 + \omega^2[g_{m1}(C_2+C_{\bar{c}m1}+C_{o2})]^2}$
BP Ib	$\omega g_{m2} C_1$
BP II	$\sqrt{[\frac{1}{R_A}(g_{m3}+\frac{1}{R_B}) - \omega^2 C_A C_{d3}]^2 + \omega^2[\frac{C_{d3}}{R_A} + C_A(g_{m3}+\frac{1}{R_B})]^2}$
HP	$\sqrt{[\omega^2 C_1 C_A]^2 + \omega^2[\frac{C_1}{R_A}]^2}$
N a	$\sqrt{[g_{m1}g_{m2} + \frac{1}{R_A R_{d2}} - \omega^2 C_A (C_1+C_{d2})]^2 + \omega^2[\frac{C_A}{R_{d2}} + \frac{C_1+C_1}{R_A}]^2}$

Table 4.4 Lumped Model Magnitude Response Numerator Polynomials

FILTER TYPE	MAGNITUDE NUMERATOR POLYNOMIAL
N b	$\sqrt{c^2+d^2}$ $c = \left[g_{m1}g_{m2} + \frac{1}{R_A R_{d2}} + \frac{g_{m1}}{R_{o2}} - \omega^2 C_A (C_1 + C_{d2})\right]$ $d = \omega\left[\frac{C_A}{R_{d2}} + \frac{C_1 + C_{d2}}{R_A} + g_{m1}(C_{\overline{cm}1} + C_{o2})\right]$

Table 4.4 Continued

values for either C_1 and C_2 or g_{m1} and g_{m3} and use equations 4.3 and 4.4 to determine the remaining two values.

Once the component values have been determined, the bias currents can be derived from consideration of the relationship between the OTA transconductance and its bias current. The magnitude response of the actual filter can then be determined through the use of the magnitude response equations shown in Table 4.4.

While this is the easiest method, it has several drawbacks. First, and foremost, such a method almost never results in the desired filter performance. Use of the ideal design equations gives only the nominal component values and they may be quite different from those needed to produce the desired filter response. Proper design equations should not only allow prediction of the filter response once component values have been chosen, but should also allow the designer to accurately choose the component values to fit a desired response.

The lumped model design equations, 4.12 and 4.13, are much more complex than those for the ideal case, and thus much harder to use. To achieve a solution, it is again assumed that g_{m1} and g_{m2} are equal. The designer then chooses either C_1 and C_2 or g_{m1} and g_{m3} and iterates equations 4.12 and 4.13 to obtain the remaining component values. As the majority of OTA parameters in those equations are bias current relative, each iteration requires approximating all of the parameters from their relationships to bias current determined in Chapter 3. This is an extremely time consuming task.

4.5 Program Development for Filter Design

Two programs were written to reduce the amount of design time. The first of these is to allow the determination of filter parameters, and the second to predict the actual filter performance.

The first program [9] is based upon the ideal design equations, 4.3 and 4.4. The pseudo code for this program is shown in Figure 4.3. The designer is required to determine the OTA's which will be used, their bias currents or transconductances (it will work out one from the other) and the center frequency and Q of the desired filter. Once the program knows the OTA which is being used, it reads the definition file for that OTA. A definition file is basically a list of the equations defining the various OTA parameters. The definition files for the seven OTA's developed here are given in [9]. Table 4.5 gives the parameter

```
begin
        get OTA choice from USER
        read OTA definition file
        USER chooses gm or IBIAS values
        if (gm values chosen) then
                get gm values from USER
                calculate bias currents
        else
                get bias currents from USER
        endif
        get desired fn and Q values from USER
        calculate OTA parameters at chosen bias currents
        output OTA parameters
        calculate capacitor values required to get desired fn and Q
        output capacitor values
end
```

Figure 4.3 Pseudo Code for Filter Parameter Determination Program

Wilson Mirror OTA	
Parameter Equation	Units
$\ln(g_m) = 3.168 + 0.884 \cdot \ln(I_{bias}) + 0.017 \cdot \ln(I_{bias})^2$	μmhos
$\ln(R_o) = 13.795 - 0.266 \cdot \ln(I_{bias}) - 0.104 \cdot \ln(I_{bias})^2$	kΩ
$\ln(R_d) = 9.218 - 0.983 \cdot \ln(I_{bias})$	kΩ
$C_o = 9.1$	pF
$C_d = 2.885 + 0.011 \cdot I_{bias}$	pF
$C_{cm}^{+} = 6.7$	pF
$C_{cm}^{-} = 6.7$	pF

Modified Wilson Mirror OTA	
Parameter Equation	Units
$\ln(g_m) = 3.193 + 0.867 \cdot \ln(I_{bias}) + 0.017 \cdot \ln(I_{bias})^2$	μmhos
$\ln(R_o) = 11.216 - 0.664 \cdot \ln(I_{bias}) - 0.055 \cdot \ln(I_{bias})^2$	kΩ
$\ln(R_d) = 9.129 - 0.976 \cdot \ln(I_{bias})$	kΩ
$C_o = 9.4$	pF
$C_d = 3.224 + 0.009 \cdot I_{bias}$	pF
$C_{cm}^{+} = 5.8$	pF
$C_{cm}^{-} = 4.5$	pF

Table 4.5 Parameter Equations for Modified and Normal Wilson Mirror OTA's

equations for the Wilson mirror OTA and the modified Wilson mirror OTA as examples of the format of the equations needed to define the OTA parameters.

For the first program, if the user enters the OTA transconductance, the program works out the bias current necessary to produce that transconductance from the measured transconductance to bias current equation. It then calculates the capacitor values required to produce the center frequency and Q desired and gives the designer a list of the necessary component values.

The second program [9], which is to predict the actual filter response, is much more complex than the first (see Figure 4.4). This program requests from the designer the OTA and filter type chosen, as well as the component values required. The user is then required to enter the frequency range and number of output points for the prediction output. The program will then output the ideal and expected filter responses using the ideal and non-ideal magnitude response equations of Tables 4.3 and 4.4. In addition, it generates all of the ideal and non-ideal design parameters, as well as the values of the lumped parameters for each of the OTA's. The lumped parameters are determined from the equations in the OTA definition file.

As it is much easier to design with the ideal design equations, though they do not always predict accurately the actual response, a further capability was added to the second program. After the initial analysis has been done, and the filter response generated, the program asks if the designer wishes to do capacitor or gm compensation. The program takes the ideal filter center frequency and Q, as determined internally, and iterates the non-ideal design equations, 4.12 and 4.13, changing either the capacitor values or the gm values, until the non-ideal response matches the desired ideal response. This allows the designer to iterate component values to achieve the required solution, while doing the actual design with the much simpler ideal equations. After compensation, the program generates the new expected filter response curve and the component values required to produce this response.

```
begin
        get OTA choice from USER
        read OTA definition file
        get filter type from USER
        USER chooses gm or IBIAS values
        if (gm values chosen) then
                get gm values from USER
                calculate bias currents
        else
                get bias currents from USER
        endif
        get capacitor values from USER
        Ask USER for frequency range and # of points for filter prediction
        output filter component values used
        calculate OTA parameters at chosen bias currents
        output OTA parameters
        call up filter calculation and prediction routine
        Ask USER if capacitor compensation is desired
        if (capacitor compensation desired) then
                do
                        iterate capacitor values
                until (lumped model fn and Q equal original ideal values)
                output new filter component values
                call up filter calculation and prediction routine
        else
                Ask USER if gm compensation is desired
                if (gm compensation desired) then
                do
                        iterate gm values
                        calculate new bias currents
                        calculate new OTA parameters
                until (lumped model fn and Q equal original ideal values)
                output new filter component values
                call up filter calculation and prediction routine
        endif
end
```

Figure 4.4 Pseudo Code for Filter Prediction Program

The above two programs thus enable the designer to get a complete filter design, including all component values and a file containing the expected filter response, from a knowledge of the desired filter center frequency and Q, with practical values for the transconductance of the OTA's used. The results from application of the programs and comparison between its predictions and the actual measurements are covered in Chapter 5.

CHAPTER 5

BIQUAD FILTER PERFORMANCE

Measurement of OTA based biquad filter response is not a simple task. OTA's have a limited dynamic range, and are temperature sensitive [4]. For these reasons the input signal to the filter structure was limited to $10mV_{p-p}$, and an HP Network Analyzer was used for the measurement because of its high sensitivity. To eliminate temperature change, the entire circuit was installed in a test oven, and the temperature was maintained at 25°C.

5.1 Prediction of Filter Performance

The usefulness of any set of design equations becomes readily apparent when the circuit resulting from their application is implemented and its performance compared with that desired. The conventional design methods using HSPICE do not adequately predict the performance of OTA based biquad filters. Figure 5.1 shows a comparison of the HSPICE prediction (dotted line) and the measured results (solid line) for a biquad bandpass II filter using Wilson Mirror OTA's with

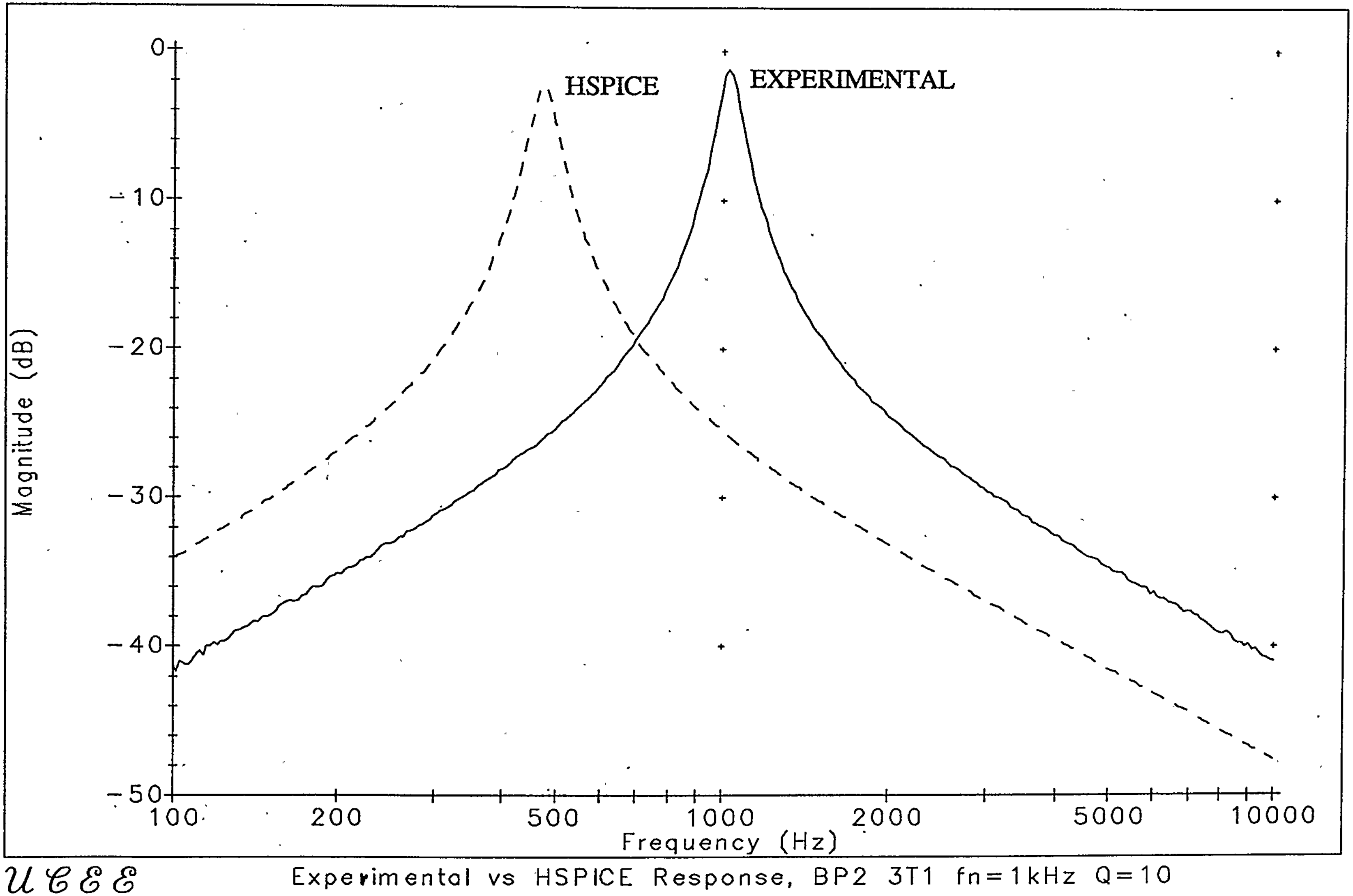

Figure 5.1 HSPICE Prediction of Bandpass II Performance

f_n = 1kHz and Q = 10. The technology file for HSPICE was provided by LTI [7], but does not appear to have been sufficient to enable satisfactory prediction of filter response.

Various methods were employed to bring the HSPICE prediction closer to that of the experimental results. The transistor parameters provided by LTI were changed, and a noticeable improvement was generated in this manner. However, as there was no theoretical basis for the changes made, this was not considered a practical solution. Temperature variation was also considered a possibility, but reasonable temperature variation in HSPICE did not account for the difference. It appears that the OTAs are just too sensitive to slight variations in the technology to allow for the use of standard CAD tools.

To show the adequacy of the design process developed here, filters were again designed using the Wilson Mirror OTA. The center frequency f_n was set to 1kHz for all the test designs and Q was varied from 5 to 20.

For all nine possible filter types the filter measurement results are shown in Figures 5.2 - 5.10. In all of these figures, graph (a) corresponds to a Q of 5 and graph (b) to a Q of 20. In the graphs the dotted line is the predicted performance using the equations developed in Chapter 4, and the solid line is the actual measured response. The measured center frequency magnitudes may not always be accurate. The measurement system allowed for only a limited number of data

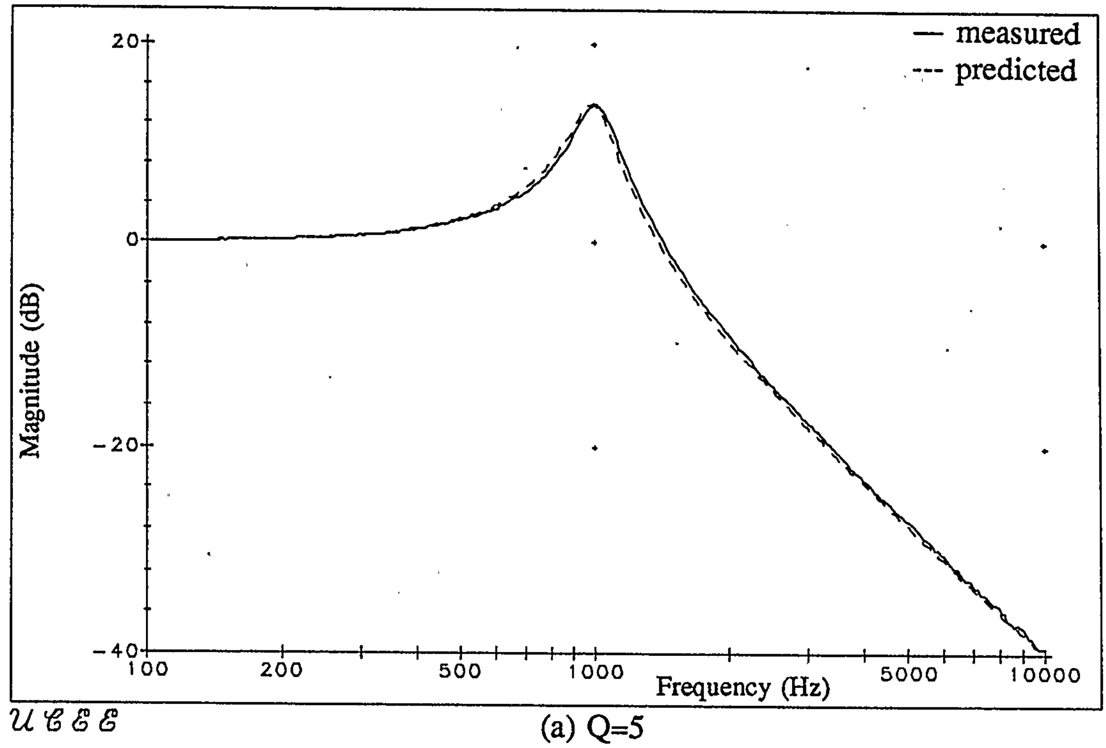

(a) Q=5

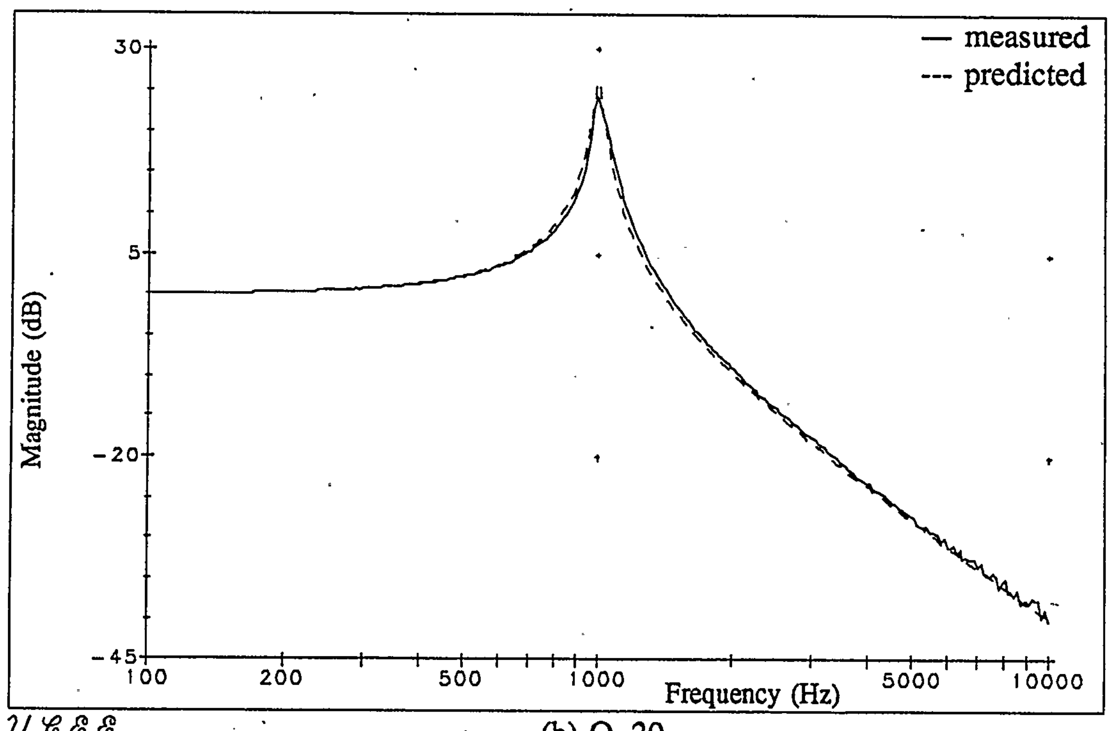

(b) Q=20

Figure 5.2 Lumped Model Prediction of 3T1 Lowpass Ia Performance

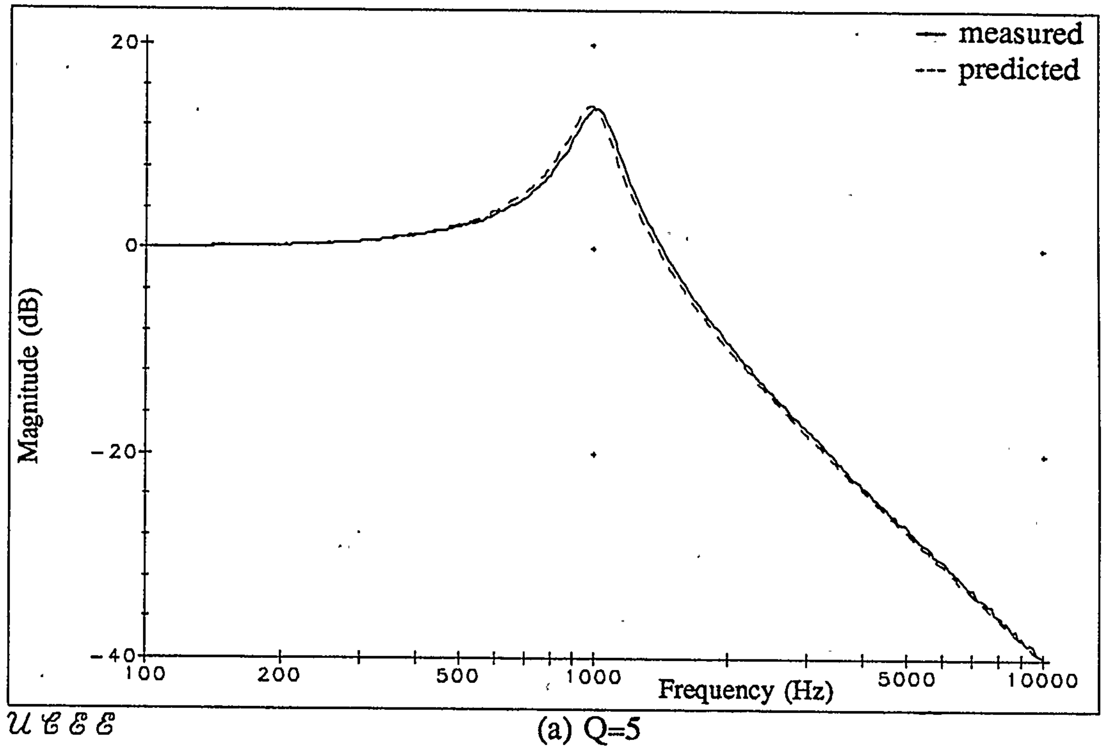

(a) Q=5

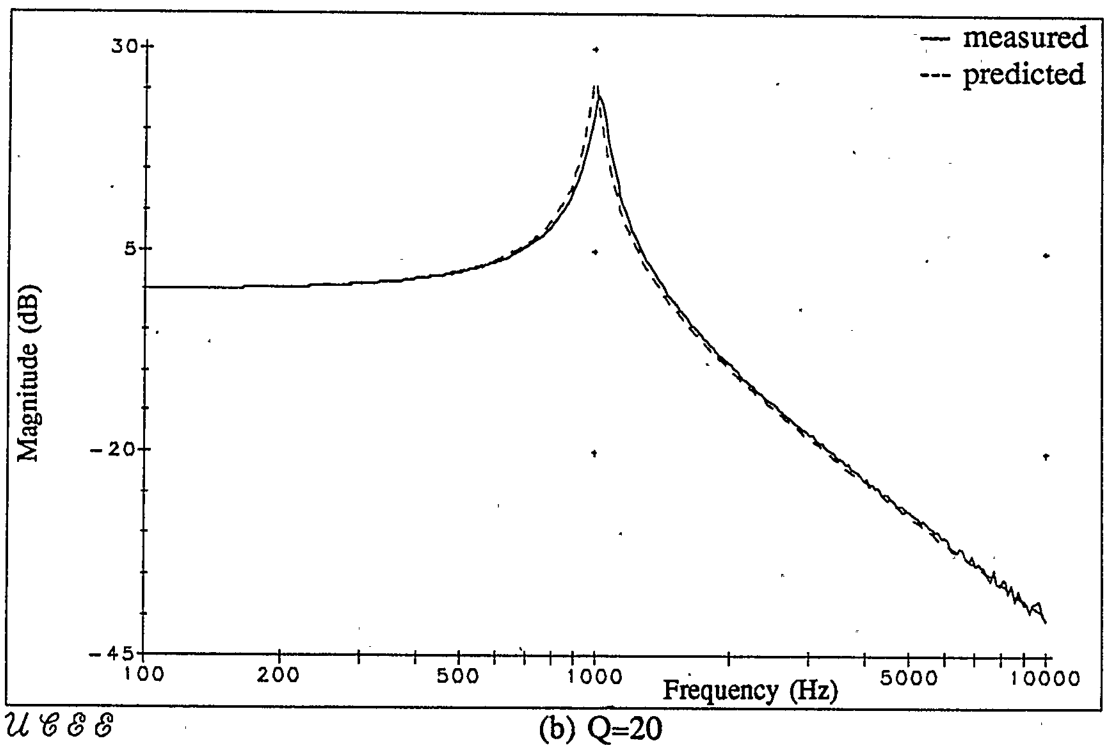

(b) Q=20

Figure 5.3 Lumped Model Prediction of 3T1 Lowpass Ib Performance

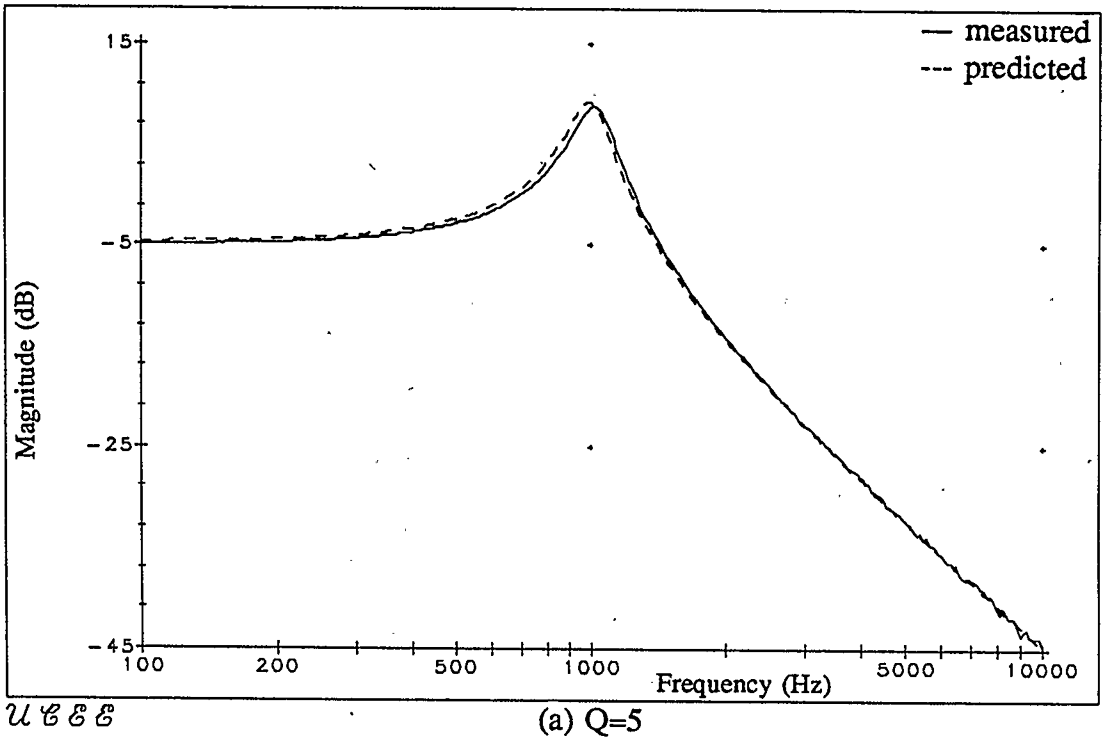

(a) Q=5

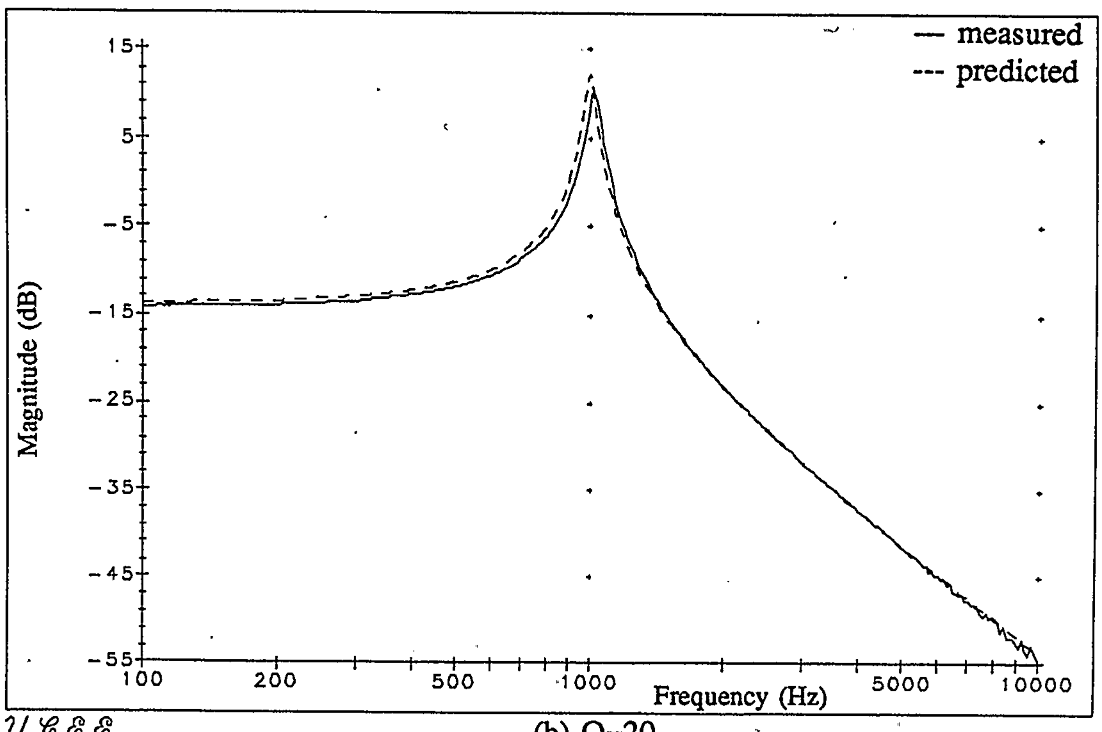

(b) Q=20

Figure 5.4 Lumped Model Prediction of 3T1 Lowpass II Performance

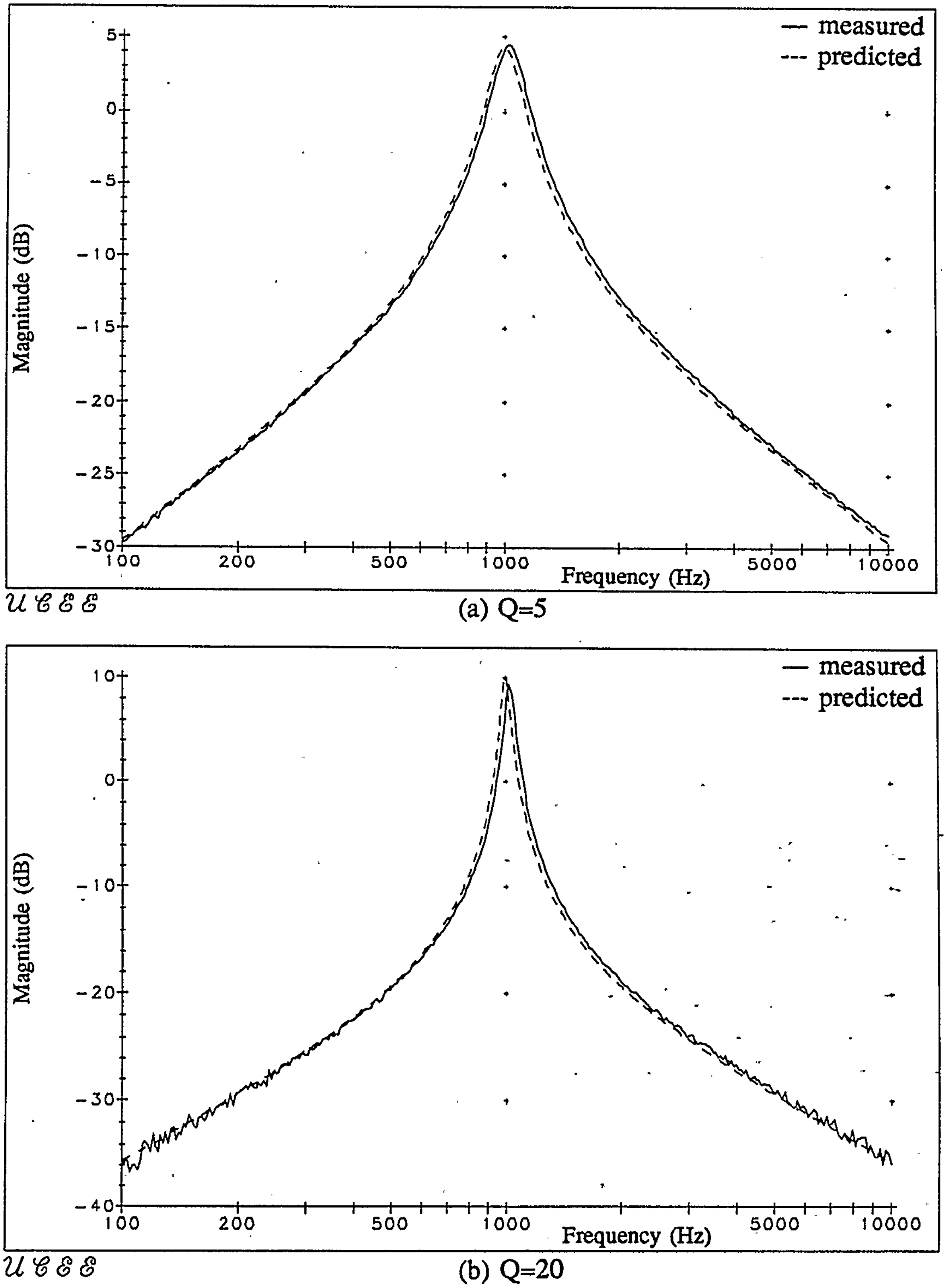

Figure 5.5 Lumped Model Prediction of 3T1 Bandpass Ia Performance

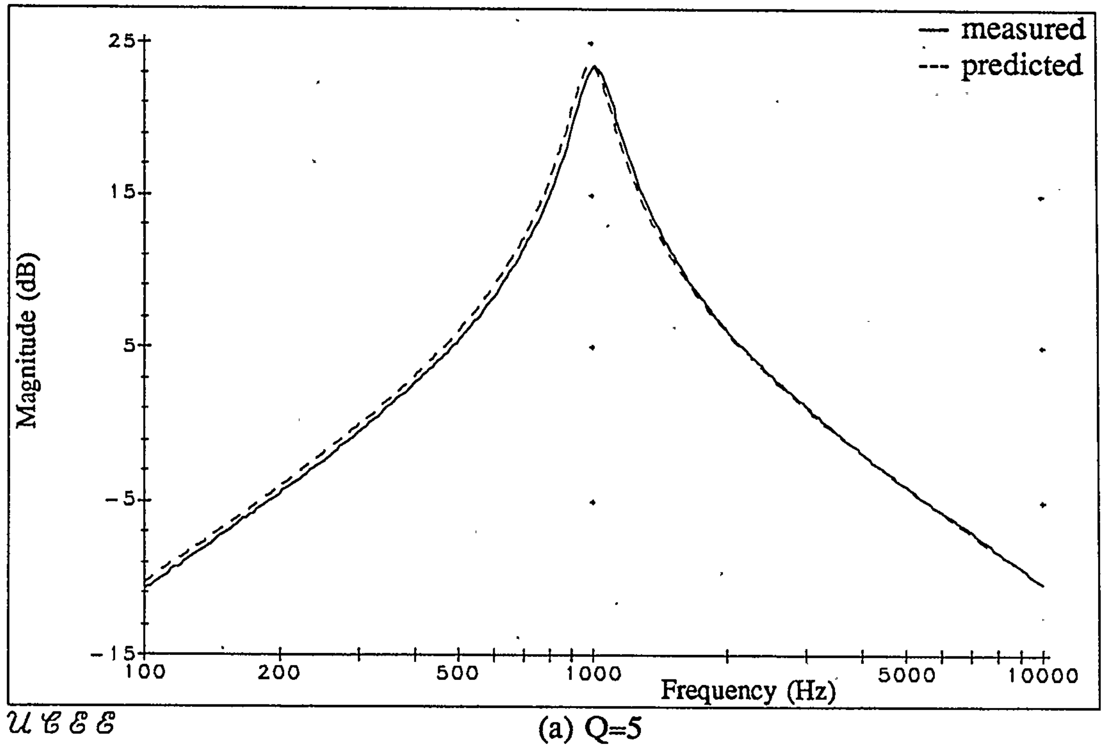

(a) Q=5

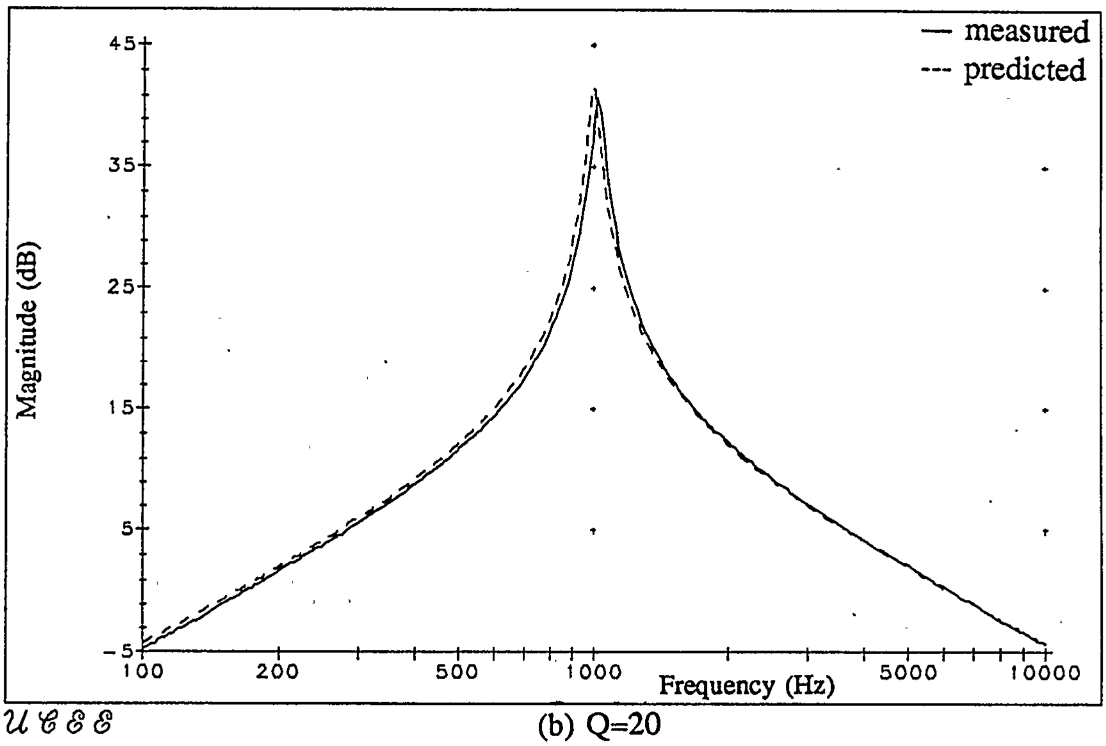

(b) Q=20

Figure 5.6 Lumped Model Prediction of 3T1 Bandpass Ib Performance

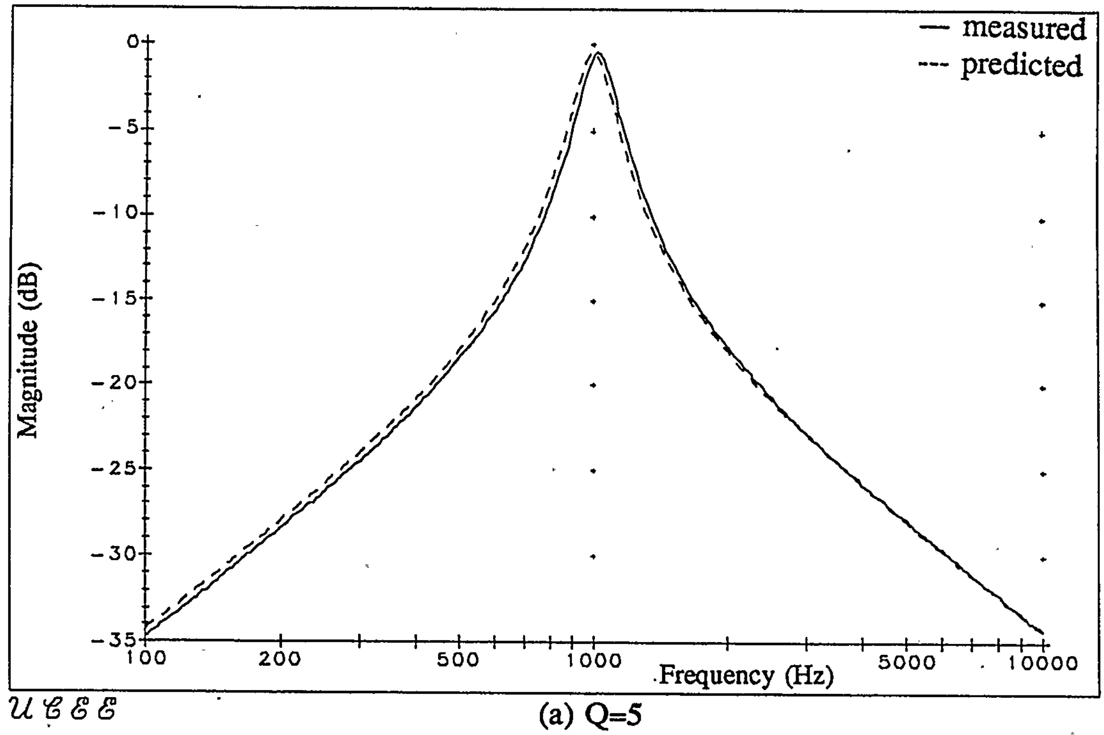

(a) Q=5

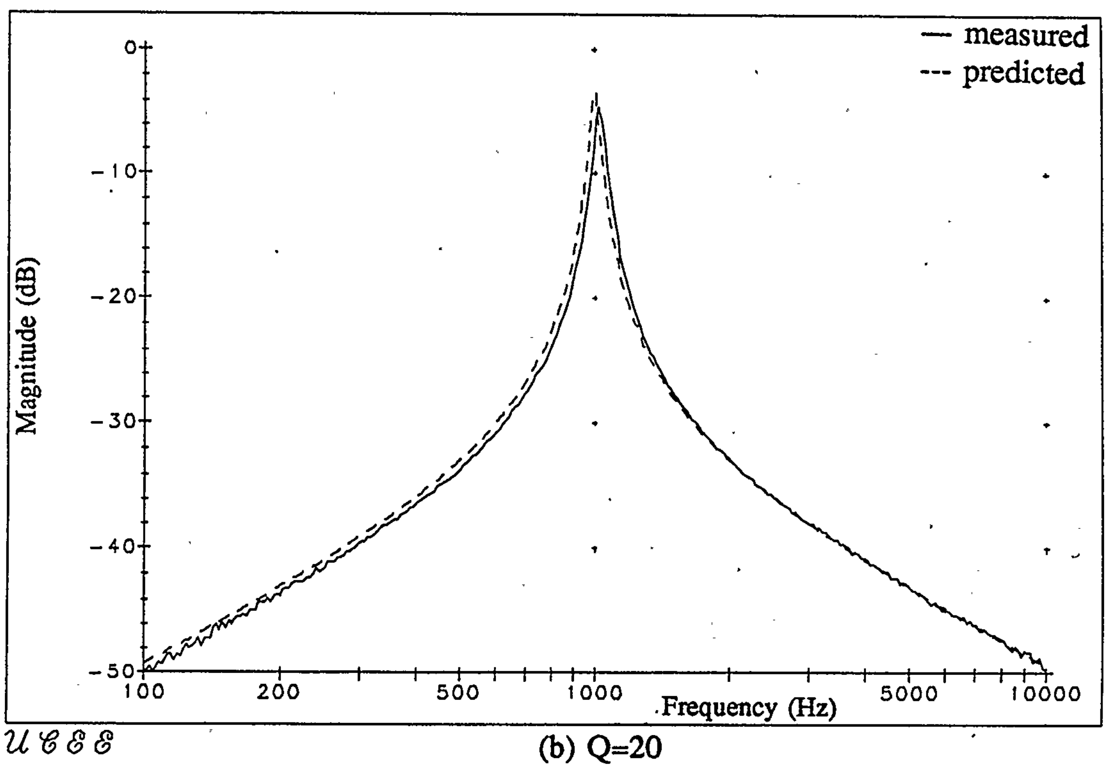

(b) Q=20

Figure 5.7 Lumped Model Prediction of 3T1 Bandpass II Performance

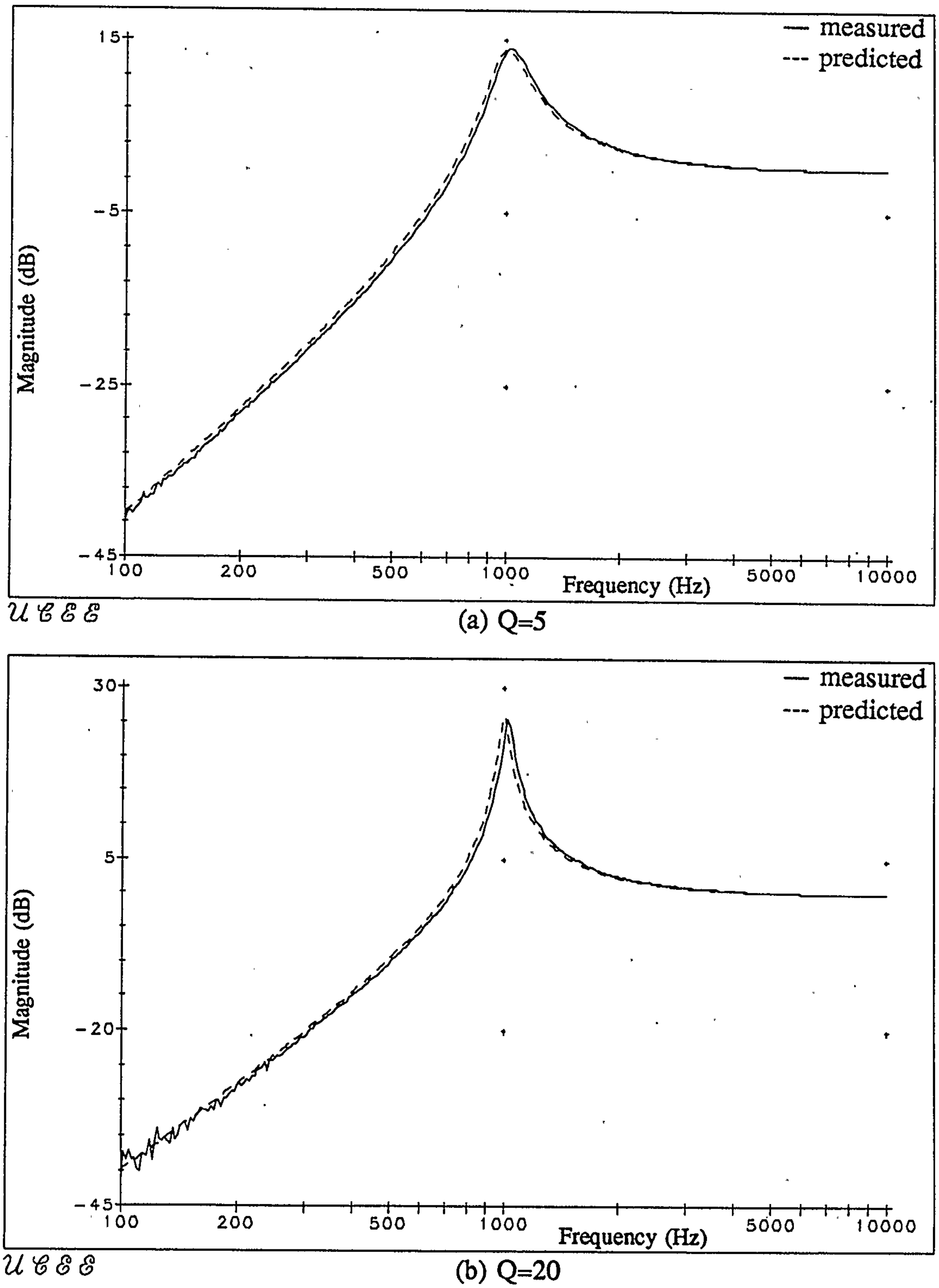

Figure 5.8 Lumped Model Prediction of 3T1 Highpass Performance

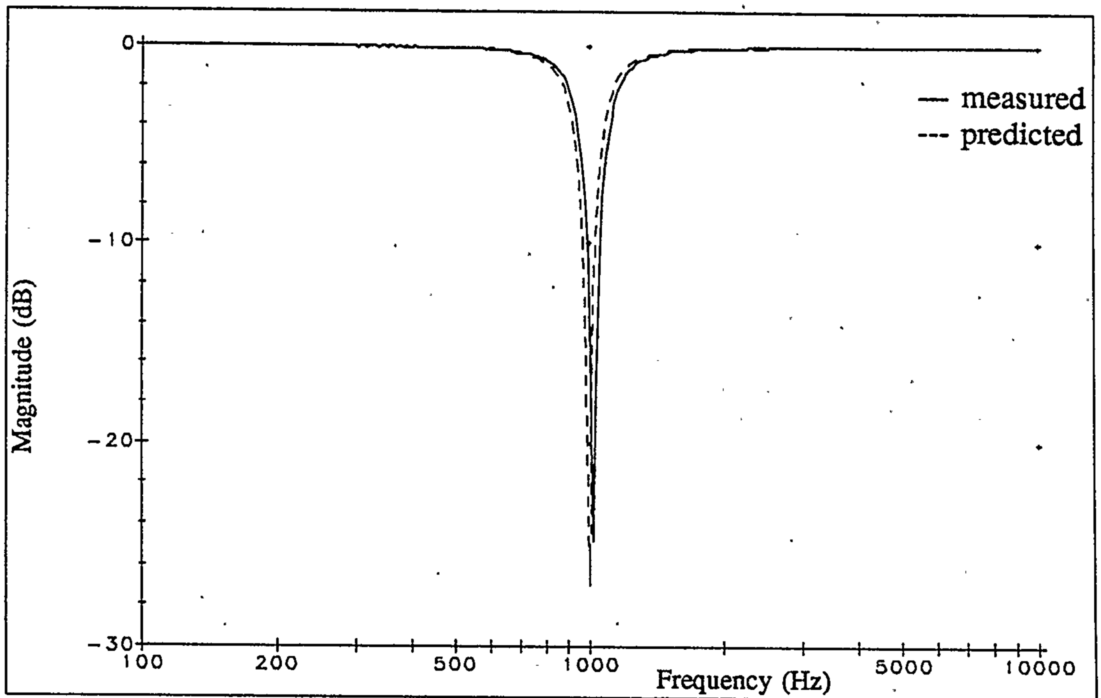

𝒰𝒞ℰℰ

(a) Q=5

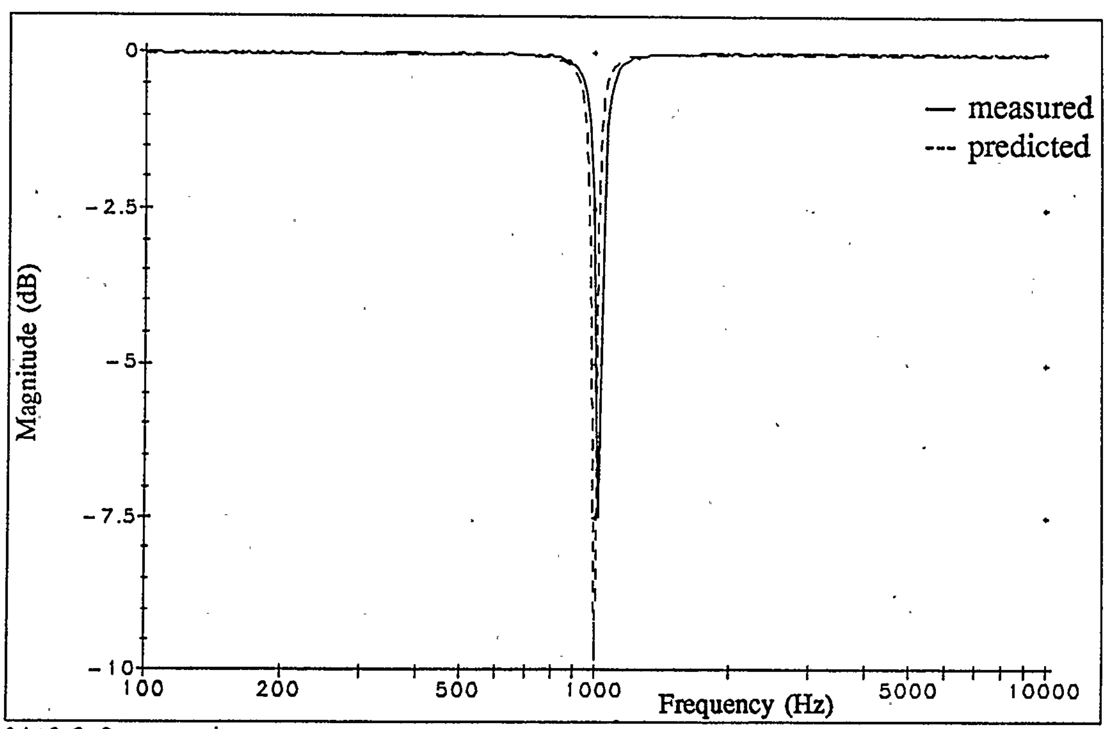

𝒰𝒞ℰℰ

(b) Q=20

Figure 5.9 Lumped Model Prediction of 3T1 Notch a Performance

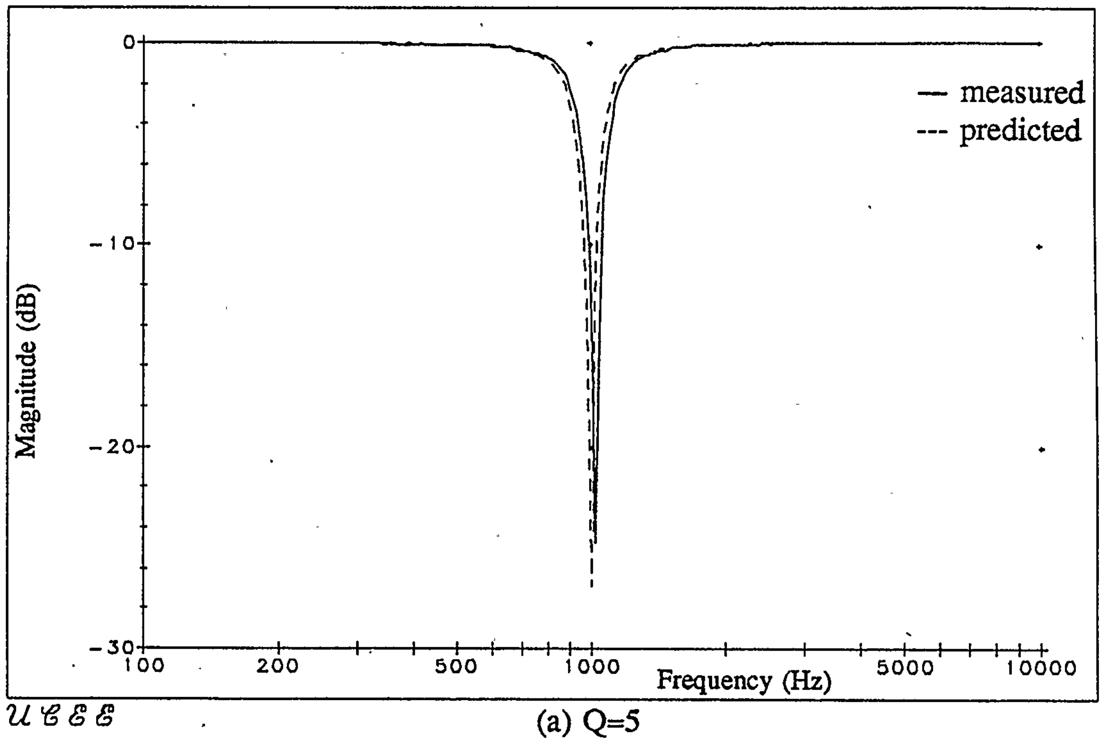

(a) Q=5

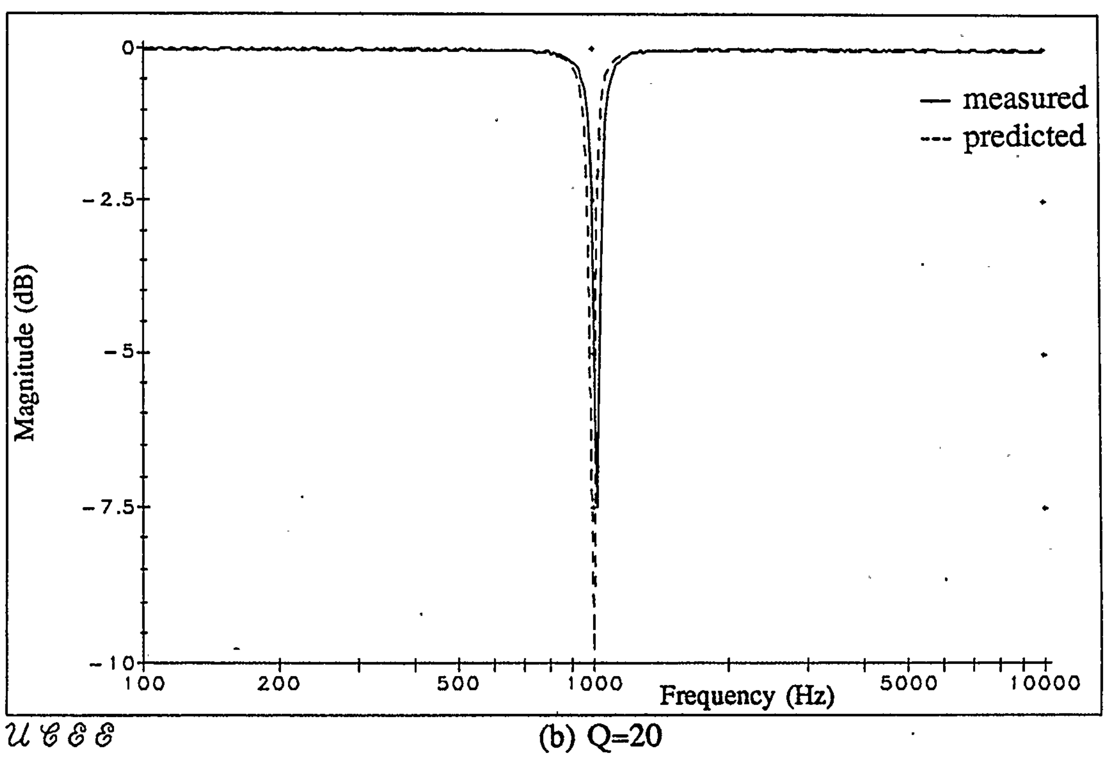

(b) Q=20

Figure 5.10 Lumped Model Prediction of 3T1 Notch b Performance points, and it was not possible to make sure that one fell at exactly the center frequency. With the sharp variation in magnitude around the center frequency, especially in the case of notch filters, the apparent center frequency magnitude is likely to be somewhat different from that actually achieved.

It becomes evident after inspection of these graphs that the predicted performance can be up to around 4% different from the actual performance. While this is much better than the HSPICE prediction, and is small enough that it can be eliminated through tuning, or even neglected, it is relevant to determine what causes it. Through closer inspection of the OTA parameter plots shown in Chapter 3, specifically those of transconductance (Figure 3.2), the error bars, which represent the maximum and minimum values measured, while not overly large, actually correspond to a variation of up to 10%. If the transconductance of the OTA's are 5% different (the prediction uses the average) from those used in the prediction, it is quite possible to get the errors noticed above.

It is unfortunate, but there is very little that can be done to rectify this problem. The variation in OTA parameters is mainly due to process variations, over which there is little control. Specifications for commercial OTA's, such as the CA3080 [10], predict the possibility of up to 100% variation in the value of g_m for the same bias current. With such inaccuracies in the implementation technology for OTA's, the only complete solution is to measure accurate parameter variation for all of the OTA's used in a design and there after use only those OTA's. This is hardly an acceptable solution, as parameter measurement is extremely time consuming.

With this in mind, the best solution appears to be to separately tune each filter circuit after it has been designed and built. Some possibility exists of integrating a compensation circuit onto the chip with the OTA's. The increase in complexity required by this, and the need for recalibration of all the parameter measurements, limits this approach to those applications which are highly demanding.

Another possible source of variation is that due to the temperature sensitivity of the OTA. The transconductance of an OTA is inversely proportional to temperature [4]. Since ω_n is directly proportional to g_m (Eqn. 4.12) it follows that it must be inversely proportional to temperature as well. The equation for Q (Eqn 4.13) shows that the variations of g_m will cancel, and only negligible variations of Q will result from the non-idealities. This is shown to be the case in the plot of Figure 5.11.

Such a result can also be predicted theoretically. Manipulation of equation 3.5 allows for an estimate of the center frequency variation due to temperature change. A temperature change from 25°C to 75°C corresponds to approximately a 14% variation in the center frequency by such a method. The actual variation for such a range shown in Figure 5.11 is closer to 10%. The difference is most likely due to temperature variation of OTA parameters not taken into account by equation 3.5 and due to slight variation in the bias chain which sets the operating point. Prediction of this effect would require measurement of all OTA parameters over the full temperature range, and was not practical to do.

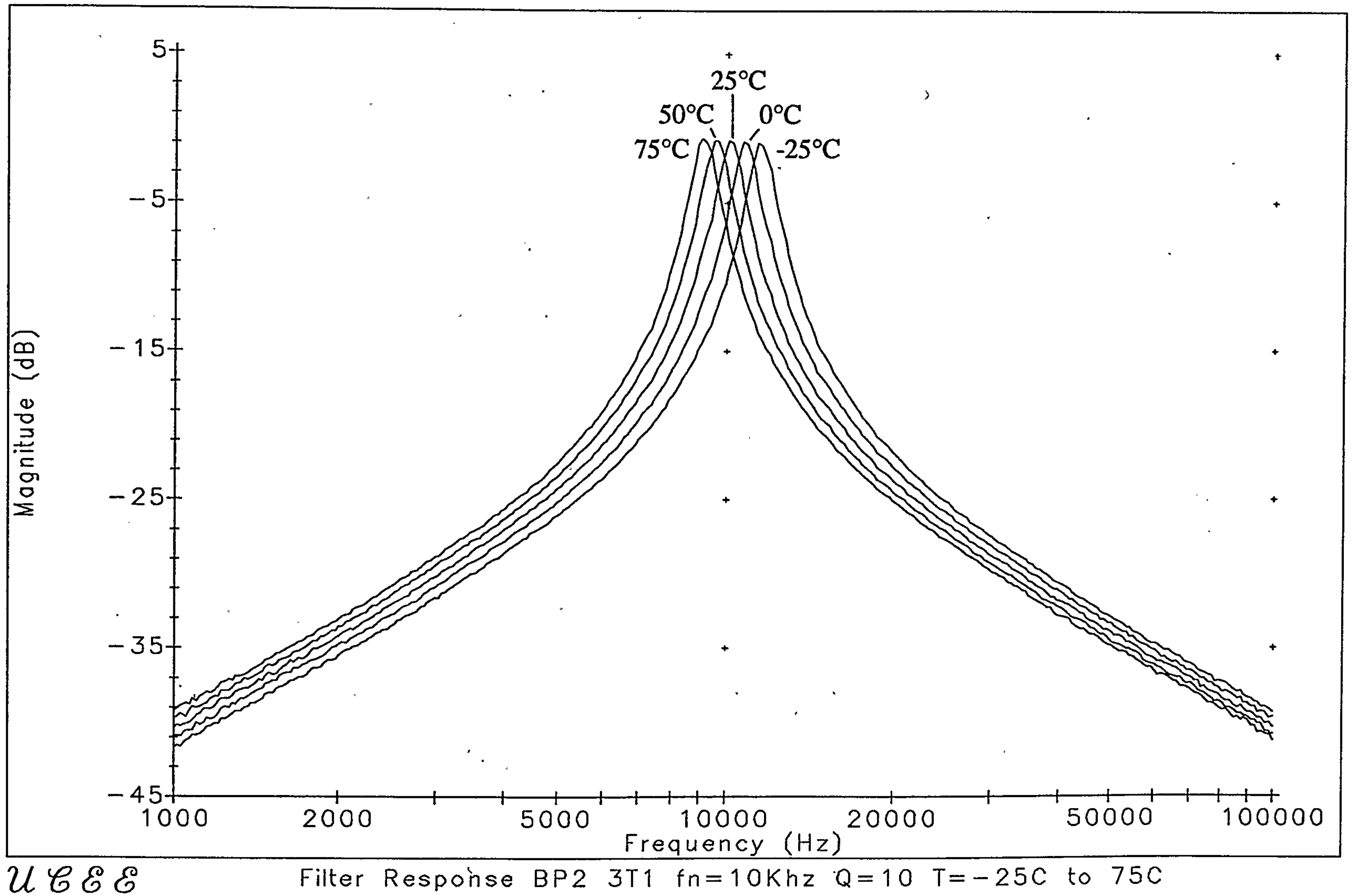

Figure 5.11 Temperature Variability of Biquad Filter Response

Again, it is possible to create compensation circuitry for the temperature variation, and many such circuits have been proposed [11]-[12]. Unfortunately, the operation of such circuitry is usually quite complex and often has stability problems. Other graduate students are researching this problem currently and have chips under manufacture. For now, it is sufficient to realize that such a problem exists. It is for this reason that the filter circuits were installed in an oven to enable the elimination of temperature variation during the measurements.

5.2 Performance of OTA Based Biquad Filters

To properly test the performance of the biquad filter structure it is necessary to vary its operating parameters as much as practical. However, the large quantity of plots this produces, precludes the inclusion of all of them here. With this in mind, it was decided that only six of the nine possible filter structures would be necessary. The selection was made as follows. The two type I bandpass filters give essentially the same response, so only one was included. Similarly, only one of the type I lowpass filters was necessary. And finally, the notch filters are so similar that only one was included. The type II bandpass and lowpass filters were included to show type II filter response, and the highpass filter was included to show highpass response.

To show the flexibility of these filters they were configured for three different center frequencies (1kHz, 10kHz, 100kHz) and for three different Q's (5, 10, 20). For each OTA, this will require 18 different plots (six filter types times three frequencies). As there are seven OTA types, it again becomes impractical to show the results for all OTA types, and is not really necessary. The majority of filter designs will use the best structure possible.

To choose the best OTA structure for building biquad filters it is necessary to define what is meant by best. As was indicated earlier, the definition of best rests on the tradeoff between size and performance. If minimum size is required, performance is likely to be sacrificed somewhat. If maximum performance is desired, the size is likely be larger. As the OTA's can be split into two categories based upon size, those requiring two cells and those requiring only one, the optimal OTA's of both size categories will best show the performance capabilities of these filters.

From consideration of the plots and tables of Chapter 3 the choice of the best OTA's can be made. The overall best OTA is that using only Wilson mirrors, and which requires two cells. It thus remains to choose a single cell OTA. Again considering the plots and tables of Chapter 3, it was determined that the modified Wilson mirror configuration is somewhat better than the other single cell designs. Thus, the two OTA's chosen for the filter evaluation were the Wilson mirror OTA (Figure 2.12) and the modified Wilson mirror OTA (Figure 2.14).

The results of the filter performance capabilities for the Wilson mirror OTA are shown in Figures 5.12 - 5.14. Those for the modified configuration are shown in Figures 5.15 - 5.17. In each figure there are six plots, labeled from a to f, corresponding to the six different filter types chosen (lowpass Ia, lowpass II,

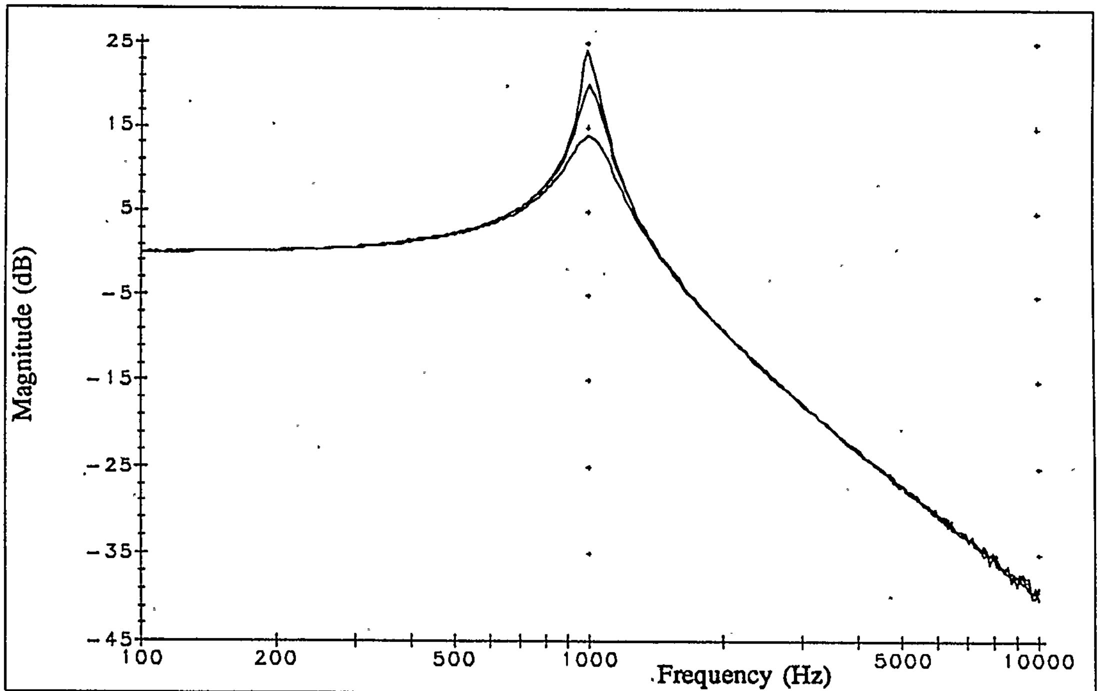

UCEE (a) LP1a 1kHz Q=5,10,20

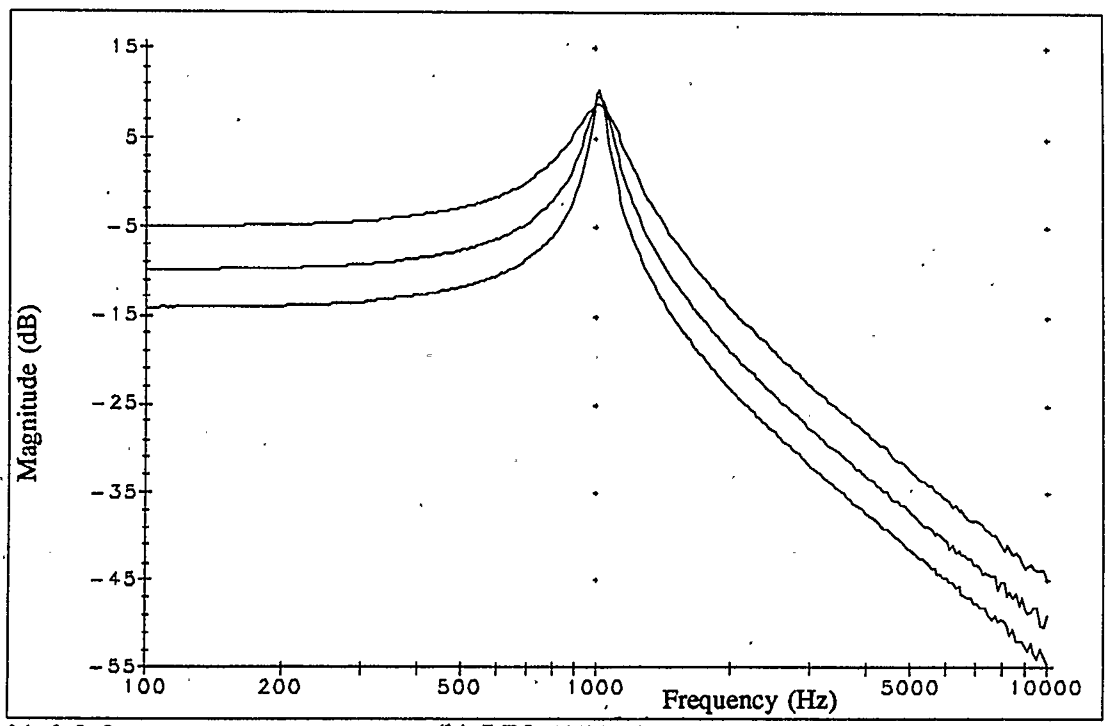

UCEE (b) LP2 1kHz Q=5,10,20

Figure 5.12 1kHz Filter Response Using Wilson Mirror OTA's

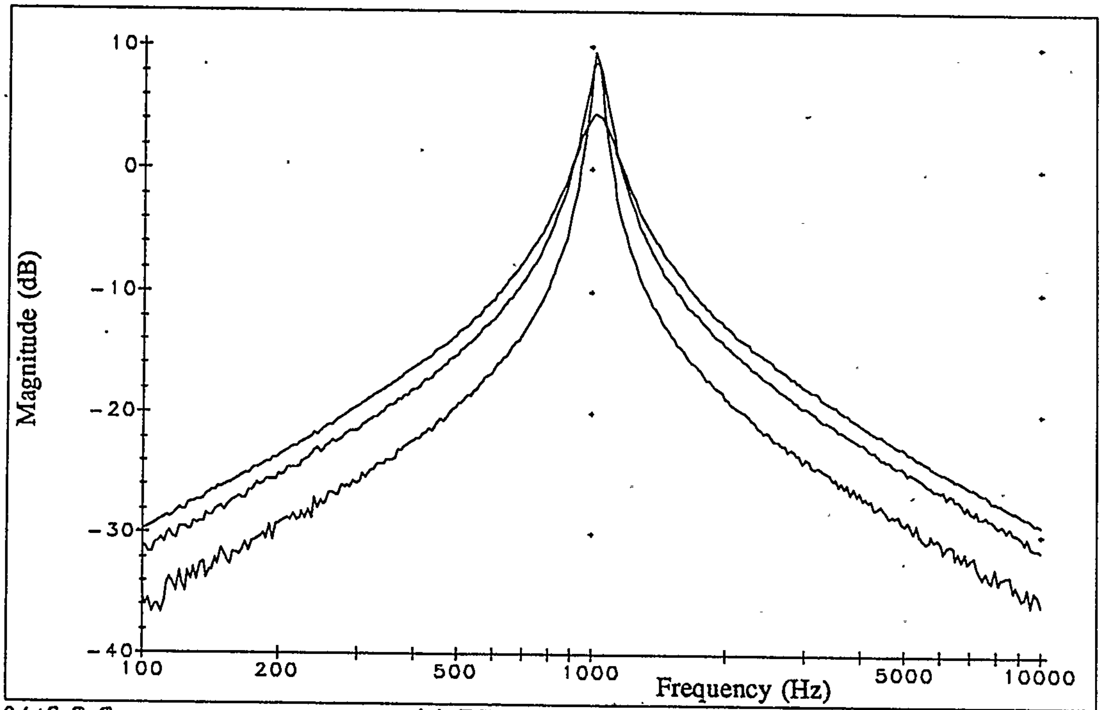

𝒰𝒞ℰℰ (c) BP1a 1kHz Q=5,10,20

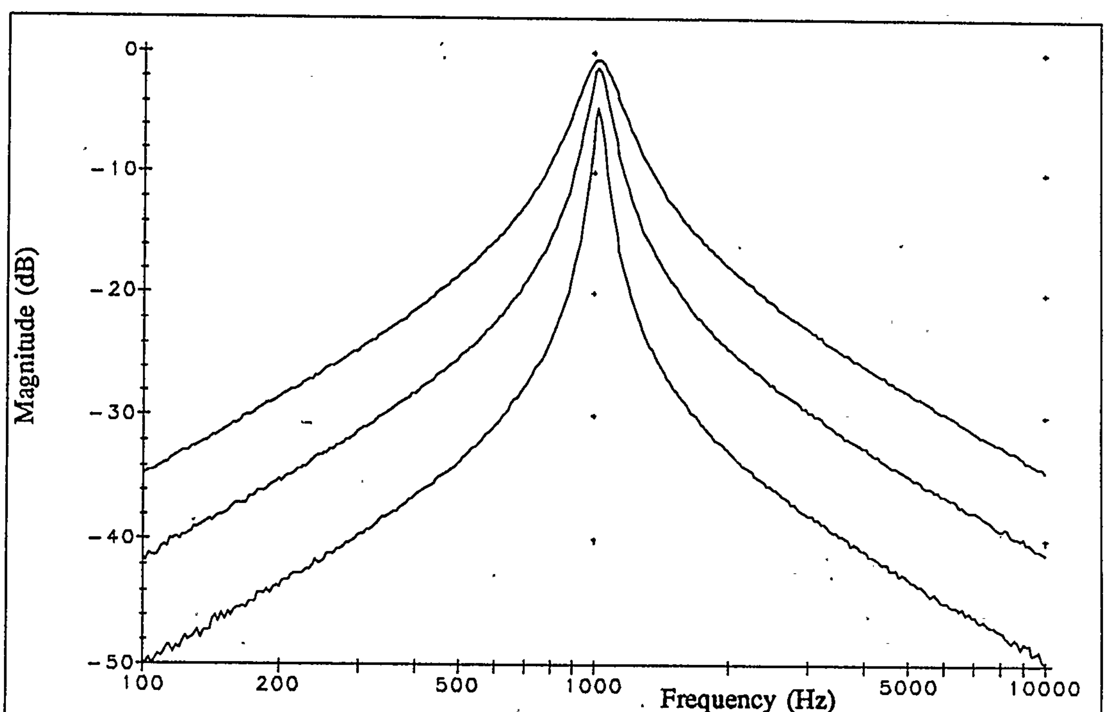

𝒰𝒞ℰℰ (d) BP2 1kHz Q=5,10,20

Figure 5.12 Continued

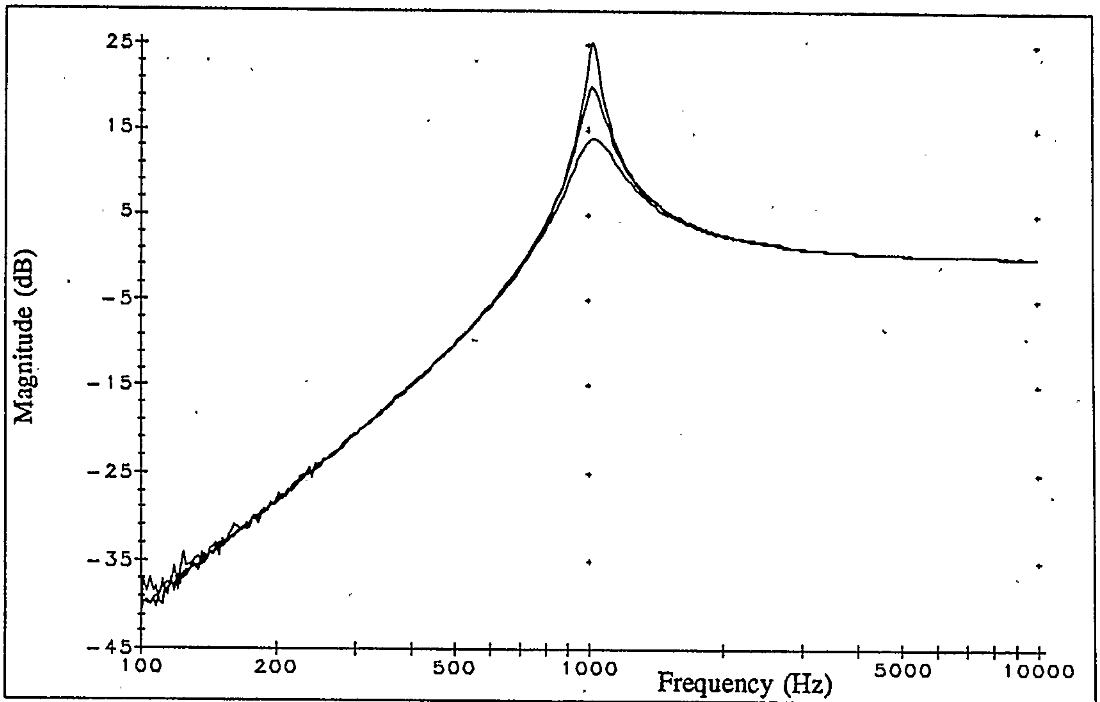

UCEE

(e) HP 1kHz Q=5,10,20

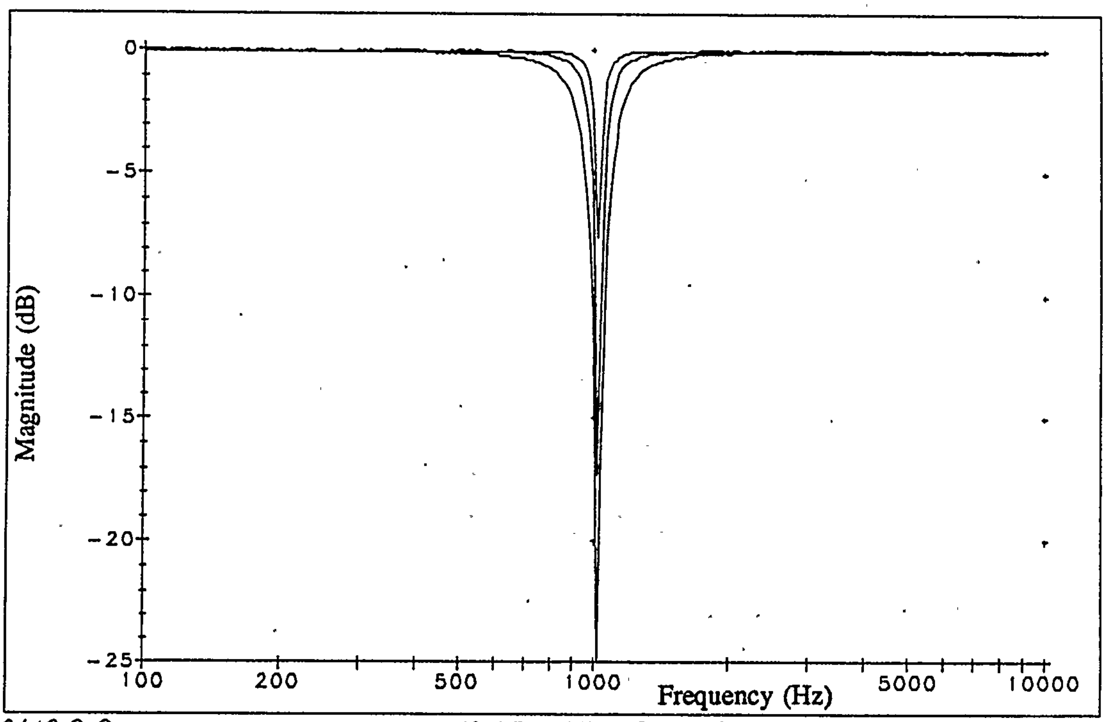

UCEE

(f) Na 1kHz Q=5,10,20

Figure 5.12 Continued

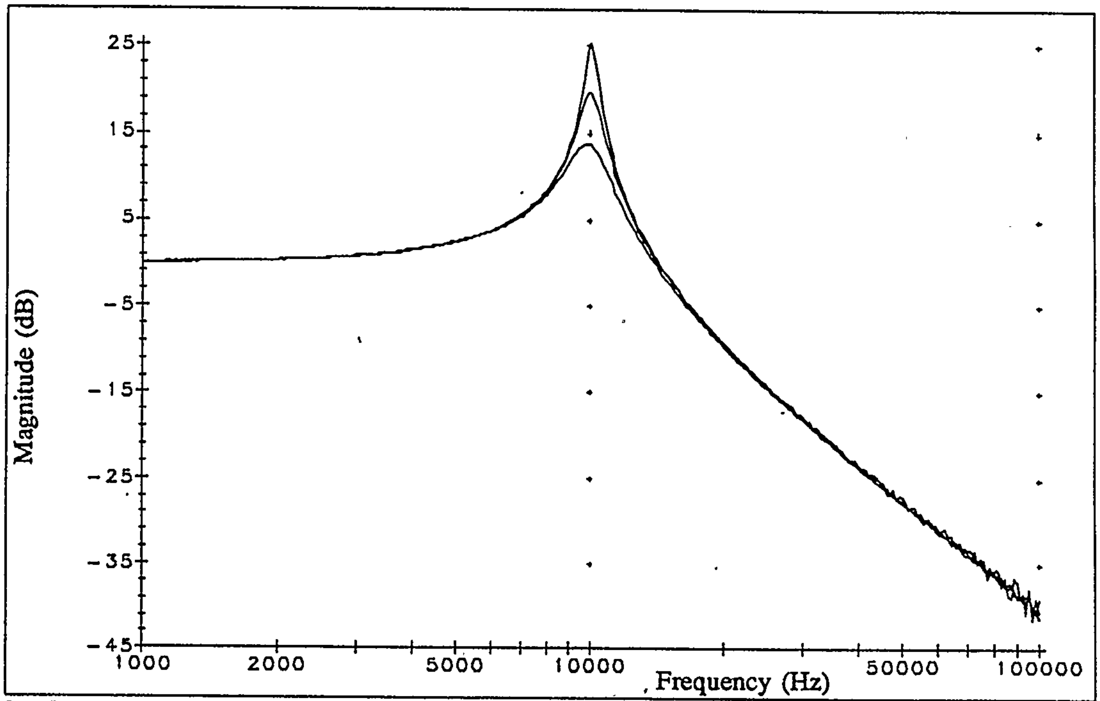

(a) LP1a 10kHz Q=5,10,20

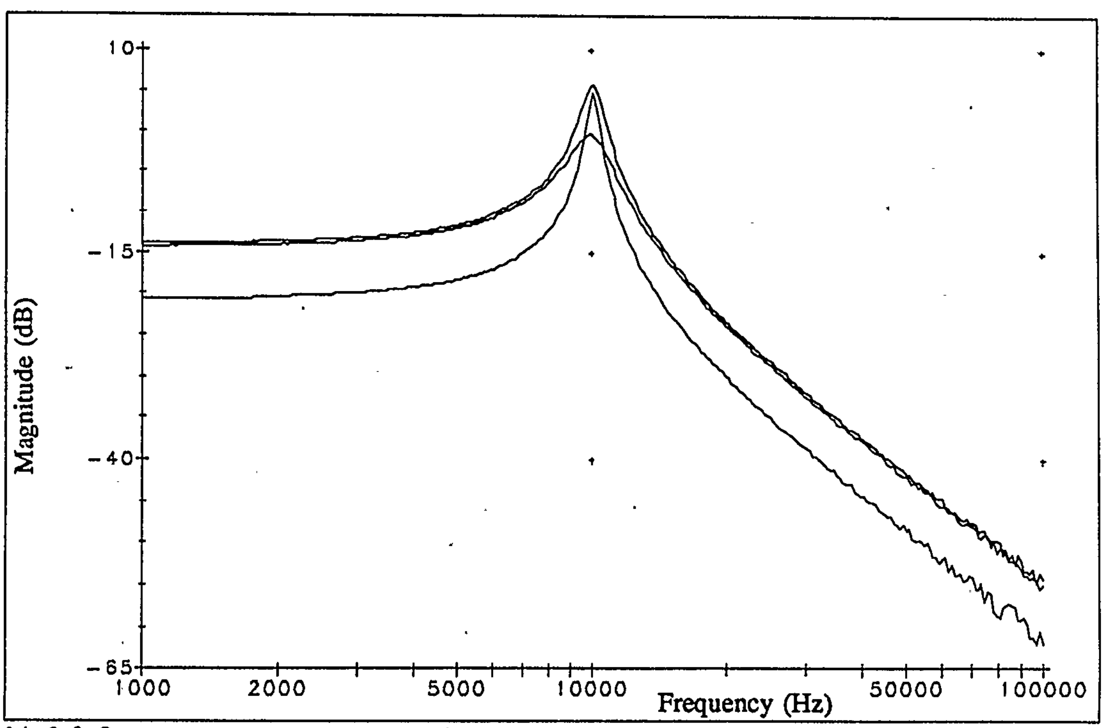

(b) LP2 10kHz Q=5,10,20

Figure 5.13 10kHz Filter Response Using Wilson Mirror OTA's

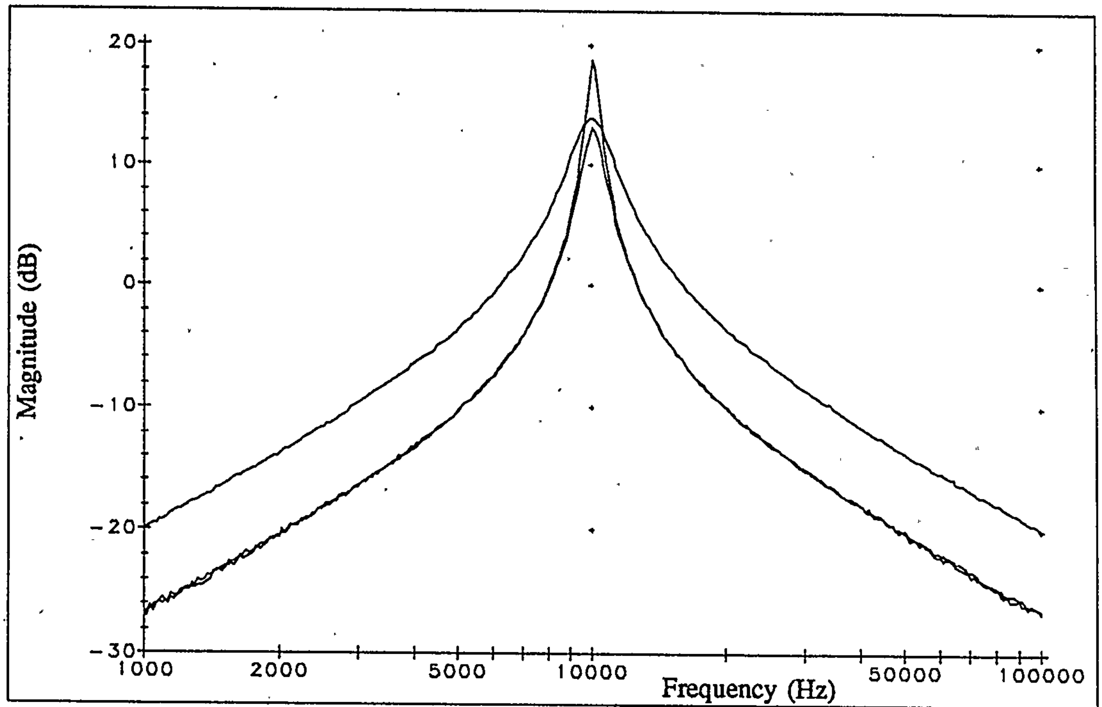

𝒰𝒞ℰℰ (c) BP1a 10kHz Q=5,10,20

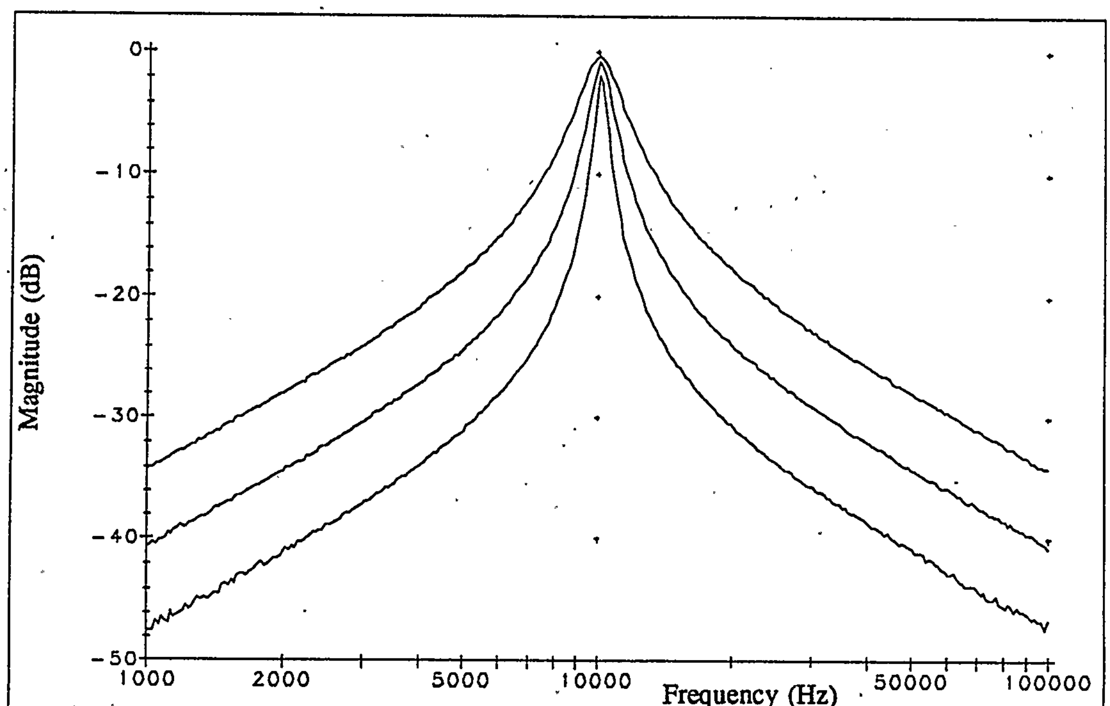

𝒰𝒞ℰℰ (d) BP2 10kHz Q=5,10,20

Figure 5.13 Continued

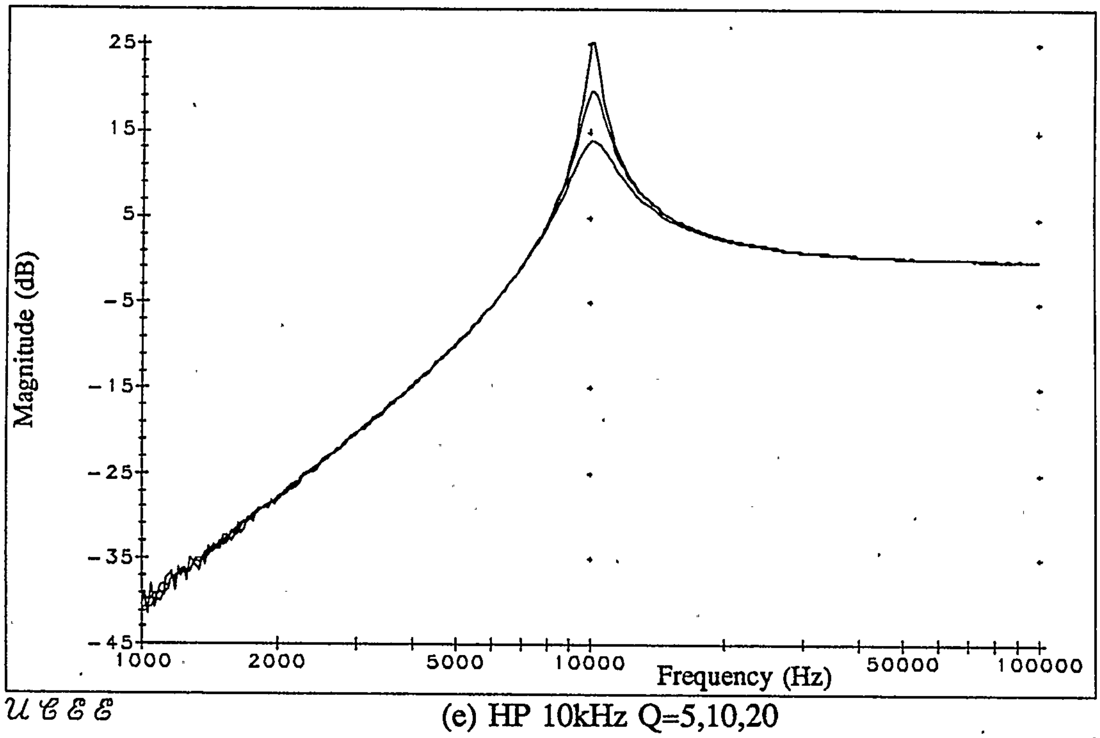

(e) HP 10kHz Q=5,10,20

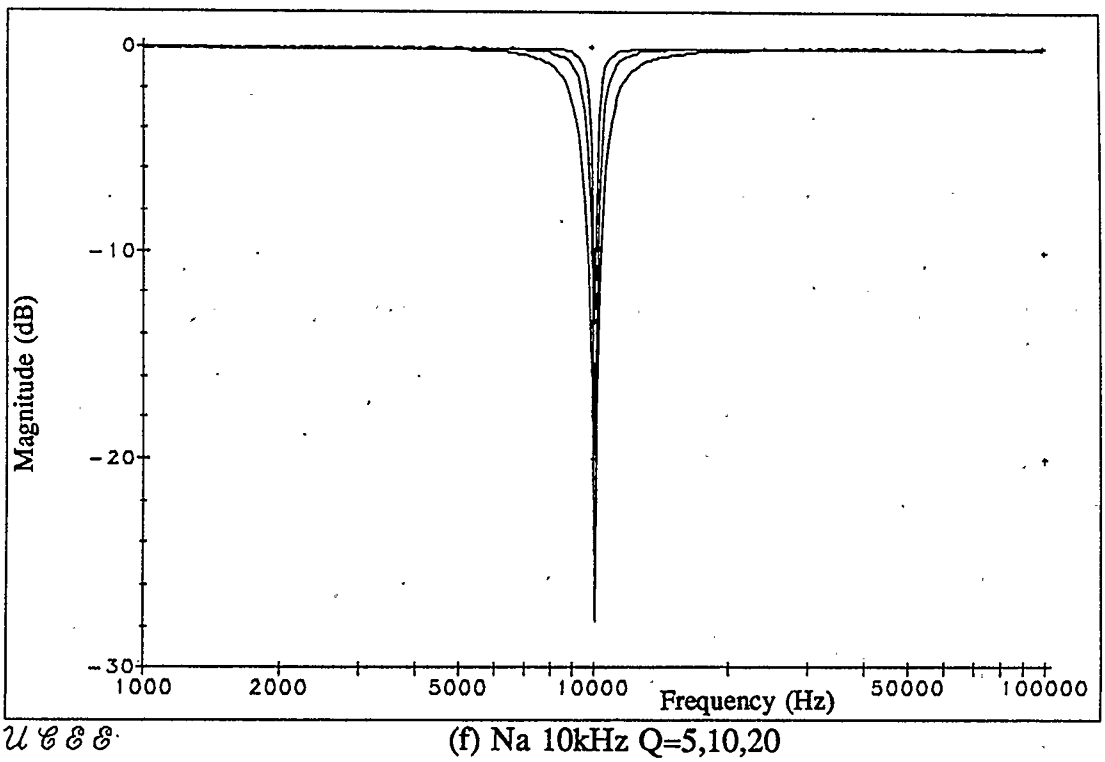

(f) Na 10kHz Q=5,10,20

Figure 5.13 Continued

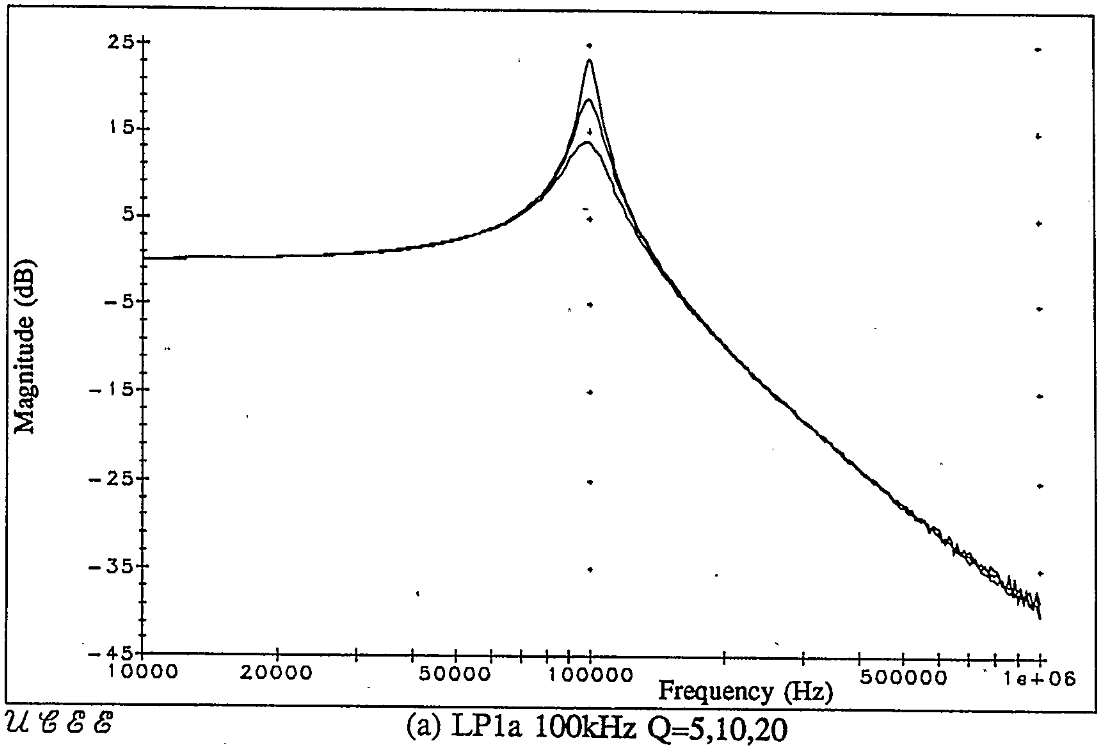

(a) LP1a 100kHz Q=5,10,20

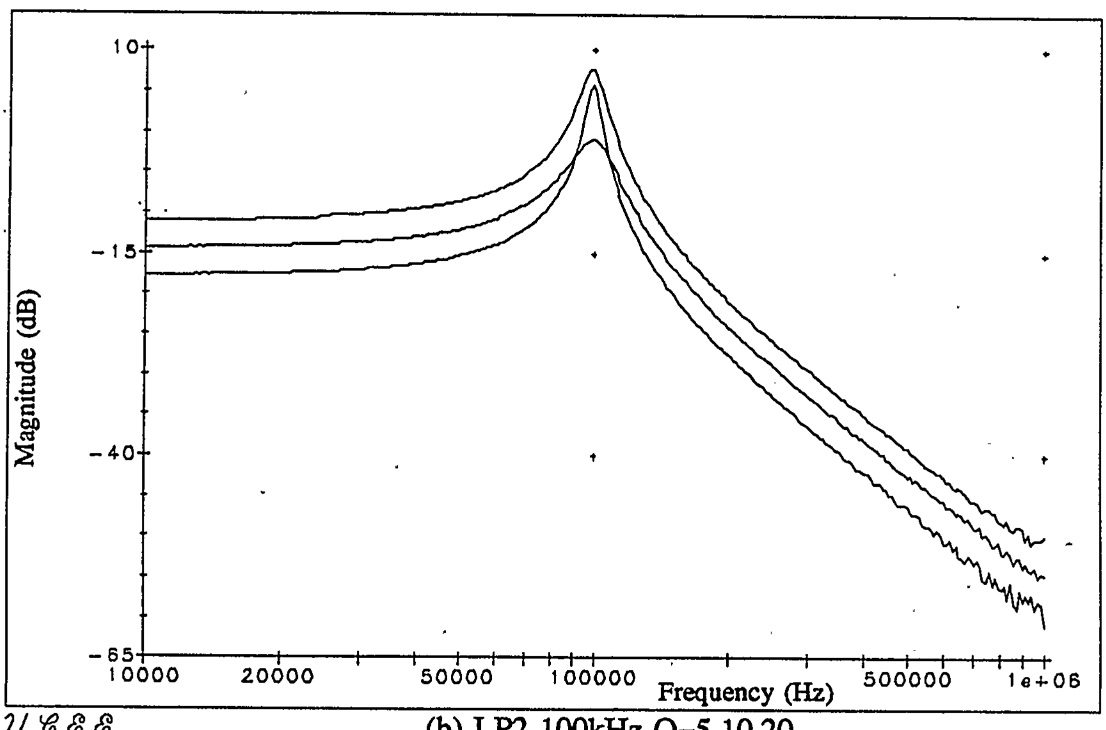

(b) LP2 100kHz Q=5,10,20

Figure 5.14 100kHz Filter Response Using Wilson Mirror OTA's

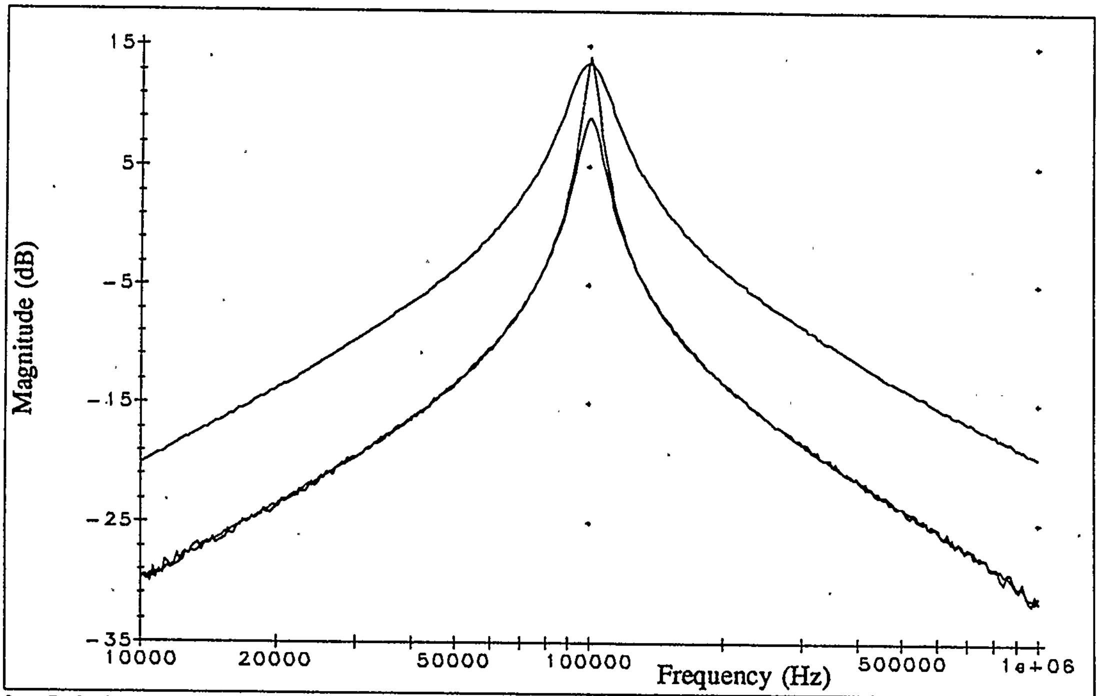

UCEE (c) BP1a 100kHz Q=5,10,20

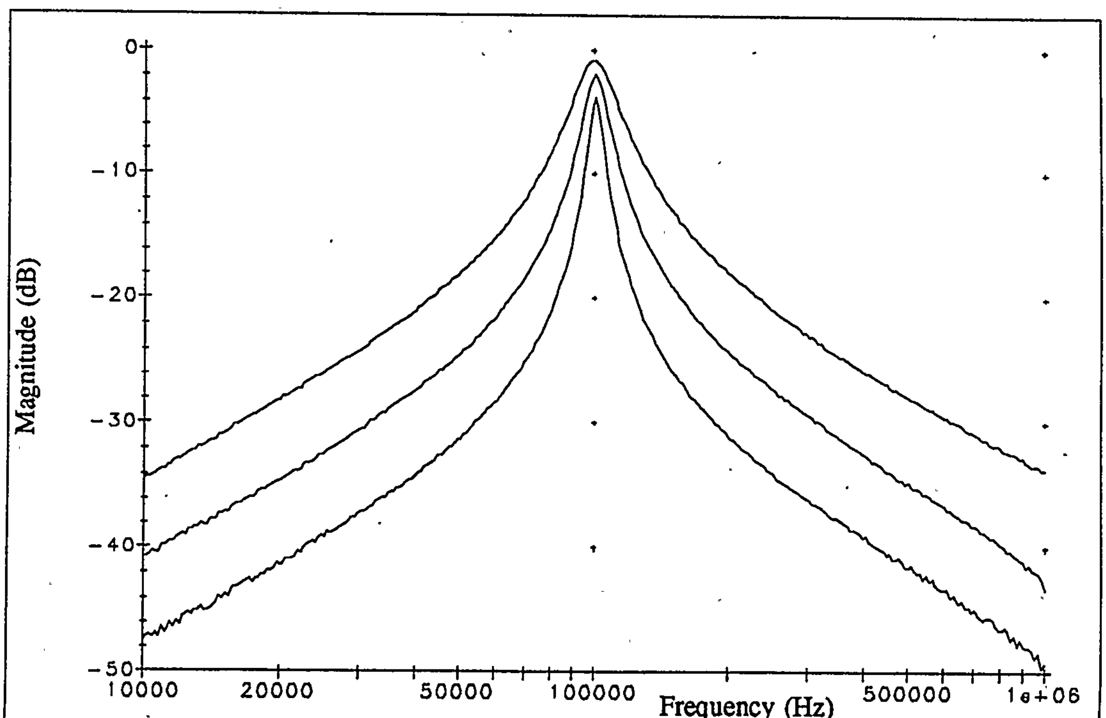

UCEE (d) BP2 100kHz Q=5,10,20

Figure 5.14 Continued

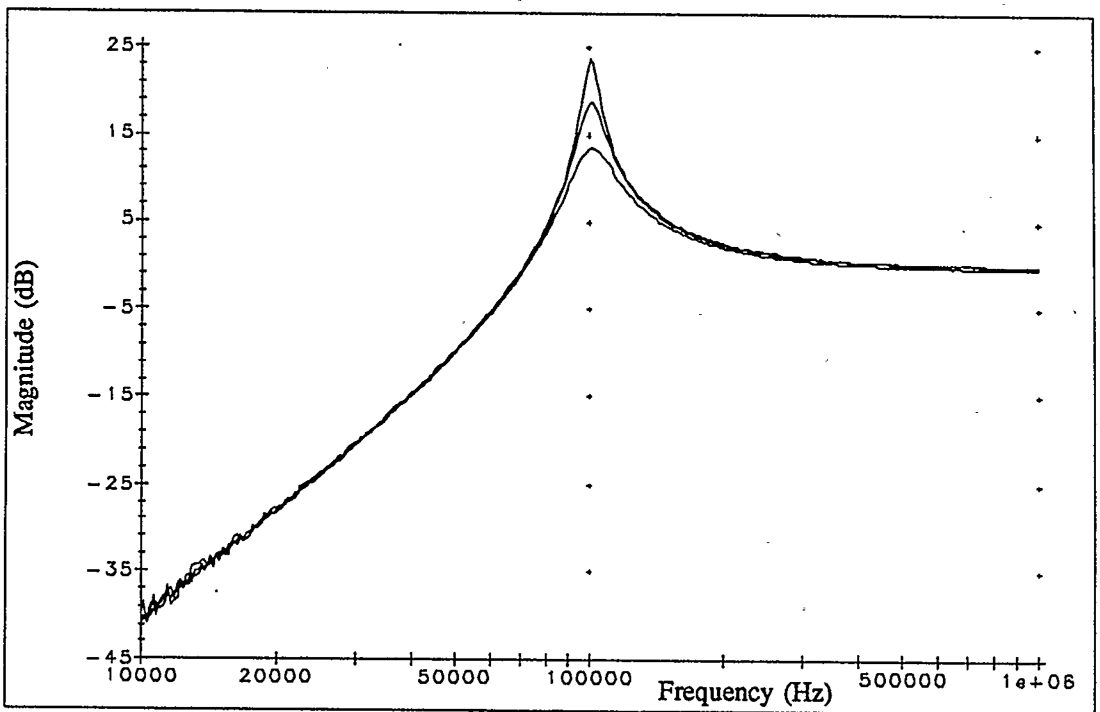

UCEE (e) HP 100kHz Q=5,10,20

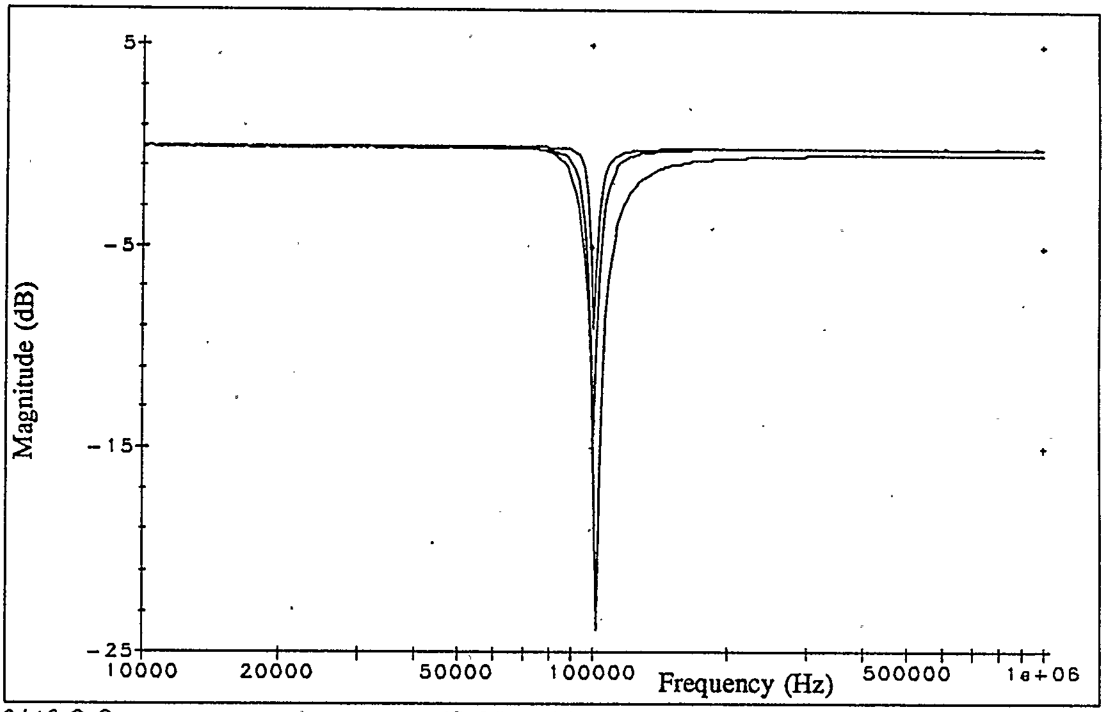

UCEE (f) Na 100kHz Q=5,10,20

Figure 5.14 Continued

bandpass Ia , bandpass II, highpass and notch a, respectively). Each plot shows a family of curves corresponding to a Q variation of 5, 10, and 20.

5.3 Evaluation of Filter Performance

Several details can be noticed from examination of the plots of filter performance. The difference between the type I and type II lowpass and bandpass filters can be seen to be the behaviour at the center frequency with changes in filter Q. Type I filters have varying gain at the center frequency, while type II filters maintain almost unity gain. Ideally, type I filters would have linearly increasing gain with increasing Q and type II filters would have exactly unity gain at the center frequency [2], but this can be seen not always to be the case. However, the algorithms developed in Chapter 4 predict such a performance quite well (see Figures 5.2 - 5.10).

While the Wilson mirror OTA's are by far the best in theory, when integrated into the biquad filters, the modified Wilson mirror OTA's perform equally well. Non-ideal variation of center frequency magnitude is due to variation of capacitor values with Q. For these filter designs it is often not practical to keep the capacitor values constant, especially at low frequencies, because of the limited range of transconductance values. However, in some of the filter types the output magnitude is relative to capacitor value, so variation of capacitor values will effect the results obtained from those filters. Even though they are not ideal, all of the results achieved are well predicted by the algorithms developed in Chapter 4.

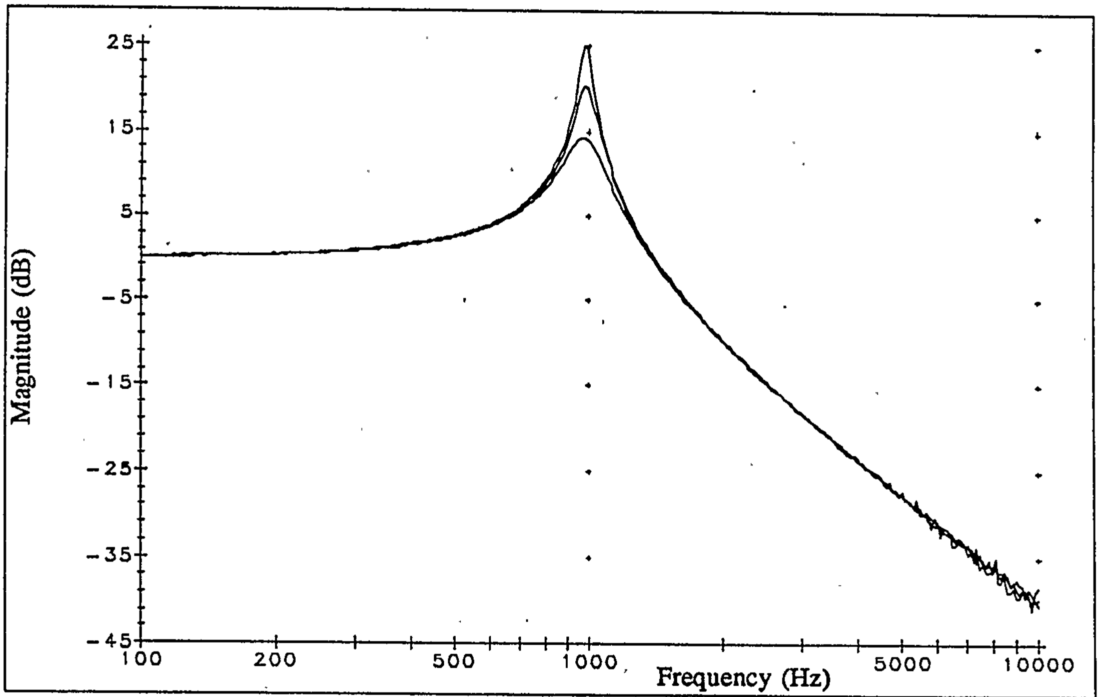

(a) LP1a 1kHz Q=5,10,20

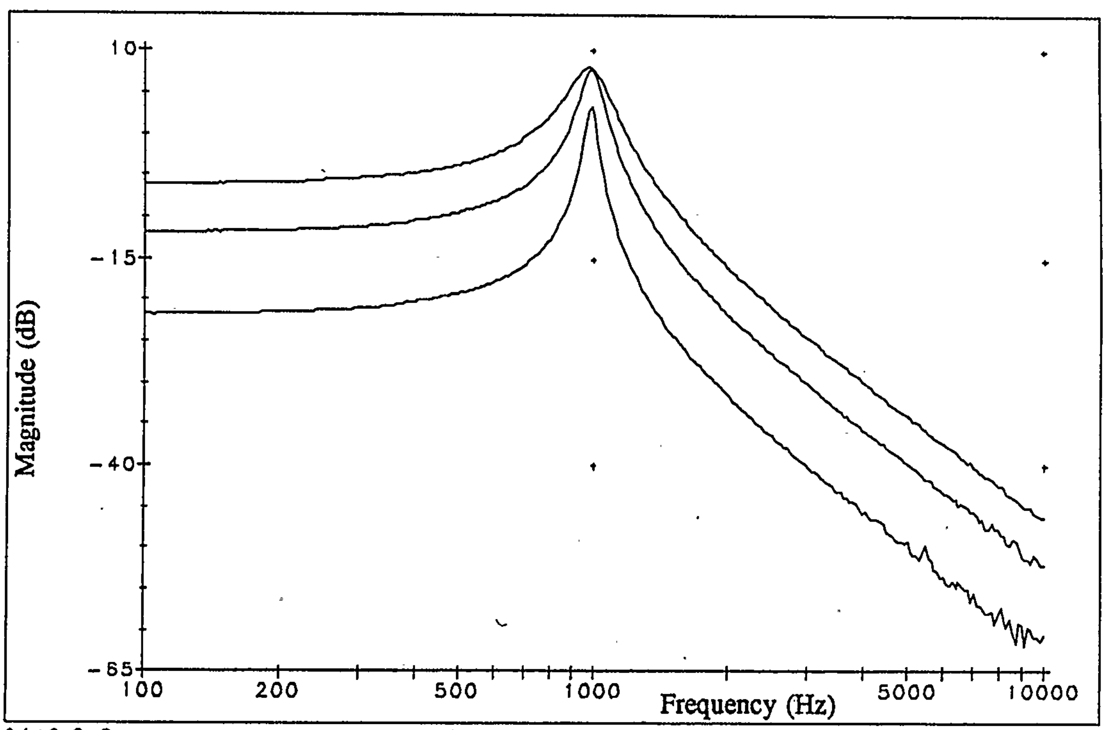

(b) LP2 1kHz Q=5,10,20

Figure 5.15 1kHz Filter Response Using Modified Wilson Mirror OTA's

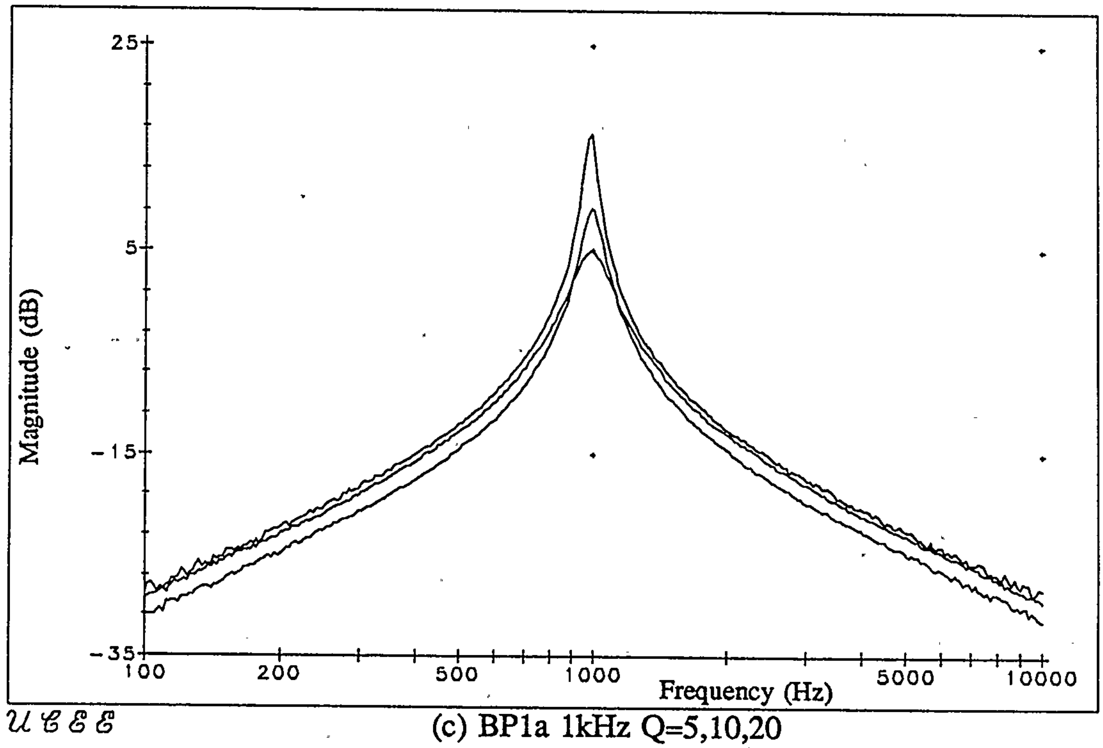

(c) BP1a 1kHz Q=5,10,20

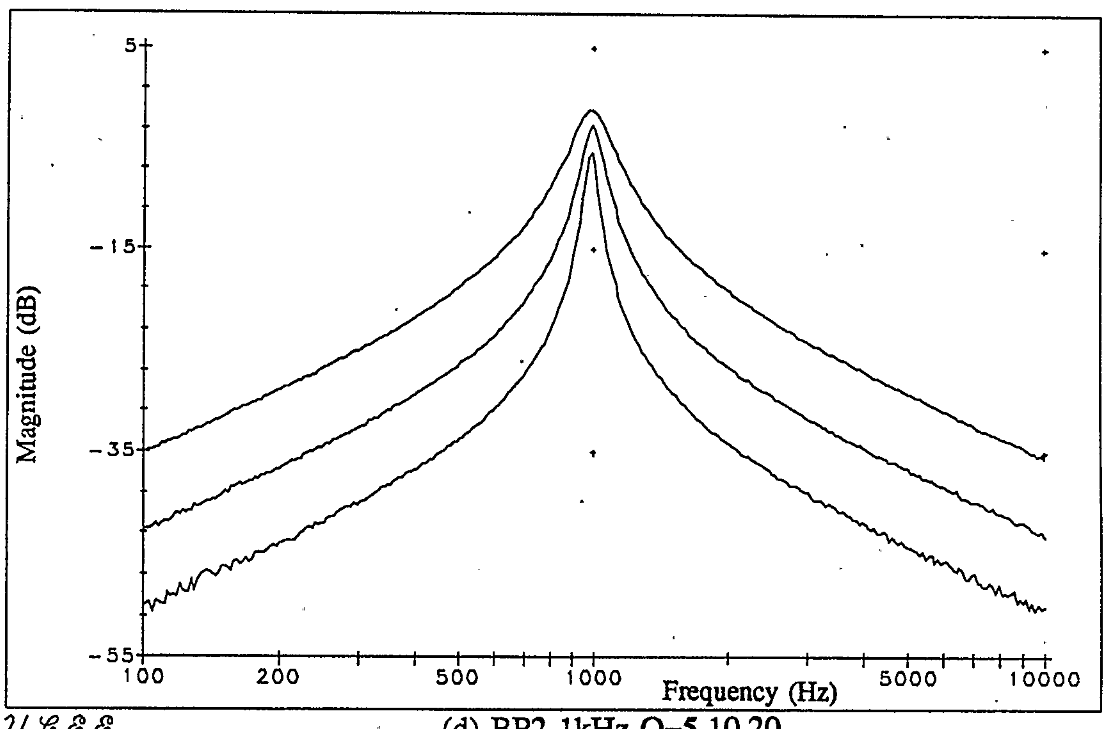

(d) BP2 1kHz Q=5,10,20

Figure 5.15 Continued

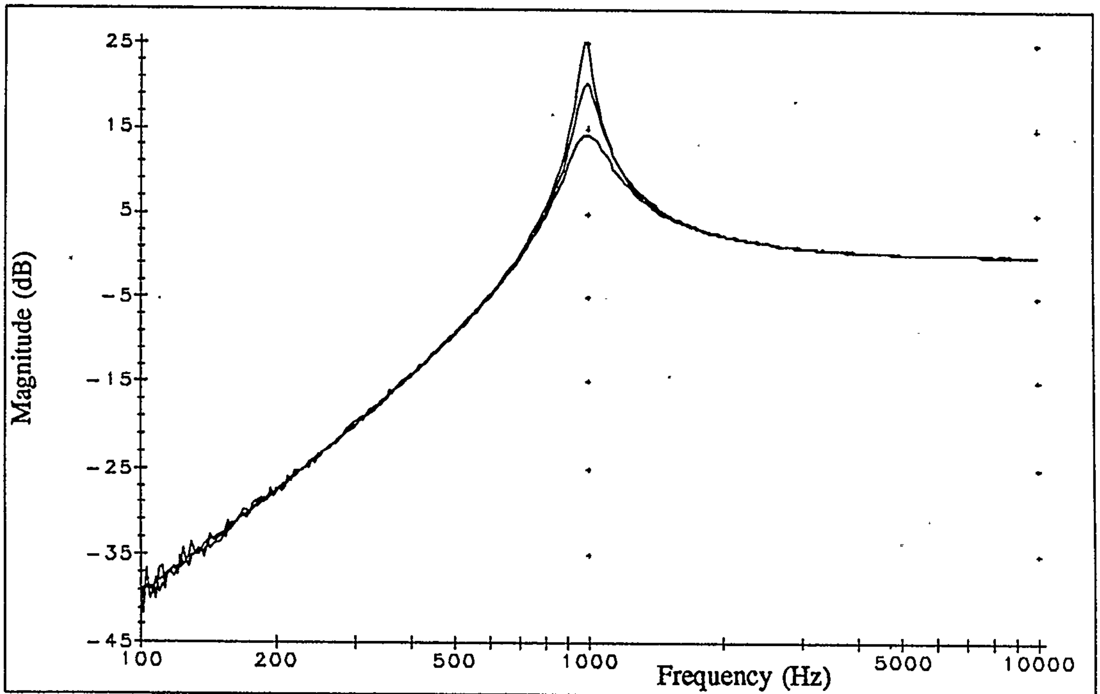

UCEE (e) HP 1kHz Q=5,10,20

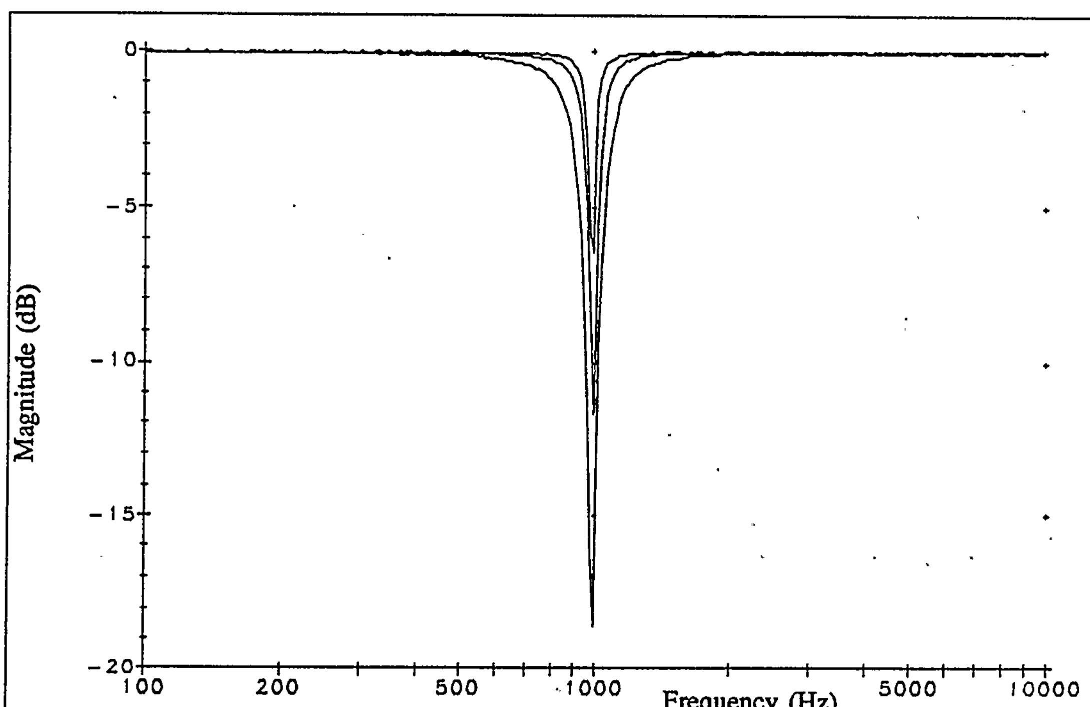

UCEE (f) Na 1kHz Q=5,10,20

Figure 5.15 Continued

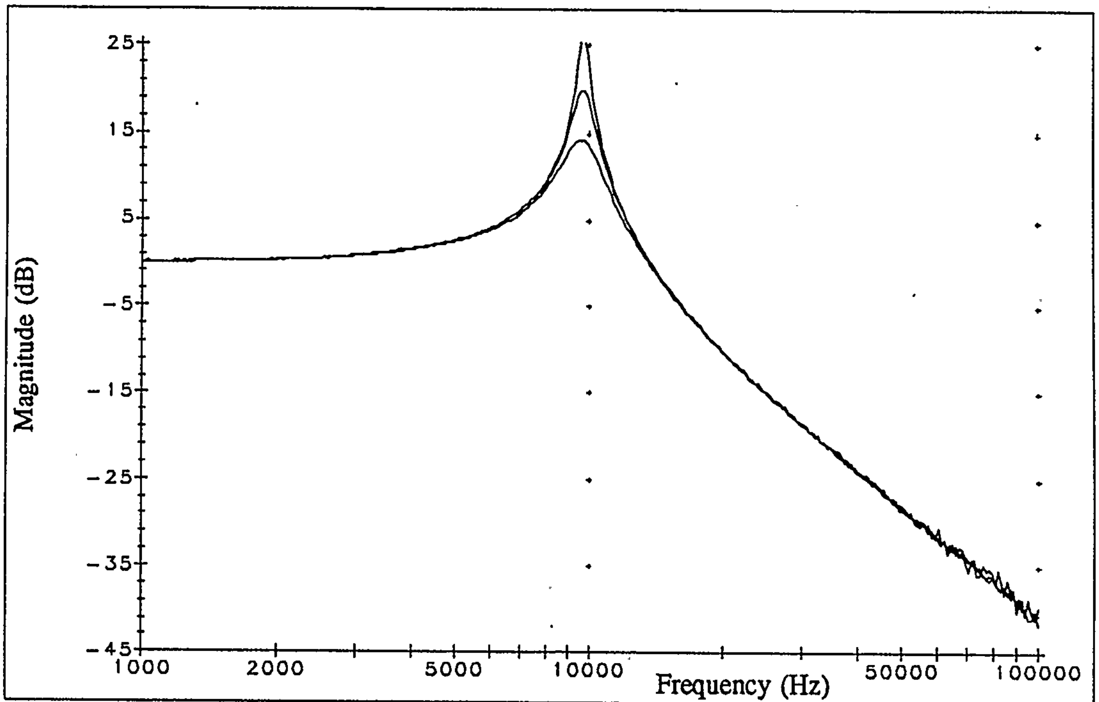

UCEE

(a) LP1a 10kHz Q=5,10,20

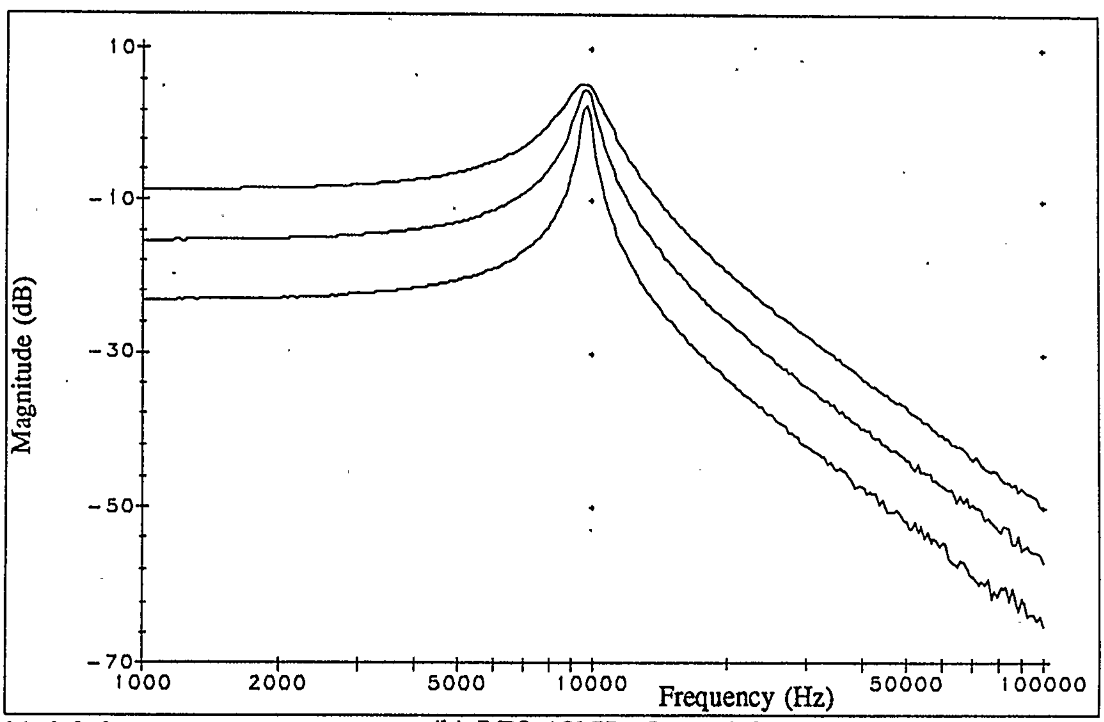

UCEE

(b) LP2 10kHz Q=5,10,20

Figure 5.16 10kHz Filter Response Using Modified Wilson Mirror OTA's

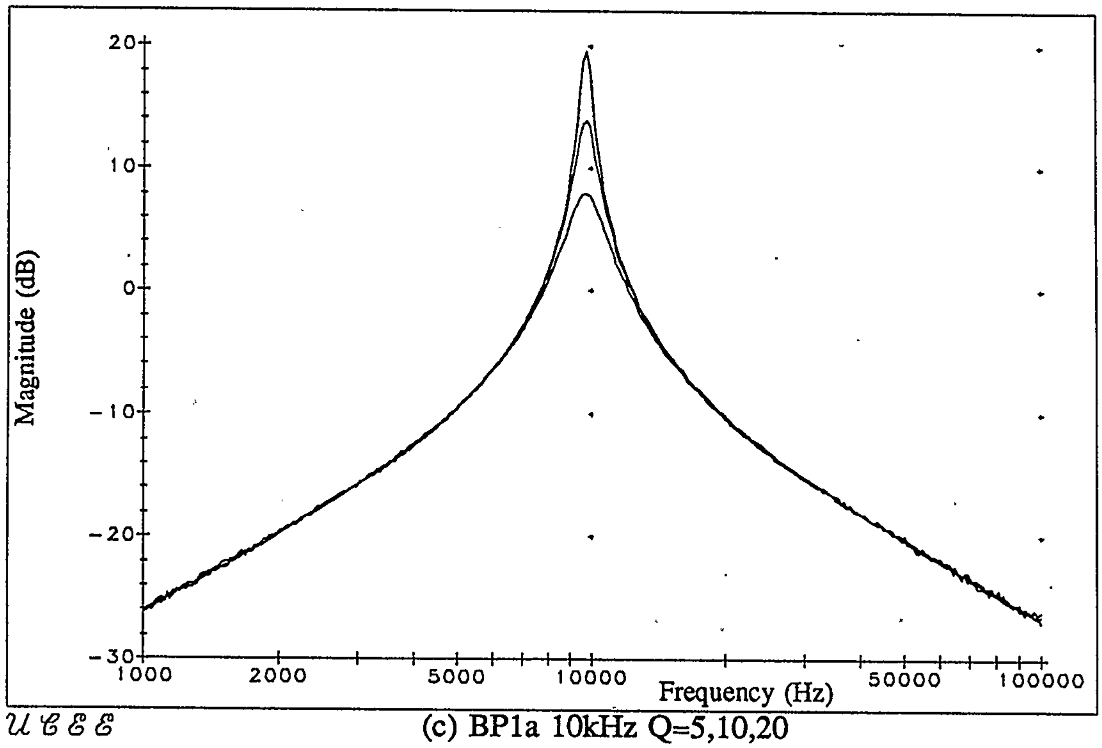

(c) BP1a 10kHz Q=5,10,20

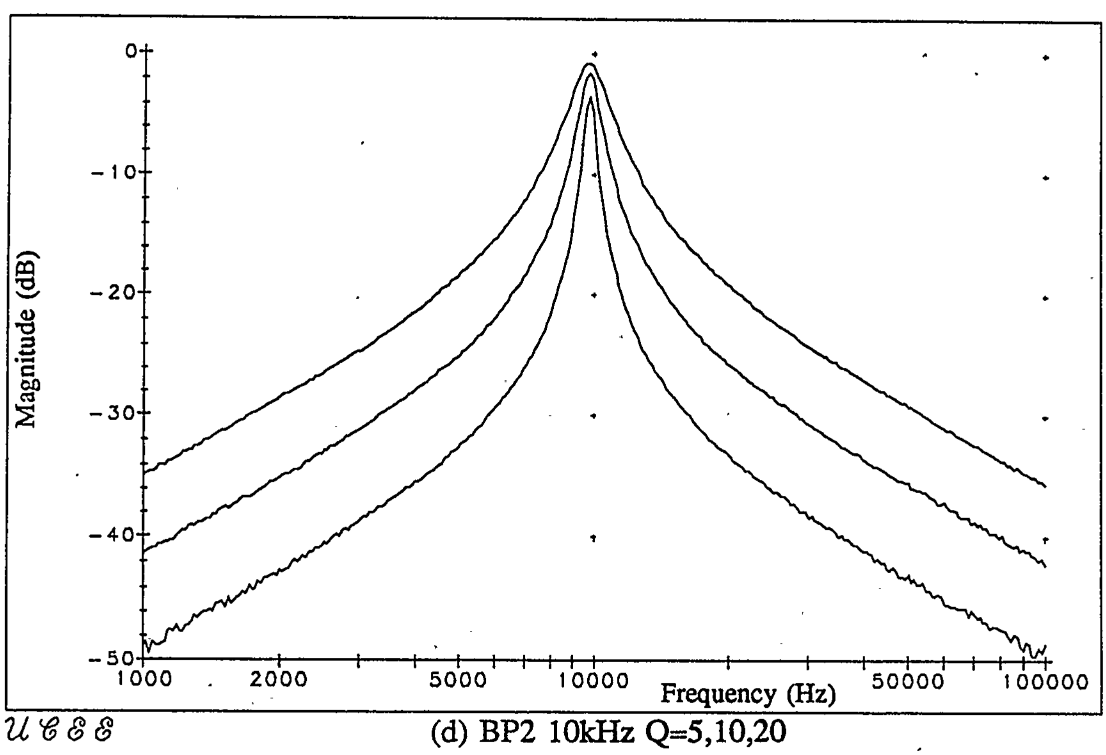

(d) BP2 10kHz Q=5,10,20

Figure 5.16 Continued

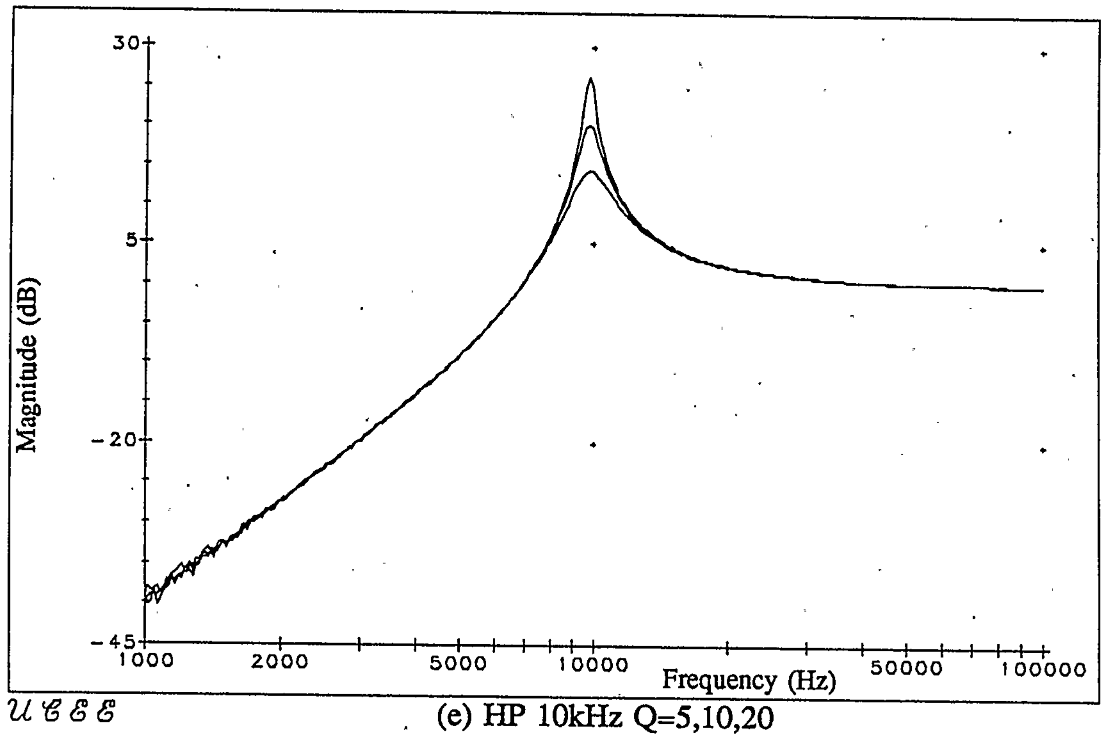

(e) HP 10kHz Q=5,10,20

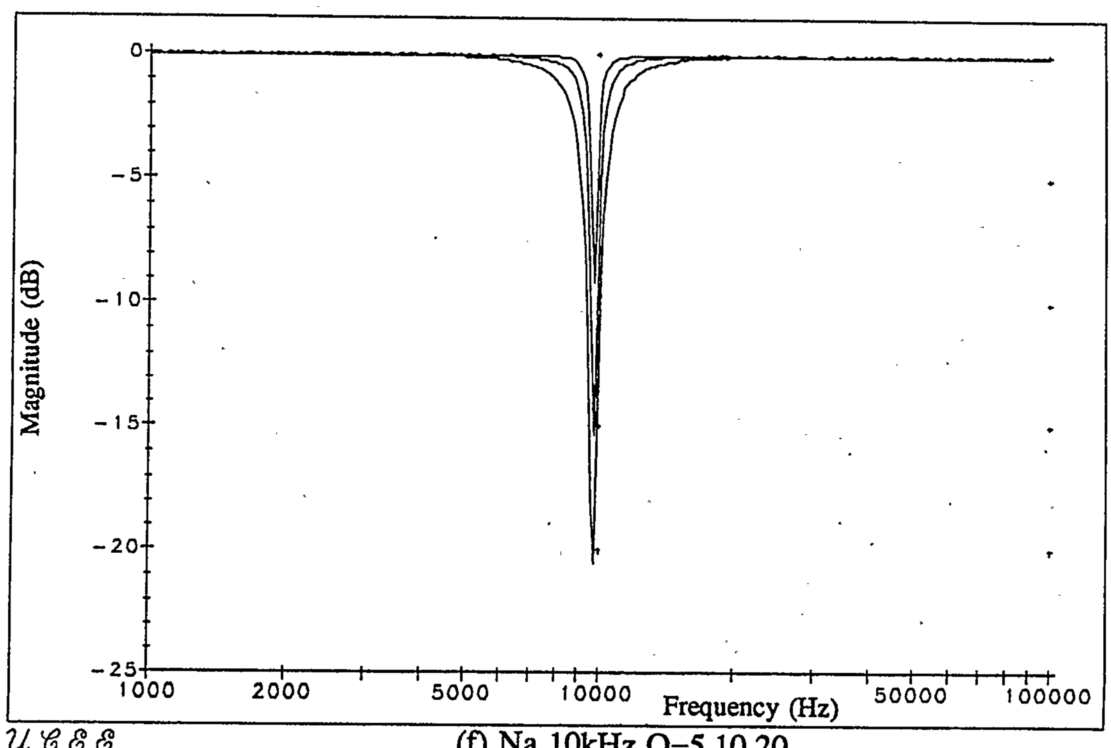

(f) Na 10kHz Q=5,10,20

Figure 5.16 Continued

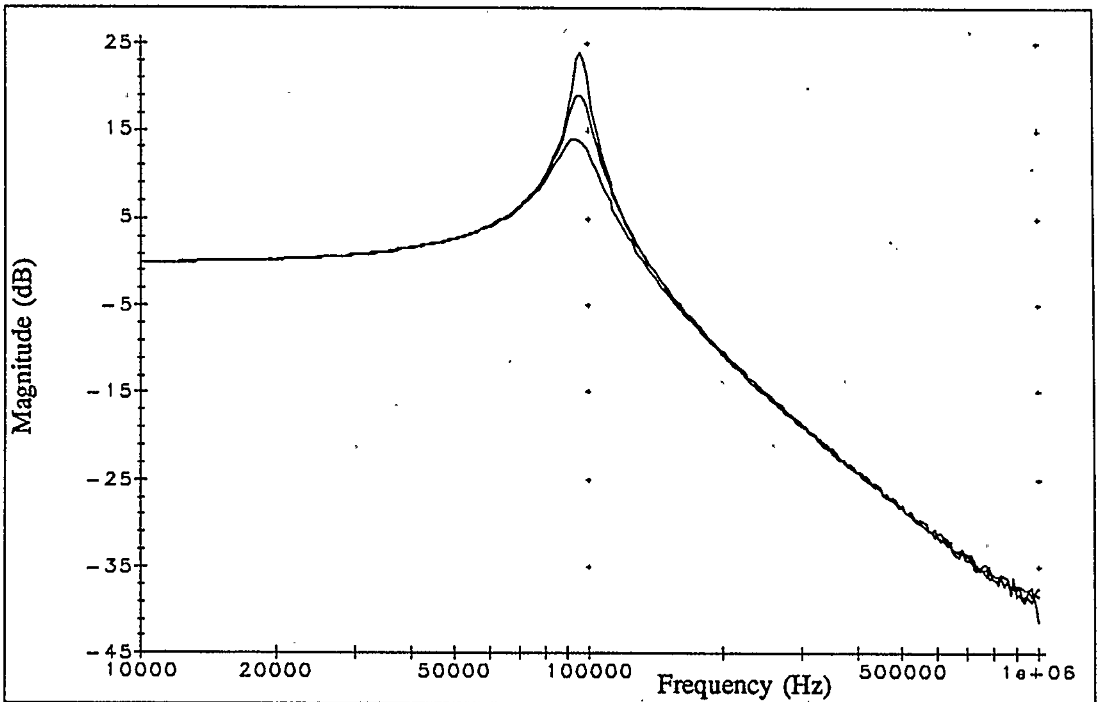

UCEE (a) LP1a 100kHz Q=5,10,20

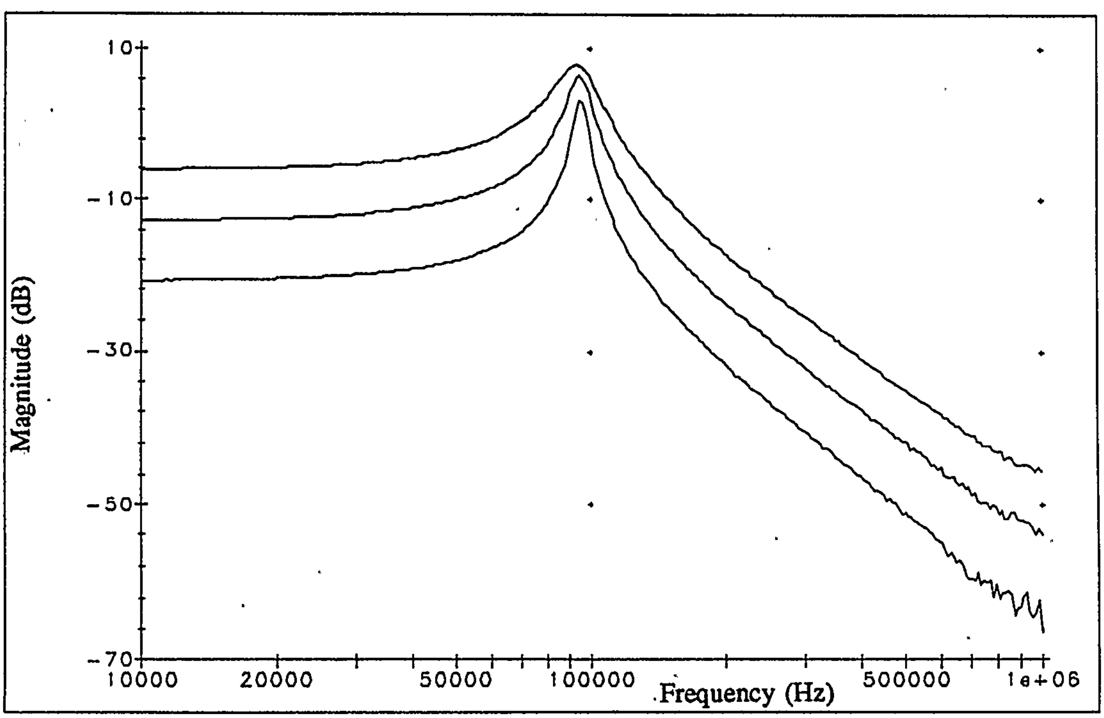

UCEE (b) LP2 100kHz Q=5,10,20

Figure 5.17 100kHz Filter Response Using Modified Wilson Mirror OTA's

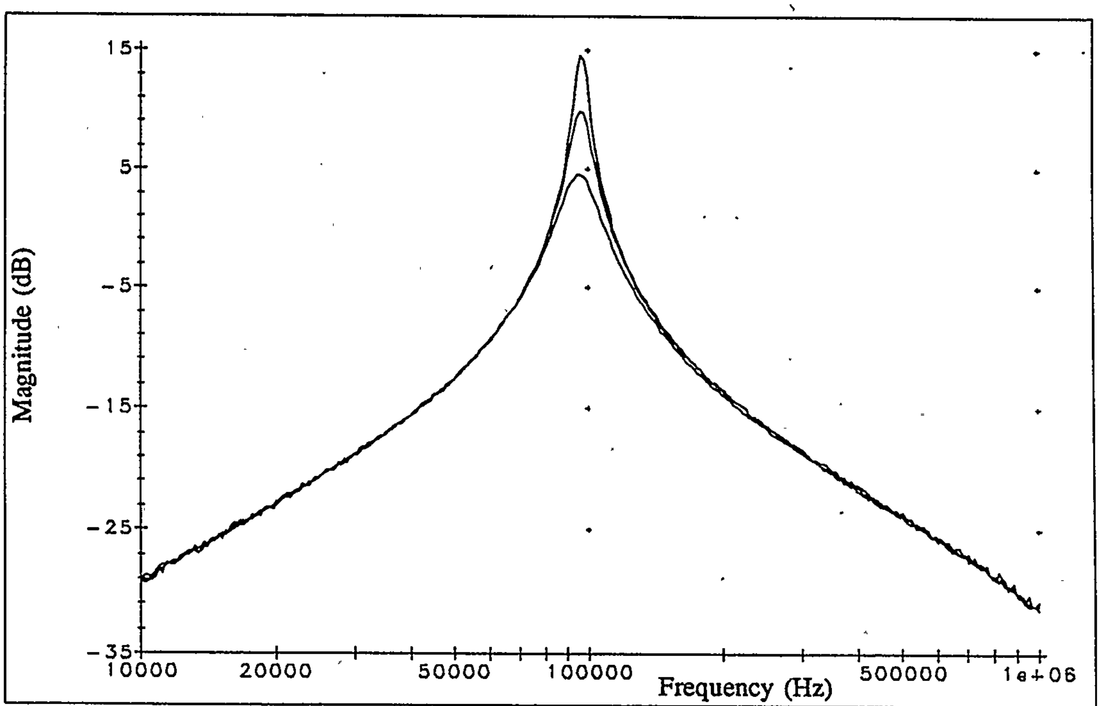

𝒰𝒞ℰℰ

(c) BP1a 100kHz Q=5,10,20

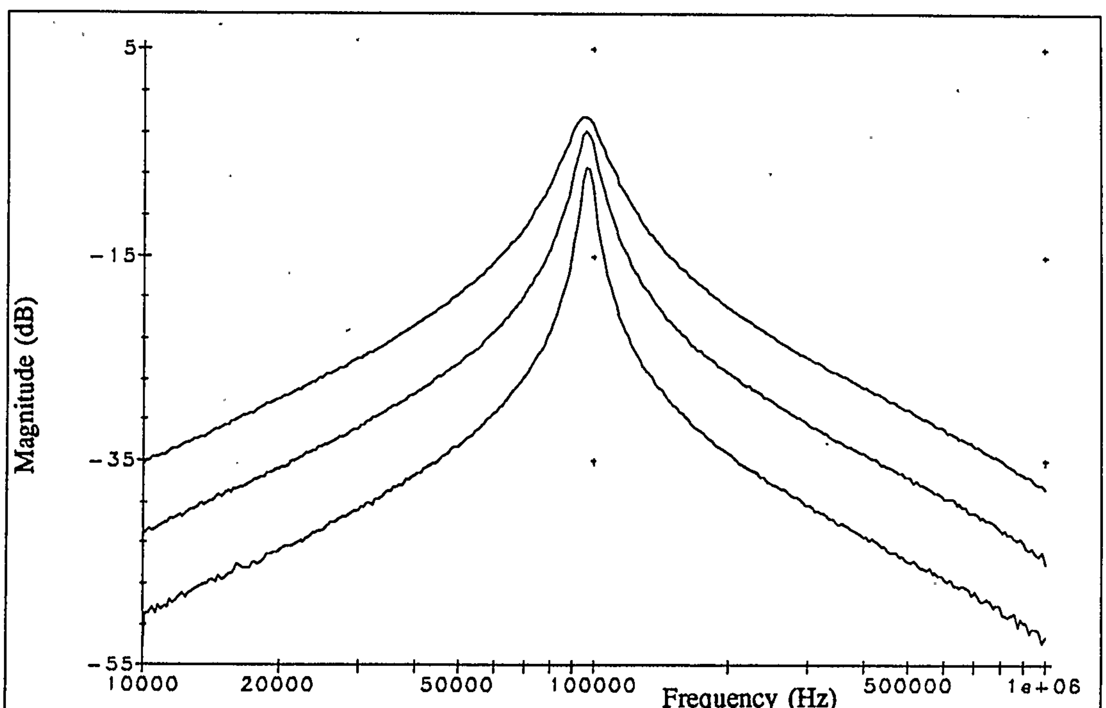

𝒰𝒞ℰℰ

(d) BP2 100kHz Q=5,10,20

Figure 5.17 Continued

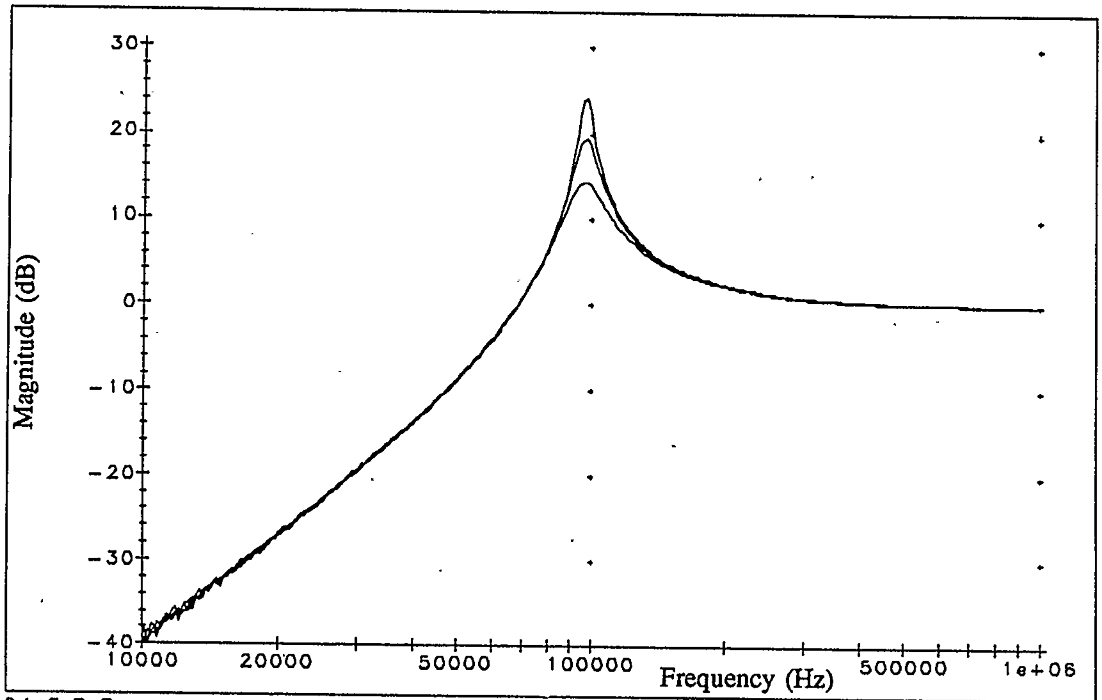

(e) HP 100kHz Q=5,10,20

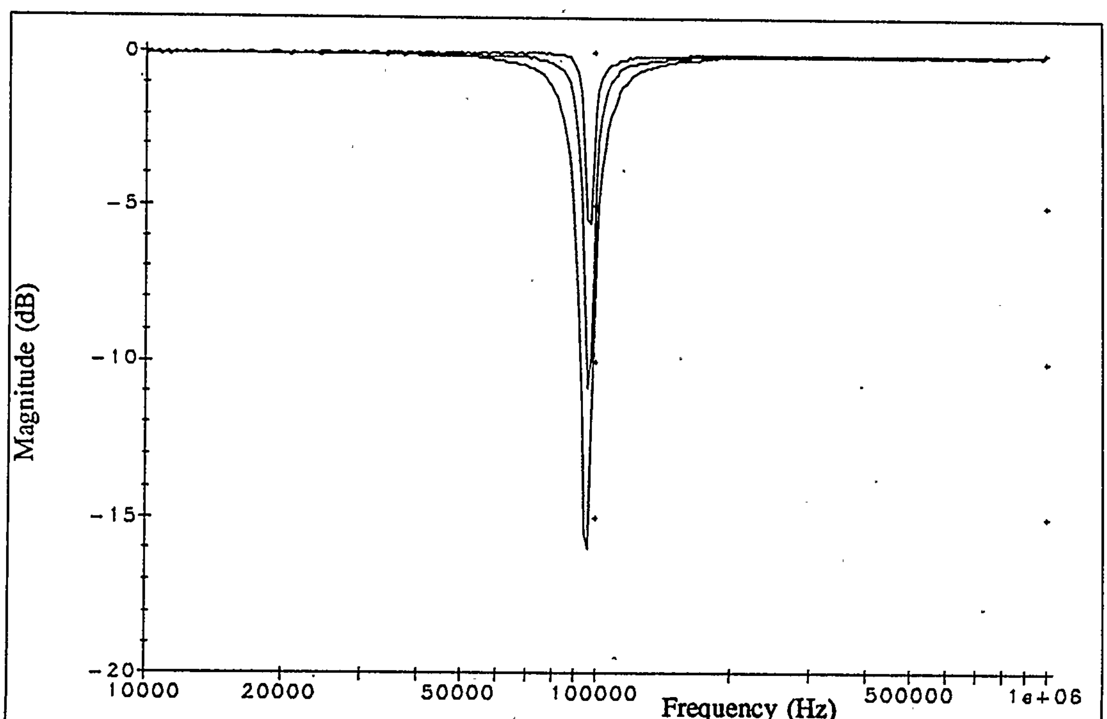

(f) Na 100kHz Q=5,10,20

Figure 5.17 Continued

However, due to the large volume of data generated by such predictions they could not be included here.

That filter structures using the single cell modified Wilson mirror OTA's perform equally well as those using the Wilson mirror OTA's is quite useful. As the modified OTA configuration only requires a single cell, an entire biquad filter structure could be integrated in only three cells with such an OTA, as opposed to the six cells which would be required using the straight Wilson mirror configuration.

Analysis using the lumped model technique was applied to all six of the filter types used over the frequency ranges and Q variations chosen above. In addition, the remaining three filter types were implemented and analyzed for the same range. The results achieved were consistent with those shown in Figures 5.2 - 5.10. For those interested in the full set of results and predictions they may be found in [13].

CHAPTER 6

CONCLUSIONS AND RECOMMENDATIONS

Standard design techniques do not work well in the prediction of OTA based biquad filter responses. To overcome this equations were derived which enabled the easy design of these filters and prediction of their responses. To show the use of this design technique, OTA structures were developed and integrated, and then the design technique was applied to the development of filters utilizing these OTA's.

6.1 OTA Design

Five different OTA designs were developed based upon the standard current mirror structure of an OTA (Figure 2.2), and two more were developed by modifying this structure to reduce the overall size. All the designs were tested using kit part transistors and were found to work well. The designs were then integrated through LTI's semi-custom bipolar process.

The integrated OTA's were characterized relative to the applied bias current. This enabled the development of a lumped model for each OTA which in turn allowed for a better understanding of their performance.

6.2 Filter Design

Using the lumped models developed for the OTA's, a set of biquad filter design equations was developed. A further set of equations was developed to enable the prediction of filter performance. A program was then written to allow the designer to easily perform filter design, and to predict the filter response with a fair degree of accuracy. An additional capability was added to the second program to allow prewarping of the design to take into account non-idealities.

The OTA based biquad filters worked very well over three decades of frequency. They performed well with quality factors up to 20, and there was no indication that they would not be able to perform well for higher Q's too. Two OTA's were used for the filters, the best of the single cell OTA's (the modified Wilson mirror OTA) and the best of the dual cell OTA's (the normal configuration Wilson mirror OTA). The filter responses of both OTA's are equally good. Thus, the best OTA for implementation in these filters is that of the modified Wilson mirror OTA, as it is a single cell OTA with a performance equal to that of the best dual cell OTA.

6.3 Future Work

It was found that OTA parameters varied significantly from chip to chip. This meant that the design equations which used those parameters could not be as accurate as desired. If a method could be found to reduce the process variations, this would greatly enhance the usefulness of the design equations. Unfortunately, this is extremely unlikely, if not impossible.

The OTA parameters are temperature sensitive, and for applications in which temperature change is possible, it will be necessary to design a compensation ciruit. The simplest method is making the bias current source proportional to the absolute temperature. If full integration is desired, however, it would be better to remove the entire bias current structure and replace it with one which is temperature dependant. This will entail remeasurement of all the OTA parameters, as the parameters are all bias current dependant, but if temperature independance is required the old parameters will no longer be valid anyway.

There is a possibility that a biquad filter with mixed types of OTA's would produce a better response than one with all the same type of OTA. However, with the seven different OTA structures created here, and three OTA's used in the biquad filter structure, there are an extremely large number of possible combinations, so this was left for future consideration. It is also possible that in-depth consideration of the actual biquad filter structure would lead to a design which eliminates redundancies in the structure of the individual OTA's (such as bias chains, etc.), and thus reduces the amount of silicon area required by the design. These possibilities are left for future work.

6.4 Conclusions

A design technique was developed here which enables the designer to quite easily design and predict the response of OTA based biquad filters. In any design technique there are always deviations which can not be accounted for. In some cases these deviations can be ignored, in other cases it is impossible to do so. The process variations encountered here are enough to be noticeable, but can be removed through tuning if desired, or even ignored in many cases. However, if these filters were to be used on a commercial scale, the need for fine tuning may render them impractical.

Once the OTA's have been characterized, the design process becomes straight forward and simple. The designer need only know the frequency at which to operate, the quality factor desired in the filter, and practical values for some of the filter components, such as the capacitor values, the transconductance values or the bias current values. Computer program were developed to take the design data and to produce the remaining component values as well as a prediction of the performance expected.

As even a simple single cell OTA produces a biquad filter with good response, it is practical to fully integrate such a design provided the need for fine tuning can be tolerated. The wide frequency range through which operation is possible, and the flexibility of the structure lead to a circuit which has many possible applications.

The end question becomes as to whether the designer can tolerate the slight error in the design equations due to process variations, and the somewhat larger error which would result if temperature variations are encountered. If the error is not tolerable, the circuit can be manually tuned to whatever tolerance is required to at least remove process variations. If this is not a viable alternative, as will be the case in some high production commercial applications, or if temperature variations will be encountered, other schemes must be adopted. It is impractical, if not impossible, to improve the integration technology to remove the process variations. The best alternative appears to be integration of a compensation circuit directly onto the chip with the filter for highly demanding applications.

BIBLIOGRAPHY

1. A. S. Sedra and Kenneth C. Smith, *Microelectronic Circuits*. New York: CBS College Publishing, 1982.

2. H. S. Malvar, "Electronically Controlled Active-C Filters and Equalizers with Operational Transconductance Amplifiers," *IEEE Transactions on Circuits and Systems*, vol. CAS-31, No. 7, pp. 645-649, July 1984.

3. R. L. Geiger and E. Sánchez-Sinencio, "Active Filter Design Using Operational Transconductance Amplifiers: A Tutorial," *IEEE Circuits and Devices Magazine*, pp. 20-32, March 1985.

4. H.S. Malvar, "Electronically Tunable Active Filters with Operational Transconductance Amplifiers," *IEEE Transactions on Circuits and Systems*, vol. CAS-29, No. 5, pp. 333-336, May 1982.

5. I. A. Khan and M. T. Ahmed, "Wide-Range Electronically Tunable Multifunction OTA-C Filter for Instrumentation Applications," *IEEE Transactions on Instrumentation and Measurement*, vol. IM-36, No. 1, pp 13-17, March 1987.

6. Meta-Software, *HSPICE User's Manual*, Campbell, California: Meta-Software Inc., June 1987.

7. LTI, *LTI Design Manual,* Burlington, Ontario: Linear Technology Inc., 1985.

8. J. W. Haslett and J. L. LaFrenz, "Detailed Characterization of Linear Technology Transconductance Amplifiers," *LTI Reports,* April 1987.

9. J. L. LaFrenz, *Programs for Design and Prediction of OTA Biquad Filters,* Internal Report 54 CO 88 JLaF, March 1988.

10. RCA, "CA3080, CA3080A," *RCA Integrated Circuits for Linear Applications,* U.S.A.: RCA Corporation, 1986, pp. 266-274.

11. J. S. Brugler, "Silicon Transistor Biasing for Linear Collector Current Temperature Dependance," *IEEE Journal of Solid-State Circuits,* pp. 57-58, June 1967.

12. P. R. Gray and R. G. Meyer, *Analysis and Design of Analog Integrated Circuits.* New York: John Wiley & Sons Inc., 1977, pp. 239-261.

13. J. L. LaFrenz, *Performance of OTA Biquad Filters,* Internal Report 56 CO 88 JLaF, March 1988.

14. J. W. Haslett and J. L. LaFrenz, "Operational Transconductance Amplifier Characterization," *LTI Reports,* December 1985.

15. J. W. Haslett, "Predicting Operational Transconductance Amplifier Noise Performance," *LTI Reports,* January 1986.

16. J. W. Haslett and J. L. LaFrenz, "Operational Transconductance Amplifier Configurations Suitable for Single and Dual Cell Fabrication Using LTI's Semicustom Process," *LTI Reports,* March 1986.

17. J. W. Haslett and J. L. LaFrenz, "LTI Transconductance Amplifier Characterization," *LTI Reports,* October 1986.

18. J. O. Voorman, W. H. A. Brüls and P. J. Barth, "Integration of Analog Filters in a Bipolar Process," *IEEE Journal of Solid-State Circuits,* vol. SC-17, No. 4, pp 713-722, August 1982.

19. K. Fukahori, "A Bipolar Voltage-Controlled Tunable Filter," *IEEE Journal of Solid-State Circuits,* vol. SC-16, No. 6, pp. 729-737, December 1981.

20. P. E. Allen, "A Model for Slew-Induced Distortion in Single-Amplifier Active Filters," *IEEE Transactions on Circuits and Systems,* vol. CAS-25, No. 8, pp. 565-572, August 1978.

21. T. Sugawara and H. Yamada, "A Volume and Frequency Response Control IC for Audio," *IEEE Journal of Solid-State Circuits,* vol. SC-15, No. 6, pp. 968-971, December 1980.

22. K. Tan and P. R. Gray, "Fully Integrated Analog Filters Using Bipolar-JFET Technology," *IEEE Journal of Solid-State Circuits,* vol. SC-13, No. 6, pp. 814-821, December 1978.

23. R. Nawrocki and U. Klein, "New OTA-Capacitor Realisation of a Universal Biquad," *Electronics Letters,* vol. 22, No. 1, pp. 50-51, 2 January 1986.

24. I. A. Khan and M. T. Ahmed, "OTA-Based Integrable Voltage/Current-Controlled Ideal C-Multiplier," *Electronics Letters,* vol. 22, No. 7, pp. 365-366, 27 March 1986.

25. J. Silva-Martínez and E. Sánchez-Sinencio, "Analogue OTA Multiplier Without Input Voltage Swing Restrictions, and Temperature-Compensated," *Electronics Letters,* vol. 22, No. 11, pp. 599-600, 22 May 1986.

26. A. Nedungadi and T. R. Viswanathan, "Design of Linear CMOS Transconductance Elements," *IEEE Transactions on Circuits and Systems,* vol. CAS-31, No. 10, pp. 891-894, October 1984.

27. C. S. Park and R. Schaumann, "A High-Frequency CMOS Linear Transconductance Element," *IEEE Transactions on Circuits and Systems,* vol. CAS-33, No. 11, pp. 1132-1138, November 1986.